Cover page:
Landsat 8 image of Jambi acquired on 27 June 2013
Source: NASA

LAND USE AND LAND COVER CHANGES IN SOUTH EAST ASIA: THE EFFECTS OF LAND TRANSFORMATIONS ON BIOPHYSICAL VARIABLES IN INDONESIA

Dissertation

zur Erlangung des Doktorgrades

der Fakultät für Forstwissenschaften und Waldökologie

der Georg-August-Universität Göttingen

vorgelegt von

C.R. Sabajo

aus Paramaribo, Suriname

Göttingen, 2018

Betreuer: Prof. Dr. Alexander Knohl (Georg-August-Universität Göttingen)
Co-Betreuer: Dr. Guerric LeMaire (CIRAD/AgroParisTech, Montpellier)

Gutachter:
Prof. Dr. Alexander Knohl, Georg-August-Universität Göttingen
Prof. Dr. Dirk Hölscher, Georg-August-Universität Göttingen
Prof. Dr. Oleg Panferov, Technische Hochschule Bingen

Prüfungskommision:
Prof. Dr. Alexander Knohl, Georg-August-Universität Göttingen
Dr. Martial Bernoux, IRD Montpellier, Frankreich
Prof. Dr. Dirk Hölscher, Georg-August-Universität Göttingen
Prof. Dr. Oleg Panferov, Technische Hochschule Bingen
Dr. Agnes Bégué, CIRAD UMR TETIS Montpellier, Frankreich

Tag der mündlichen Prüfung: 22.06.2018

THÈSE POUR OBTENIR LE GRADE DE DOCTEUR DE L'INSTITUT DES SCIENCES ET INDUSTRIES DU VIVANT ET DE L'ENVIRONNEMENT - AGROPARISTECH

N°: 2018 AGPT0005

En Écologie Fonctionnelle et Sciences Agronomiques

École doctorale GAIA – Biodiversité, Agriculture, Alimentation, Environnement, Terre, Eau – n°584
Portée par l'Université de Montpellier

Unité de recherche: Ecologie fonctionnelle et biochimie des sols

LAND USE AND LAND COVER CHANGES IN SOUTH EAST ASIA:

THE EFFECTS OF LAND TRANSFORMATIONS ON BIOPHYSICAL VARIABLES IN INDONESIA

Présentée par Clifton R. Sabajo
Le 22 Juin 2018

Sous la direction de Prof. Dr. Alexander Knohl
et
Dr. Guerric Le Maire

Devant le jury composé de

Prof. Dr. Alexander Knohl, Bioclimatology, University of Göttingen	**Directeur de thèse**
Dr. Martial Bernoux, IRD Montpellier	**Co-directeur de thèse**
Prof. Dr. Dirk Hölscher, University of Göttingen	**Rapporteur**
Prof. Dr. Oleg Panferov, University of Bingen	**Rapporteur**
Dr. Agnes Bégué, CIRAD UMR TETIS Montpellier	**Examinateur**
Dr. Guerric LeMaire, CIRAD Montpellier	**Invité**
Dr. Olivier Roupsard, UMR Eco&Sols CIRAD Sénégal	**Invité**

AgroParisTech
INSTITUT DES SCIENCES ET INDUSTRIES DU VIVANT ET DE L'ENVIRONNEMENT

UNIVERSITÉ DE MONTPELLIER

Land Use and Land Cover Changes in South East Asia:

The effects of land transformations on biophysical variables in Indonesia

This research was carried out at the Bioclimatology department at the University of Göttingen, Faculty of Forest Sciences and Forest Ecology in association with the CRC 990, "EFForTS, Ecological and Socioeconomic Functions of Tropical Lowland Rainforest Transformation Systems (Sumatra, Indonesia)" (subproject A03).

This research was funded by a fellowship under the Erasmus Mundus Joint Doctorate Programme Forest and Nature for Society (EMJD-FONASO), under a co-tutelle agreement between University of Göttingen (Germany), Faculty of Forest Sciences and Forest Ecology and AgroParisTech (Montpellier, France). The research was partly supported by the German Research Foundation (DFG) in the framework of the CRC990 "EFForTS, Ecological and Socioeconomic Functions of Tropical Lowland Rainforest Transformation Systems (Sumatra, Indonesia)".

Layout and figures: C.R. Sabajo
Cover: C.R. Sabajo
Photos: C.R. Sabajo

Land Use and Land Cover Changes in South East Asia:

The effects of land transformations on biophysical variables in Indonesia

Doctoral dissertation submitted for the degree of doctor in Forest Sciences and Forest Ecology issued by the Georg-August University of Göttingen
& the degree of doctor issued by *l' Institut des Sciences et Industries du Vivant et de l'Environnement (AgroParisTech)*
Submitted by
C.R. Sabajo
from Paramaribo, Suriname

Dissertation zur Erlangung des Doktorgrades der Fakultät für Forstwissenschaften und Waldökologie der Georg-August-Universität Göttingen
& des Doktorgrades ausgestellt durch *l'Institut des Sciences et Industries du Vivant et de l'Environnement (AgroParisTech)*
Vorgelegt von
C.R. Sabajo
Aus Paramaribo, Suriname

Thèse pour obtenir le grade de docteur délivré par - la Faculté des Sciences Forestières et d' Écologie Forestière de l'Université Georg-August-Göttingen
et L'Institut des Sciences et Industries du Vivant et de l'Environnement (AgroParisTech)
présentée par
Clifton R. Sabajo
Du Paramaribo, Suriname

Proefschrift ter verkrijging van het doctoraat in de Bosbouwkunde en Bosecologie aan de Georg-August Universiteit in Göttingen en aan *l'Institut des Sciences et Industries du Vivant et de l'Environnement (AgroParisTech)*
door
C.R. Sabajo
uit Paramaribo, Suriname

Supervision / Betreuungsauschuss / Direction / Promotoren:

Prof. Dr. Alexander Knohl (Georg-August-Universität Göttingen)
Dr. Guerric LeMaire (CIRAD/AgroParisTech, Montpellier)

Referee / Gutachter / Rapporteur / Referenten:
Prof. Dr. Alexander Knohl, Georg-August-Universität Göttingen
Prof. Dr. Dirk Hölscher, Georg-August-Universität Göttingen
Prof. Dr. Oleg Panferov, Technische Hochschule Bingen

Examination committee / Prüfungskommision / Jury / Beoordelingscommissie:
Prof. Dr. Alexander Knohl (Georg-August-Universität Göttingen)
Dr. Martial Bernoux (IRD Montpellier, Frankreich)
Prof. Dr. Dirk Hölscher, Georg-August-Universität Göttingen
Prof. Dr. Oleg Panferov, Technische Hochschule Bingen
Dr. Agnes Bégué, CIRAD Montpellier, Frankreich

Date of defense: 22 June 2018
Tag der mündlichen Prüfung: 22 Juni 2018
Soutenue publiquement le : 22 Juin 2018
Openbare verdediging op: 22 juni 2018

Begin at the beginning... and go on till you come to the end: then stop.

~Lewis Carroll, *Alice's Adventures in Wonderland*

C. R. Sabajo

Land Use and Land Cover Changes in South East Asia

The effects of land transformations on biophysical variables in Indonesia

85 pages

Thesis, Göttingen University - Germany & AgroParisTech Montpellier - France

With summaries in English, German, French and Dutch

Table of contents

Summary

Over the last decades, Indonesia has experienced dramatic land transformations with an expansion of oil palm plantations at the expense of tropical forests. Indonesia is currently one of the regions with the highest transformation rate of the land surface worldwide related to the expansion of oil palm plantations and other cash crops replacing forests on large scales. As vegetation is a modifier of the climate near the ground these large-scale land transformations have major impacts on surface biophysical variables such as land surface temperature (LST), albedo, vegetation indices (e.g. the normalized difference vegetation index, NDVI), on the surface energy balance and energy partitioning.

Despite the large historic land transformation in Indonesia toward oil palm and other cash crops and governmental plans for future expansion, this is the first study so far to quantify the impacts of land transformation on biophysical variables in Indonesia. To assess such changes at regional scale remote sensing data are needed.

As a key driver for many ecological functions, LST is directly affected by land cover changes. We analyze LST from the thermal band of a Landsat image and produce a high-resolution surface temperature map (30 m) for the lowlands of the Jambi province in Sumatra (Indonesia), a region which experienced large land transformation towards oil palm and other cash crops over the past decades. The comparison of LST, albedo, NDVI, and evapotranspiration (ET) between seven different land cover types (forest, urban areas, clear cut land, young and mature oil palm plantations, acacia and rubber plantations) shows that forests have lower surface temperatures than the other land cover types, indicating a local warming effect after forest conversion. LST differences were up to 10.1 ± 2.6 ºC (mean ± SD) between forest and clear-cut land. The differences in surface temperatures are explained by an evaporative cooling effect, which offsets an albedo warming effect.

Young and mature oil palm plantations differenced in their biophysical. To study the development of surface biophysical variables during the 20 – 25 years rotation cycle of oil palm plantations, we used three Landsat images from the Jambi province in Sumatra/Indonesia covering a chronosequence of oil palm plantations.

Our results show that differences between oil palm plantations in different stages of the oil palm rotation cycle are reflected in differences in the surface energy balance, energy partitioning and biophysical variables. During the oil palm plantation lifecycle the surface temperature differences to forest gradually decrease and approach zero around the mature oil palm plantation stage of 10 years. Concurrently, NDVI increases and the albedo decreases approaching typical values of forests. The surface energy balance and energy partitioning show a development patterns related to biophysical variables and the age of the oil palm plantations. Newly established and young plantations (< 5 years) have less net radiation available than mature oil palm plantations, yet have higher surface temperatures than mature oil palm plantations. The changes in biophysical variables, energy balance and energy partitioning during the oil palm rotation cycle can be explained by the previously identified evaporative

cooling effect in which the albedo warming effect is offset. A main determinant in this mechanism is the vegetation cover during the different phases in the oil palm rotation cycle. NDVI as a proxy for vegetation cover showed a consistent inverse relation with the LST of different aged oil palm plantations, a trend that is also observed for different land use types in this study.

On a regional and longer time scale, the analysis of the LST trend between 2000 and 2015 based on MODIS data shows that the average daytime surface temperature in the Jambi province increased by 1.05 ºC, which followed the trend of observed land cover changes and exceed the effects of climate warming.

In order to assess the full climate effects of oil palm expansion the surface energy balance, energy partitioning and biophysical processes play an important role and the full rotation cycle of oil palm plantations need to be considered. Based on our result we construct the rotation cycle of oil palm plantations and the changes that occur during the development of oil palm vegetation.

This study provides evidence that the expansion of oil palm plantations and other cash crops leads to changes in biophysical variables, warming the land surface and thus enhancing the increase of air temperature because of climate change. By using high-resolution Landsat data we were able to include the effects of land use change on biophysical variables. Understanding the effects of land cover change on the biophysical variables may support policies regarding conservation of the existing forests, planning and expansion of the oil palm plantations and possible afforestation measures. Knowledge of biophysical variables, radiation balance and energy partitioning during the rotation cycle of oil palm can be used to including new management practices that could reduce the extreme environmental and microclimatic conditions in the initial phase of the oil palm plantations.

Zusammenfassung

In den letzten Jahrzehnten hat Indonesien umfassende Veränderungen der Landnutzung mit einer Ausweitung von Ölpalmplantagen auf Kosten tropischer Wälder erlebt. Derzeit ist Indonesien weltweit eine der Regionen mit der höchsten Umwandlungsrate der Landnutzung, die mit der Ersetzung von Wäldern durch Ölpalmplantagen und andere Nutzpflanzen verbunden ist. Da die Vegetation ein Einflussfaktor für das Bodenklima ist, haben diese großflächigen Landtransformationen große Auswirkungen auf die biophysikalischen Variablen wie Landoberflächentemperatur (LST), Albedo, Vegetationsindizes (z.B. der normalisierte Differenzvegetationsindex, NDVI) und auf die Energiebilanz und die verschiedenen Komponenten der ausgetauschten Energie.

Trotz des großen Umfangs der bereits vollzogenen und von der Regierung geplanten Landtransformationen in Indonesien hin zu Ölpalmplantagen und anderen Nutzpflanzen, ist dies die bisher erste Studie, welche die Auswirkungen dieser Landtransformation auf die biophysikalischen Variablen in Indonesien quantifiziert. Um solche Veränderungen auf regionaler Ebene zu bewerten, werden Fernerkundungsdaten benötigt.

Als einer der Hauptantriebsfaktoren für viele ökologische Prozesse ist die LST direkt von Veränderungen der Landnutzung betroffen.
Wir analysieren die LST aus dem thermischen Band eines Landsat-Bildes und erstellen eine hochauflösende Oberflächentemperaturkarte (30 m) für das Tiefland der Provinz Jambi auf Sumatra (Indonesien), eine Region die in den letzten Jahrzehnten eine große Landumwandlung hin zu Ölpalmen und anderen Nutzpflanzen erfahren hat. Der Vergleich von LST, Albedo, NDVI und Evapotranspiration (ET) zwischen sieben verschiedenen Landbedeckungstypen (Wald, städtische Gebiete, Brachland, junge und reife Ölpalmplantagen, Akazien- und Kautschukplantagen) zeigt, dass Wälder niedrigere Oberflächentemperaturen haben als die anderen Landbedeckungstypen, was auf einen lokalen Erwärmungseffekt nach der Umwandlung des Waldes in einen anderen Landbedeckungstyp hindeutet. Die LST-Unterschiede betrugen bis zu 10,1 ± 2,6 ºC (Mittelwert ± Standardabweichung) zwischen Wald und Brachland. Die Unterschiede in den Oberflächentemperaturen lassen sich durch einen Verdunstungskälteeffekt, der den Albedo-Erwärmungseffekt kompensiert erklären.

Auf Grundlage der beobachteten Unterschieden in den biophysikalischen Variablen zwischen reifen und jungen Ölpalmplantagen, analysieren wir drei Landsat-Bilder, die eine Chronosequenz von Ölpalmplantagen enthalten um die Entwicklung von biophysikalischen Oberflächenvariablen während des 20-25 jährigen Rotationszyklus der Ölpalmplantagen zu untersuchen.

Unsere Ergebnisse zeigen, dass sich die Unterschiede zwischen Ölpalmplantagen in verschiedenen Phasen des Ölpalmen-Rotationszyklus in Unterschieden in der Energiebilanz, Energiepartitionierung und biophysikalischen Variablen widerspiegeln. Während des Lebenszyklus der Ölpalmplantage nehmen die Oberflächentemperaturunterschiede allmählich ab und nähern sich grob den Werten der reifen Ölpalmphase mit einem Alter von 10 Jahren.

Gleichzeitig nimmt der NDVI zu und der Albedo ab und beide Größen nähern sich den typischen Werten von Wäldern. Die Energiebilanz und die Energiepartitionierung zeigen einen Entwicklungstrend, der mit den biophysikalischen Variablen und mit dem Alter der Ölpalmplantagen zusammenhängt. Neu etablierte und junge Plantagen (<5 Jahre) haben eine geringere Nettostrahlung als reife Ölpalmplantagen, aber eine höhere Oberflächentemperaturen als reife Ölpalmplantagen. Die Veränderungen der biophysikalischen Variablen, der Energiebilanz und der Energieaufteilung während des Ölpalmen-Rotationszyklus können durch den zuvor identifizierten Verdunstungskälteeffekt erklärt werden, durch den der Albedo-Erwärmungseffekt kompensiert wird. Eine Hauptdeterminante in diesem Mechanismus ist die Vegetationsbedeckung während der verschiedenen Phasen im Rotationszyklus der Ölpalme. Der NDVI als Proxy für die Vegetationsbedeckung zeigt einen inversen Zusammenhang zur LST der Ölpalmplantagen unterschiedlichen Alters; ein Trend, der auch für andere Landnutzungstypen in dieser Studie beobachtet wurde.

In einer auf MODIS Daten basierenden regionalen und langfristigeren Analyse des LST-Trends zwischen den Jahren 2000 und 2015 zeigt sich, dass die durchschnittliche Tagesoberflächentemperatur in der Provinz Jambi um 1,05 °C gestiegen ist, was dem Trend der beobachteten Landbedeckungsänderungen folgt und die Auswirkungen der Klimaerwärmung übersteigt.

Um die volle Auswirkungen der Ölpalmenexpansion auf das Klima abzuschätzen, spielen die Energiebilanz, die Energiepartitionierung und biophysikalische Prozesse eine wichtige Rolle, wobei der gesamte Rotationszyklus von Ölpalmplantagen berücksichtigt werden muss. Basierend auf unseren Ergebnissen entwickeln wir eine Struktur des Rotationszyklus von Ölpalmplantagen der die während der Entwicklung der Ölpalmenvegetation auftretenden Veränderungen darstellt.

Diese Studie belegt, dass die Ausweitung von Ölpalmplantagen und anderen Nutzpflanzen zu Veränderungen der biophysikalischen Variablen führt, die die Landoberfläche erwärmen und somit den Anstieg der Lufttemperatur aufgrund des Klimawandels verstärken. Durch den Einsatz von hochauflösenden Landsat-Daten konnten wir die Auswirkungen von Landnutzungsänderungen auf biophysikalische Variablen in unserer Analyse einbeziehen. Ein besseres Verständnis der Auswirkungen von Landbedeckungsänderungen auf die biophysikalischen Variablen kann Maßnahmen zur Erhaltung der bestehenden Wälder, zur Planung und zum Ausbau von Ölpalmplantagen und zu möglichen Aufforstungsmaßnahmen unterstützen. Wissen über biophysikalische Variablen, Strahlungsbilanz und Energieaufteilung während des Rotationszyklus der Ölpalme können verwendet werden, um neue Managementpraktiken einzubeziehen, die die extreme ökologischen und mikroklimatischen Bedingungen in der Anfangsphase der Ölpalmplantagen reduzieren könnten.

Resumé

Au cours des dernières décennies, l'Indonésie a connu des transformations spectaculaires des terres avec une expansion des plantations de palmiers à huile au détriment des forêts tropicales. L'Indonésie est actuellement l'une des régions ayant le plus haut taux de transformation de la surface terrestre dans le monde à cause de l'expansion des plantations de palmiers à huile et d'autres agricultures qui remplacent les forêts à grande échelle. Comme la végétation est un modificateur du climat près du sol, ces transformations à grande échelle ont des impacts majeurs sur les variables biophysiques de surface telles que la température de surface, l'albédo, les indices de végétation (NDVI), sur le bilan énergétique de surface et le partitionnement énergétique.

Ce travail de thèse vise à quantifier les impacts des changements d'usage des terres en Indonésie sur les variables biophysiques de surface. Pour évaluer ces changements à l'échelle régionale, des données de télédétection sont nécessaires.

Étant une variable clé de nombreuses fonctions écologiques, la température de surface (LST) est directement affectée par les changements de la couverture terrestre. Nous avons analysé la LST à partir de la bande thermique d'une image Landsat et produit une carte de température de surface avec une haute résolution (30m) pour les basses terres de la province de Jambi à Sumatra (Indonésie), une région qui a subi de grandes transformations au cours des dernières décennies. La comparaison des LST, albédo, NDVI et évapotranspiration (ET) entre sept différents types de couverture terrestre (forêts, zones urbaines, terres incultes, plantations de palmiers à huile jeunes et matures, plantations d'acacias et de caoutchouc) montre que les forêts ont des températures de surface inférieures à celles des autres types de couvert végétal, ce qui indique un effet de réchauffement local après la conversion des forêts vers des plantations. Les différences de LST atteignaient 10,1 ± 2,6 ºC (moyenne ± écart-type) entre les forêts et les terres déforestées. Les différences de températures de surface s'expliquent par un effet de refroidissement évaporatif des forêts, qui compense l'effet de réchauffement de l'albédo.

Basé sur des différences observées dans les variables biophysiques entre les plantations de palmiers à huile jeunes et matures, nous avons analysé trois images Landsat couvrant une chronoséquence de plantations de palmiers à huile pour étudier la dynamique des variables biophysiques de surface pendant le cycle de rotation de 20-25 ans des plantations de palmiers à huile.

Nos résultats montrent que les différences entre les plantations de palmiers à huile à différents stades du cycle de rotation du palmier à huile se reflètent dans les différences du bilan énergétique de surface, du partitionnement énergétique et des variables biophysiques. Au cours du cycle de rotation des plantations de palmiers à huile, les différences de température à la surface diminuent graduellement et se rapprochent de zéro autour du stade mature de la plantation de palmiers à huile de 10 ans. Parallèlement, le NDVI augmente et l'albédo diminue à proximité des valeurs typiques des forêts. Le bilan énergétique de surface et le partitionnement énergétique montrent des tendances de développement liés aux variables biophysiques et à l'âge

des plantations de palmiers à huile. Les nouvelles plantations et les jeunes plantations (<5 ans) ont un rayonnement net plus faible que les plantations de palmiers à huile matures, mais ont des températures de surface plus élevées que les plantations de palmiers à huile matures.
Les changements dans les variables biophysiques, le bilan énergétique et la répartition de l'énergie au cours du cycle d'une rotation du palmier à huile peuvent s'expliquer par l'effet de refroidissement évaporatif précédemment identifié dans les forêts, qui compense l'effet de réchauffement de l'albédo. L'un des principaux déterminants de ce mécanisme est la couverture végétale au cours des différentes phases du cycle de rotation du palmier à huile. Le NDVI en tant qu'indicateur du couvert végétal a montré une relation inverse cohérente avec LST de différentes plantations de palmiers à huile âgés, une tendance qui est également observée pour différents types d'utilisation des terres dans cette étude.

Une analyse régionale et à plus long terme de la tendance LST entre 2000 et 2015 basée sur les données MODIS montre que dans la journée la température moyenne de Jambi a augmenté de 1,05 ºC, suivant la tendance des changements observés et dépassant les effets du réchauffement climatique.

Afin d'évaluer les effets de l'expansion du palmier à huile sur le climat, le bilan énergétique de surface, le partitionnement énergétique et les processus biophysiques jouent un rôle important et le cycle complet de rotation des plantations de palmiers à huile doit être envisagé. Basé sur nos résultats, nous construisons le cycle de rotation des plantations de palmiers à huile et les changements qui se produisent au cours du développement de la végétation de palmiers à huile.

Cette étude fournit des preuves que l'expansion des plantations de palmiers à huile et d'autres cultures commerciales entraîne des changements dans les variables biophysiques, réchauffant la surface du sol et augmentant ainsi l'augmentation de la température de l'air à cause du changement climatique. En utilisant des données Landsat à haute résolution, nous avons pu inclure les effets du changement d'utilisation des terres sur les variables biophysiques. Comprendre les effets du changement de la couverture terrestre sur les variables biophysiques peut soutenir des politiques concernant la conservation des forêts existantes, la planification et l'expansion des plantations de palmiers à huile et les mesures de boisement possibles. La connaissance des variables biophysiques, du bilan radiatif et de la répartition énergétique au cours du cycle de rotation du palmier à huile peut inclure de nouvelles pratiques de gestion susceptibles de réduire les conditions environnementales et microclimatiques extrêmes dans la phase initiale des plantations de palmiers à huile.

Samenvatting

In de afgelopen decennia heeft Indonesië te maken gehad met dramatische landtransformaties als gevolg van de uitbreiding van oliepalmplantages ten koste van tropische bossen. Momenteel is Indonesië wereldwijd een van de regio's met de hoogste transformatiegraad van het landoppervlak door de uitbreiding van oliepalmplantages en andere gewassen die bossen op grote schaal vervangen. Aangezien de vegetatie het klimaat nabij de grond kan modificeren, hebben deze grootschalige landtransformaties grote gevolgen voor de biofysische variabelen, zoals de landoppervlaktetemperatuur (LST), albedo, vegetatie-indexen (bijv. NDVI), en op de energiebalans en energiepartitie.

Ondanks de grote historische landtransformatie in Indonesië, ten gunste van oliepalm en andere gewassen, en de overheidsplannen voor toekomstige uitbreiding, is dit de eerste studie die de gevolgen van landtransformatie op de biofysische variabelen in Indonesië kwantificeert. Om zulke veranderingen op regionale schaal te beoordelen, zijn satellietdata nodig.

Als belangrijke variabele voor veel ecologische functies, wordt LST direct beïnvloed door veranderingen in landbedekking. We analyseren de temperatuur aan de hand van de thermische band van een satellietbeeld (Landsat) en produceren een hoge-resolutie oppervlaktetemperatuurkaart (30 m) voor de laaglanden van de Jambi-provincie in Sumatra (Indonesië), een gebied dat grote landtransformaties door de uitbreiding van oliepalmplantages en andere landbouwgewassen in de afgelopen decennia heeft doorgemaakt. Een analyse waarbij de LST, albedo, NDVI en evapotranspiratie (ET) van zeven verschillende landtypen (bos, stedelijke gebieden, braakland, jonge en volwassen oliepalmplantages, acacia en rubberplantages) met elkaar vergeleken worden, toont aan dat bossen lagere oppervlaktetemperaturen dan de andere landtypen hebben, wat op een lokaal opwarmingseffect na bosconversie duidt. Verschillen in LST tussen bos en open braakland kunnen tot 10,1 ± 2,6 ^{o}C (gemiddelde ± SD) oplopen. De verschillen in oppervlaktetemperaturen worden verklaard door een koelingseffect als gevolg van verdamping waarbij het verwarmende effect van albedo gecompenseerd wordt.

Op basis van de waargenomen verschillen in biofysische variabelen tussen jonge en volwassen oliepalmplantages analyseerden we drie satellietbeelden (Landsat), gebruikmakend van een chronosequentie van oliepalmplantages om de ontwikkeling van biofysische variabelen tijdens de rotatiecyclus van 20 - 25 jaren van oliepalmplantages te bestuderen.

Onze resultaten tonen aan dat verschillen tussen oliepalmplantages in verschillende stadia van de oliepalmrotatiecyclus worden weerspiegeld in verschillen in de energiebalans, energiepartitie en biofysische variabelen. Tijdens de rotatiecyclus van de oliepalmplantages nemen de verschillen in oppervlaktetemperatuur tussen bos en oliepalmplantages geleidelijk af en naderen nul in de volgroeide oliepalmfase rond 10 jaar. Tegelijkertijd neemt de NDVI toe en de albedo af en naderen waarden die typisch voor bossen zijn. De energiebalans en energieverdeling tonen een ontwikkelingspatroon dat in relatie staat tot de biofysische variabelen en de leeftijd van de oliepalmplantages. Nieuwgevestigde en jonge plantages (<5

jaar) hebben minder nettostraling dan volwassen oliepalmplantages, maar hebben hogere oppervlaktetemperaturen dan volgroeide oliepalmplantages. De veranderingen in biofysische variabelen, energiebalans en energiepartitie tijdens de oliepalmrotatiecyclus kunnen worden verklaard door het eerder geïdentificeerde verdampingskoelingseffect waarbij het albedo-opwarmeffect wordt gecompenseerd. Een belangrijke bepalende factor in dit mechanisme is de vegetatiebedekking tijdens de verschillende fasen in de oliepalmrotatiecyclus. NDVI als een proxy voor vegetatiebedekking vertoonde een consistente inverse relatie met de LST van oliepalmplantages van verschillende leeftijden, een trend die ook wordt waargenomen voor verschillende landgebruikstypen in deze studie.

Een regionale studie en een langere tijdsreeksanalyse van de LST-trend tussen 2000 en 2015 op basis van MODIS-data, toont aan dat de gemiddelde dagtemperatuur van het oppervlak in de Jambi-provincie met 1,05 ºC steeg, een trend die parallel liep met de waargenomen veranderingen in landbedekking en die de effecten van klimaatopwarming overschreed.

Om de volledige klimaateffecten van de uitbreiding van oliepalmplantages te beoordelen, spelen de energiebalans, energiepartitie en biofysische processen een belangrijke rol en moet de volledige rotatiecyclus van oliepalmplantages worden overwogen. Op basis van onze resultaten construeren we de rotatiecyclus van oliepalmplantages en de veranderingen die optreden tijdens de ontwikkeling van oliepalmvegetatie.

Deze studie toont aan dat de uitbreiding van oliepalmplantages en andere gewassen leidt tot veranderingen in biofysische variabelen, opwarming van het landoppervlak en een verhoging van de luchttemperatuur als gevolg van klimaatverandering. Door satellietdata met een hoge resolutie te gebruiken (Landsat), konden we de effecten van veranderingen in landgebruik op biofysische variabelen meerekenen. Inzicht in de effecten van veranderingen in bodembedekking op de biofysische variabelen kan het beleid met betrekking tot het behoud van de bestaande bossen, planning en uitbreiding van de oliepalmplantages en mogelijke bebossingsmaatregelen ondersteunen. Kennis van biofysische variabelen, stralingsbalans en energieverdeling tijdens de rotatiecyclus van oliepalmen kan worden gebruikt om nieuwe beheermethoden op te nemen die de extreme milieu- en micro-klimatologische omstandigheden in de beginfase van oliepalmplantages zouden kunnen verminderen.

List of tables

List of figures

1 Introduction

1.1 Land use change in South East Asia, Indonesia, Sumatra

The extent of forests in Asia and the Pacific has changed dramatically over the past two decades: the area of primary forests decreased, with South-East Asia experiencing the largest decline in the region during the last ten years (Verstraeten et al., 2005). Countries like Cambodia, Indonesia, Myanmar and Papua New Guinea reported large forest losses in the last decade (FAO, 2010).

The main cause for deforestation in these regions is the clearance of forests and the conversion into agricultural land or agro-forestry systems (Nepstad et al., 1999; Achard et al., 2002; Hertel et al., 2009) driven by the continuing expansion of the main tree crops rubber (*Hevea brasiliensis*), coconut (*Cocos nucifera*), oil palm (*Elaeis guineensis*), and coffee (*Coffea sp*.) (Bridhikitti and Overcamp, 2012; Miyamoto, 2006). This occurs especially in countries like Indonesia and Malaysia, where land use changes during the last decades lead to biodiversity loss and greenhouse gas (GHG) emissions due to carbon stock changes in biomass and soil and (peat land) forest fires (Wakker, 2004; Wicke et al., 2008; Wicke et al., 2011).

The expansion of cash crop monocultures such as acacia (timber plantations), rubber, oil palm plantations and smallholder agriculture has drastically reduced the area of primary forest in the last 2.5 decades (Bridhikitti and Overcamp, 2012; Drescher et al., 2016; Marlier et al., 2015; Miettinen et al., 2012; Verstraeten et al., 2005) in Indonesia. This large-scale conversion of rainforest for agricultural use has been observed on the island of Sumatra, which has experienced the highest primary rainforest cover loss in all of Indonesia (Drescher et al., 2016; Margono et al., 2012; Miettinen et al., 2011). Forest cover in the Sumatran provinces of Riau, North Sumatra and Jambi declined from 93 to 38%of provincial area between 1977 and 2009 (Miettinen et al., 2012). These large-scale transformations, observed as land cover change, and land use intensification have led to substantial losses in animal and plant diversity, ecosystem functions and changed microclimatic conditions (Clough et al., 2016; Dislich et al., 2016; Drescher et al., 2016). Additionally, these changes directly alter vegetation cover and structure and land surface properties such as albedo, emissivity and surface roughness, which affect gas and energy exchange processes between the land surface and the atmosphere (Bright et al., 2015).

The expansion of the area of oil palm plantations in Indonesia to meet the domestic and world demand for oil palm (Kongsager and Reenberg, 2012) has occurred at the expense of tropical forests (Koh *et al.* 2011 and Carlson *et al.* 2013). Currently Indonesia has become the world's leading palm oil producer, producing 46% of the world's palm oil in 2009 (Kongsager and Reenberg, 2012) and is ranked number 3 in rubber export (Miyamoto, 2006). As of early 2011, oil palm plantations covered 7.8 million ha in Indonesia, out of which 6.1 million ha were productive plantations under harvest (Obidzinski et al., 2012). In 2010, these plantations produced 22 million tons of crude palm oil (CPO) and the production increased further to 23.6

million tons by the end of 2011 (Obidzinski et al., 2012). Further expansions are planned to meet the growing demand for oil palm (Wicke et al., 2011).

1.2 Land use change and the effects on biophysical variables, energy balance and energy partitioning

Effects of land use and land cover (LULC) conversions are land fragmentation, land degradation, and loss of habitats and biodiversity in different rates, amounts and directions (Evrendilek et al., 2011).
The economic benefits of cash crops, like oil palm, cause land use changes in Indonesia that have effects on ecological and socio-economic functions (Drescher et al., 2016 and Clough et al., 2016). Land use and land cover changes (LULCC) also influence local or regional climate change caused by global alterations of atmospheric carbon dioxide (CO_2) concentrations and albedo (Dale et al., 2011) but studies on the local climatic and microclimatic effects of land use change are scarce.

Replacing natural vegetation with another land cover modifies the surface albedo, which affects the amount of solar radiation that is absorbed or reflected and consequently alters net radiation and local surface energy balance. A lower or higher albedo results in a smaller or greater reflection of shortwave radiation. As a result, the higher or lower amounts of net radiation absorption may increase or decrease the surface temperature and change evapotranspiration (ET) (Mahmood et al., 2014).

Changes in land cover also alter surface emissivity, i.e. the ratio of radiation emitted from a surface to the radiation emitted from an ideal black body at the same temperature following the Stefan–Boltzmann law. Emissivity of vegetated surfaces varies with plant species, density, growth stage, water content and surface roughness (Snyder et al., 1998; Weng et al., 2004). A change of emissivity affects the net radiation because it determines the emission of longwave radiation that contributes to radiative cooling (Mahmood et al., 2014).

Water availability, surface type, soil humidity, local atmospheric and surface conditions affect the energy partitioning into latent (LE), sensible (H) and ground heat (G) fluxes (Mildrexler et al., 2011). Surface roughness affects the transferred sensible and latent heat by regulating vertical mixing of air in the surface layer (van Leeuwen et al., 2011), thereby regulating land surface temperature (LST). Through its association with microclimate, net radiation and energy exchange (Coll et al., 2009; Sobrino et al., 2006; Voogt and Oke, 1998; Weng, 2009; Zhou and Wang, 2011), LST is a major land surface parameter, and as a climatic factor it is regarded to be a main driver of diversity gradients related to the positive relationships between temperature and species richness (Wang et al., 2016).

The replacement of natural vegetation also changes ET (Boisier et al., 2014) and LST because the surface biophysical variables (i.e. surface albedo, LST, emissivity and indirectly leaf area index (LAI) and normalized difference vegetation index (NDVI)) are interconnected through the surface radiation balance. When ET decreases, for example, surface temperatures and

sensible heat fluxes increase; in contrast, when ET increases, the increased LE fluxes lower surface temperatures and decrease H fluxes (Mahmood et al., 2014) under equal net radiation conditions because with a change in vegetation, soil and ecosystem heat flux and net radiation also change due to an alteration of the biophysical variables. Vegetation structure, represented by NDVI, LAI and vegetation height, is in this respect an important determinant of the resistances or conductivities to heat, moisture and momentum transfer between the canopy and the atmosphere (Bright et al., 2015), facilitating the amounts/ratios of sensible heat to water vapor dissipation away from the surface (Hoffmann and Jackson, 2000).

To understand the effects of land cover changes on LST, the associated biophysical variables must be evaluated. This can be done through the surface radiation budget and energy partitioning which unite these biophysical variables directly or indirectly: albedo as direct determinant of the net solar radiation, NDVI as a vegetation parameter determining the emissivity, which in turn determines the amount of reflected and emitted longwave radiation; LST directly affecting the amount of emitted longwave radiation from the surface; and ET, which affects the amount of energy that is used for surface cooling via the evaporation of water.

The effect of land cover change on LST is dependent on the scale, location, direction and type of the change (Longobardi et al., 2016). Several studies showed an LST increase after forest conversion to built-up areas, agricultural land (Zhou and Wang, 2011), crop land and pasture lands (Peng et al., 2014) in China. Similar observations were reported for South American ecosystems: low vegetation such as grasslands in Argentina were warmer than tall tree vegetation (Nosetto et al., 2005). In Brazil, the surface temperature increased after the conversion of natural Cerrado vegetation (a savanna ecosystem) into crop/pasture (Loarie et al., 2011a). Similar effects were also observed for other South American biomes (Salazar et al., 2016). In a global analysis, Li et al. (2015) showed that the cooling of forests is moderate at midlatitudes but northern boreal forests are warmer, an indication that the effect of land cover change on LST varies with the location of the land cover change (Longobardi et al., 2016). Similar studies on the Indonesian islands are lacking but surface temperature increases are expected as an effect of oil palm and cash crop land expansion in the recent decades.

Measuring LST changes is critical for understanding the effects of land cover changes, but challenging. LST can be monitored with LST products retrieved from thermal infrared (TIR) remote sensing data: e.g. the use of the thermal bands of the Moderate Resolution Imaging Spectrometer (MODIS) on board the Terra and Aqua satellite (Sobrino et al., 2008), the thermal band of the Thematic Mapper (TM) on board the LANDSAT-5 platform (Sobrino et al., 2004, 2008) or Enhanced Thematic Mapper (ETMC) on board the LANDSAT-7 platform. The advantage of MODIS data is the availability of readily processed products at high temporal resolution (daily) at medium (250–500 m) to coarse (1000–5000 m) spatial resolution scale; MODIS LST product (MOD11A1/MYD11A1), for example, is provided at a daily temporal resolution with a spatial resolution of 1 km. Landsat data are provided at a higher spatial resolution (30 m), but the temporal resolution is limited to 16 days and the retrieval of LST requires the correction of the satellite-observed radiances for atmospheric absorption and emission (Coll et al., 2009). Besides LST, the connected biophysical variables of the energy

and radiation budget can be derived from the visible and near-infrared (VIS–NIR) bands of MODIS or Landsat, making integrated monitoring of the biophysical variables related to changing land surface possible. In Indonesia, a large proportion of the land use changes is driven by smallholders (Dislich et al., 2016), and thus a combination of Landsat (for a fine spatial resolution) and MODIS (for temporal developments) seems desirable.

1.3 Changes of biophysical variables, energy balance and energy partitioning in a dynamically changing vegetation

Vegetation acts as a modifier of the climate near the ground (Hardwick et al., 2015) and different vegetation types have different effects because of local differences in biophysical variables between forest and oil palm plantations (young and mature) (Sabajo et al., 2017). After forest conversion the new vegetation types that follow after forest removal have biophysical variables that are significantly different than those of the forests they replace (Figure 1), i.e. different albedos, lower normalized difference vegetation index (NDVI), higher land surface temperatures (LST) and lower evapotranspiration (ET).

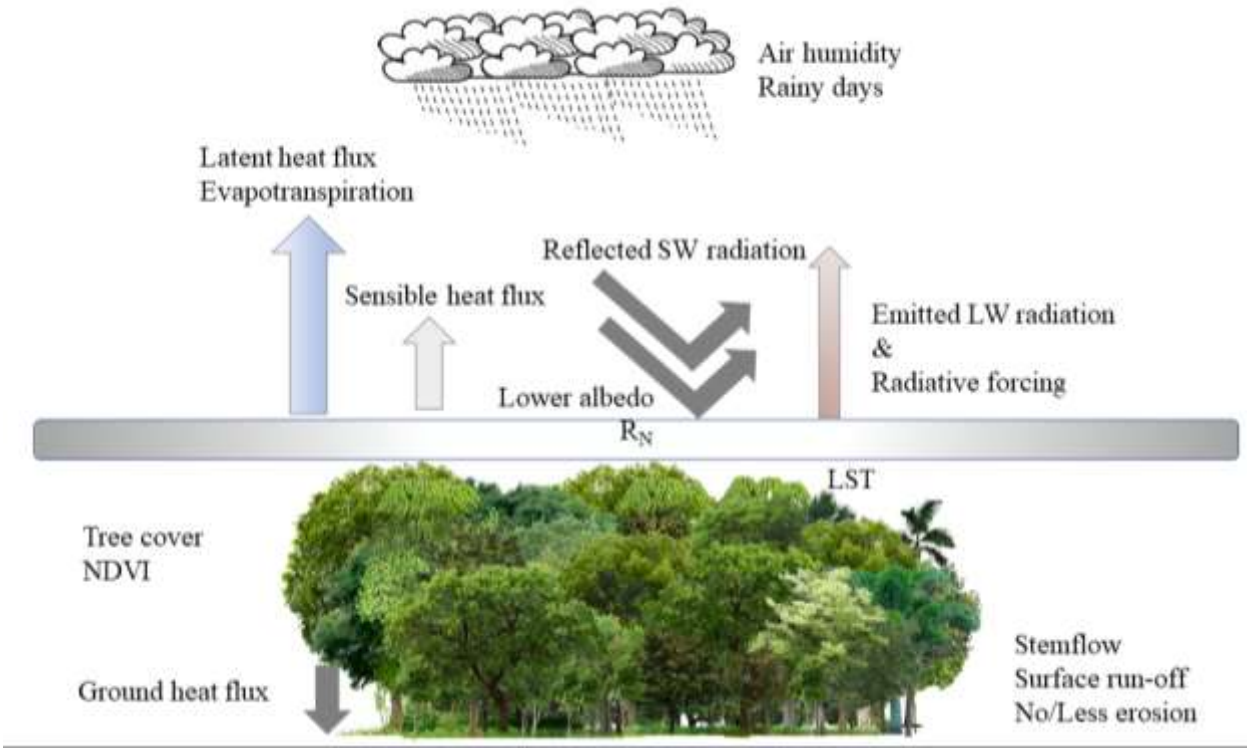

Figure 1. Energy balance and energy partitioning under forest conditions.
Forest conditions are the starting situation in this research.

Modelling studies can provide scenarios on the location and the effects of vegetation cover change on the earth's climatic and hydrological system but few Earth system models consider the effects of land use change and of dynamically changing vegetation (Arneth, 2015) on

climate change. From field observations can be deduced that in a region like Indonesia, establishment of new oil palm plantations is continuously occurring at different scales but the monitoring of the development of oil palm plantations and their associated changes and effects on the local climate and microclimate is limited. Given that an oil palm plantation has a rotation cycle of 20 – 25 years monitoring would also require such an amount of time.

The rotation cycle of an oil palm plantation starts with an initial phase in which the preceding vegetation is clear cut and planted with oil palm seedlings. In this phase the standing biomass is drastically reduced and the land surface is exposed to harsh environmental conditions characterized by high solar radiation input and windy conditions (Luskin and Potts, 2011). This phase is followed by a small unproductive oil palm tree phase (2 – 4 years after planting), followed by a mature tree phase development of 20 – 25 years during which the plantations grow to a closed canopy vegetation with a height of approximately 10 m (Zulkifli et al., 2010) yielding fruit (Corley and Tinker, 2015; Luskin and Potts, 2011) and finally when yield decreases a new rotation period starts in which the old oil palm vegetation is completely cleared and replanted, and the new cycle starts again (Figure 2).

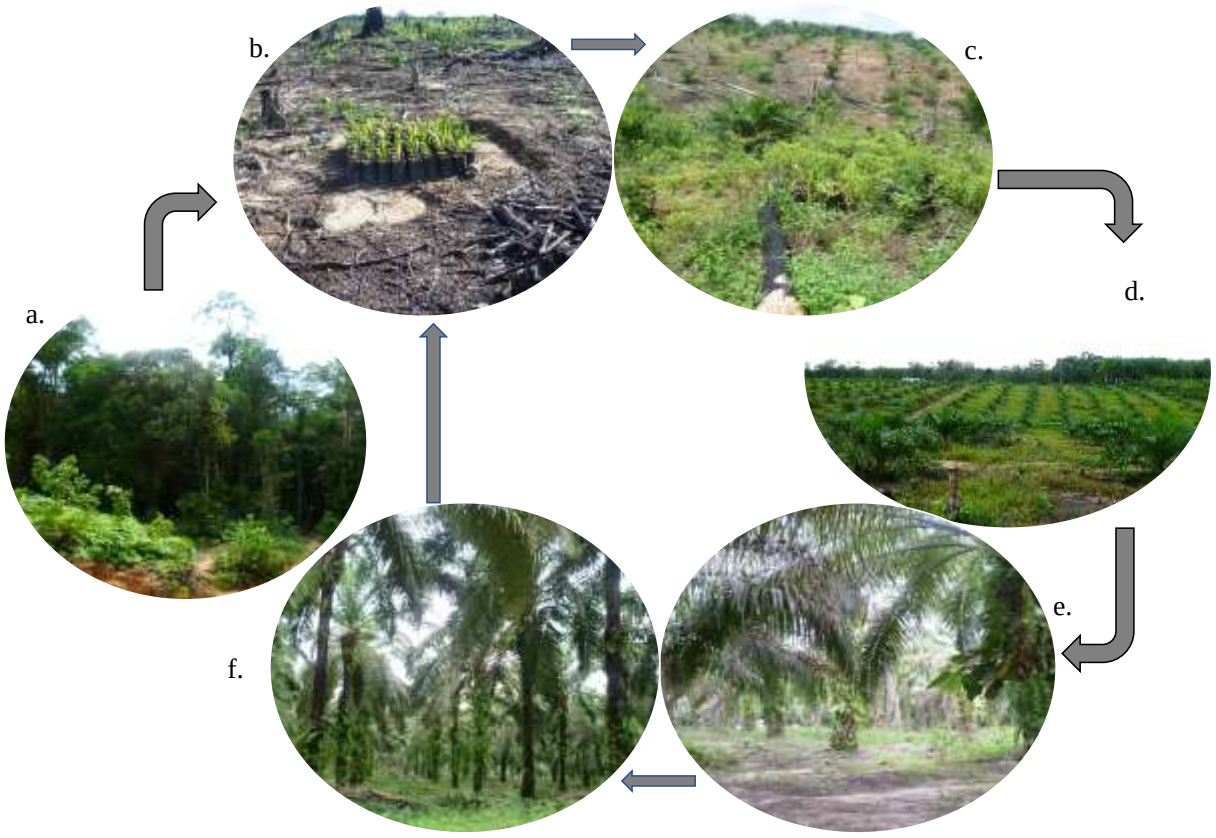

Figure 2. Rotation cycle of oil palm plantation.
Tropical forests (a) are cleared for oil palm establishment. In the initial phase (b, c) the plantation is nearly bare and exposed to large amounts of solar radiation, wind exposure and direct rainfall hit, followed by a young unproductive stage (d) in which the canopy slowly develops but does not produce any fruit. In the productive stage (3 – 4 years after planting) the plantation is productive, the canopy closes and solar radiation, wind speed and direct rainfall on the ground is reduced (e) until the trees become too old and too tall to make economic

harvesting and production possible (f). At the end of the lifecycle the plantation is cleared, new seedlings are planted and the rotation cycle of the oil palm plantation starts again (b).
Photo credits: C.R. Sabajo ©

The microclimatic conditions and the habitat features are different from the preceding vegetation the oil palm plantations replaced (Luskin and Potts, 2011) because land cover, especially the type of vegetation, affects the local and regional climates due to variation in albedo, soil water, surface roughness, plant physiology, the amount of leaf area from which heat can be exchanged, and rooting depth (Bonan, 2008). Oil palm plantations have different surface properties e.g. albedo, emissivity and surface temperature (LST). These surface properties affect the radiation balance by determining the amount of reflected solar radiation and emitted longwave radiation. Albedo for example, affects how much solar radiation is absorbed and reflected, the LST and emissivity determine thermal surface cooling by affecting the amount of longwave radiation that is emitted from the earth's surface. Depending on the net radiation, energy partitioning and feedback mechanisms that come into force, the net effect can be a cooling or warming effect.

From the few biophysical studies that exist on the difference between forest and oil palm plantations we know that there is an the age dependent relationship of the Leaf area index (LAI) of oil palm, i.e. as the oil palm grows older it produces more and larger leaves causing the leaf area to increase with age (Gerritsma & Soebagyo, 1999; Awal & Wan Ishak, 2008). Furthermore, there is a relationship between the LAI and ecologically important microclimatic variables (air temperature, relative humidity, vapor pressure deficit (VPD), specific humidity and soil temperature) in tropical forest and oil palm plantations (Hardwick et al., 2015; Meijide et al., 2018). Significant differences exist between the VPD and air temperature of forest and oil palm vegetation (Luskin & Potts, 2011). Oil palm plantations were 2.8 °C hotter and significantly less humid during the day (Luskin & Potts, 2011) and reach their maximum temperature earlier than old growth forest (Hardwick et al., 2015), maximum air temperature, soil temperature, VPD and specific humidity are largest in oil palm plantations and smallest in primary forest (Hardwick et al., 2015) and within oil palm plantations there are also differences between mature and young oil palm plantations (Sabajo et al., 2017), e.g. younger plantations were hotter and drier than older plantations (Luskin and Potts, 2011; Sabajo et al., 2017).

During the development of the vegetation the albedo decreases, causing a warming effect due to increased solar radiation absorption and the NDVI increases causing a cooling effect due to enhanced evapotranspiration that favors evaporative cooling. These contrasting processes can have a net warming or net cooling effect during the development of the oil palm plantation. Because the evaporative cooling effect is stronger than the albedo warming effect, mature oil palm plantations have lower surface temperatures than young oil palm plantations (Sabajo et al., 2017) as proven with a higher correlation between LST and NDVI and between ET and LST and a low correlation between albedo and LST. Given the dependence of ET on NDVI, a direct analysis between NDVI and LST can also be considered in studying the evaporative cooling effect on the surface temperature.

1.4 Objectives and research problem

The modification of the physical land surface properties influences climate and local microclimatic conditions via biogeochemical and biophysical processes. Therefore, given Indonesia's history of large-scale agricultural land conversion and governmental plans to substantially expand the oil palm production (Wicke et al., 2011), it is important to study the effects of the expansion of cash crop areas on the biophysical environment, especially on LST as a key land surface parameter. We focus on the Jambi province (in Sumatra, Indonesia) as it experienced large land transformation towards oil palm and other cash crops such as rubber plantations in the past, and it may serve as an example of future changes in other regions.

Given the sparsity of studies related to oil palm development and changes to microclimatic conditions, we also study the relation between the age of oil palm plantations and the surface biophysical variables, surface energy balance and energy partitioning.

Our main objective is to quantify the differences in LST across different land cover types and to assess the impact of cash crop expansion on the surface temperature in the Jambi province in the past decades (2000–2015). The aims of this study are:

(1) to evaluate the use of Landsat and MODIS satellite data as sources of a reliable surface temperature estimation in a tropical region with limited satellite data coverage by comparing the surface temperatures retrieved from both satellite sources to each other and against ground observations;
The hypothesis is that from Landsat and MODIS satellite reliable estimates of the LST can be derived for Jambi

(2) to quantify the LST variability across different land cover types;
The hypothesis is that for various landcover types different LST can be distinguished which can be related to the landcover type. We expect vegetated areas to have lower LST than non-vegetated land cover types and between vegetated land cover types different LST can also be distinguished.

(3) to assess the long-term effects of land transformation on the surface temperature against the background of climatic changes;
The hypothesis is that the surface temperature in Jambi has risen as a consequence of the observed concurrent LULCC in the period 2000 -2015.

(4) to identify the mechanisms that explain the surface temperature changes caused by alterations of biophysical variables;
In regulating the LST there are cooling and warming processes active that determine the LST; where the albedo warming effect is dominated by evaporative cooling effect LST will be lower, a process that is dependent on the vegetation cover.

(5) to study the development/relationship between land surface temperature (LST), albedo (α), NDVI, Evapotranspiration (ET), surface radiation balance and energy partitioning during the rotation cycle of oil palm plantations;
We hypothesize that as the oil palm plantation develops there is a consistent dependent relationship between the age of oil palm plantations and the surface biophysical variables, radiation balance and energy partitioning throughout the oil palm rotation cycle.

(6) to study the LST-NDVI-age relation of oil palm plantations;
There is a consistent LST-NDVI-age relationship for oil palm plantations that allows for a direct evaluation of the LST analysis.

We use forests as the vegetation to which we compare the land use types that develop after forest conversion. With the knowledge of the mechanisms on how the biophysical variables shape the local climatic conditions we construct a conceptual figure describing the relation between the dynamically changing vegetation and biophysical variables, radiation balance and energy partitioning in oil palm plantations.

1.5 Research approach

In this research we combine satellite remote sensing and meteorological data sets to estimates of biophysical variables (Jung et al., 2011) such as the albedo, emissivity and land surface temperature for Jambi. We compare the surface temperatures of different land cover types that replace forests (i.e. oil palm, rubber and acacia plantations, clear-cut land and urban areas) by using high-resolution Landsat and medium-resolution MODIS satellite data and discuss the differences by taking into account other biophysical variables such as the albedo, NDVI and ET. Although micrometeorological measurement can provide high quality and continuous data about different site conditions, the spatial coverage of micrometeorological measurements are rather limited and set up and maintenance can be expensive. Satellite data, which provide information on the land surface and land surface properties (e.g. surface temperature and albedo), can therefore serve as an additional source of data or as an alternative to surpass the limitations of micrometeorological measurements.

1.6 Significance of the Study

Remote Sensing can acquire information about the state of the ecosystems which is needed to understand our environment and to support policy makers and scientist with their decision making. The climatic effects of land use change have been been poorly studied in Indonesia and to my knowledge, this is the first study to quantify the effects of land use change on LST in Indonesia and also the first study on the relation between the oil palm plantations and surface biophysical variables, surface energy balance and energy partitioning from remote sensing.

1.7 Outline of the thesis

The study area, data and methodology that was applied in this project is described in chapter 2. In chapter 3 the results are presented, followed by the discussion in chapter 4 and the conclusions in chapter 5.

The *Materials and methods* (Ch. 2) and part of the *results* (i.e. Ch. 3.1, Ch. 3.2 and Ch. 3.7) have been published in:

Sabajo, C. R., le Maire, G., June, T., Meijide, A., Roupsard, O., and Knohl, A.: Expansion of oil palm and other cash crops causes an increase of the land surface temperature in the Jambi province in Indonesia, Biogeosciences, 14, 4619-4635, https://doi.org/10.5194/bg-14-4619-2017, 2017;

and in the the supplement of this article (Supplement of Biogeosciences, 14, 4619–4635, 2017, https://doi.org/10.5194/bg-14-4619-2017-supplement).

The remaining results (Ch. 3.3, Ch 3.4, Ch. 3.5, Ch. 3.6) will be submitted for publication.

2 Materials and methods

2.1 Study area

The study was carried out in the lowlands (approx. 25 000 km^2) of the Jambi province (total area 50 160 km^2) on Sumatra, Indonesia, between latitudes 0°30´S and 2°30´S and longitudes 101°E and 104°30´E (Figure 3). This region has undergone large land transformation towards oil palm and rubber plantations over the past decades and thus may serve as an example of expected changes in other regions of Indonesia (Drescher et al., 2016). The area has a humid tropical climate with a mean annual temperature of 26.7 ± 0.2 °C (1991 – 2011, annual mean ± SD of the annual mean), with little intra-annual variation. Mean annual precipitation was 2235 ± 381 mm and a dry season with less than 120 mm monthly precipitation usually occurred between June and September (Drescher et al., 2016). Previously logged rainforests in the Jambi province have been converted to intensively managed agro-industrial production zones and into smallholder farms to grow cash crops of rubber (*Hevea brasiliensis*) and oil palm (*Elaeis guineensis*) or fast-growing tree species such as *Acacia mangium* for pulp production (Drescher et al., 2016). The area cultivated with oil palm grew faster than the area cultivated with rubber plantations between 1990 and 2011 (Clough et al., 2016).

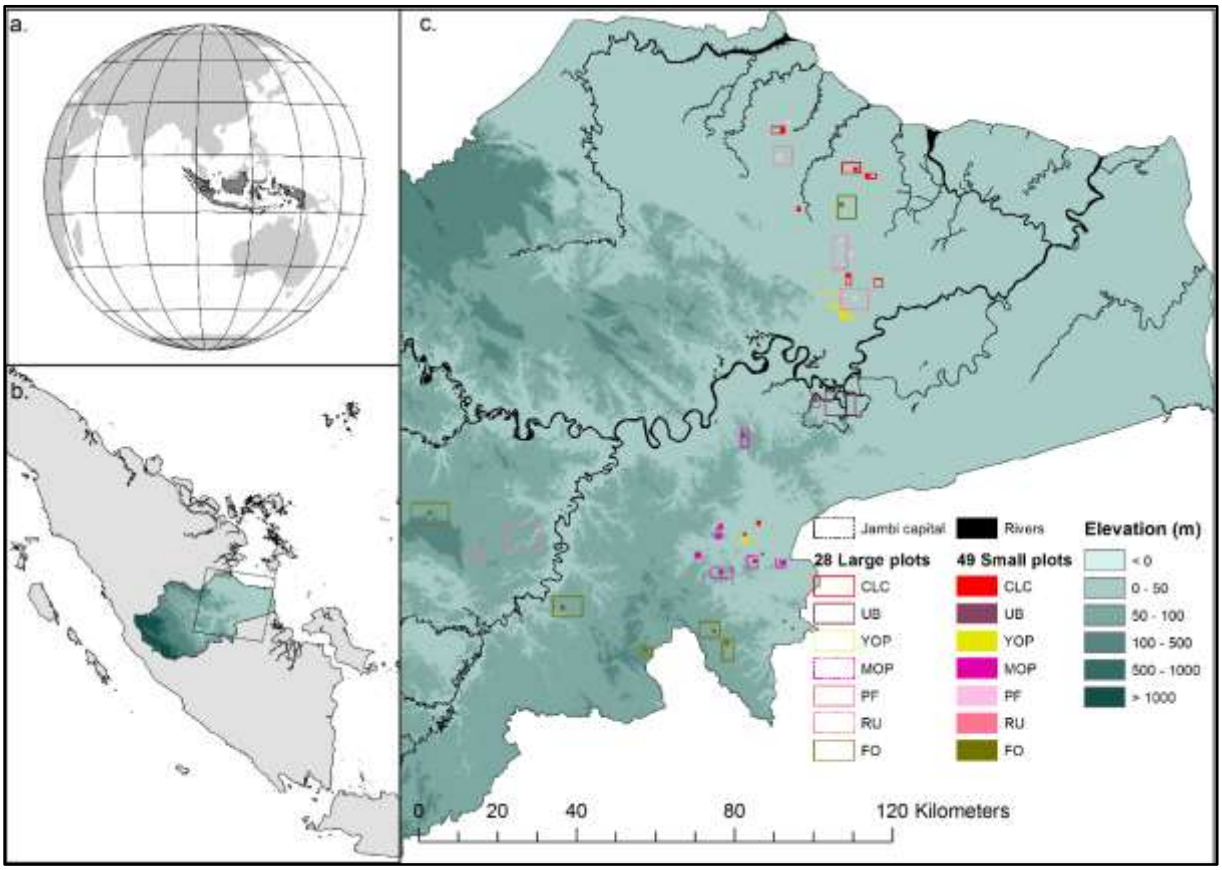

Figure 3. Geographic location of the study area.
Jambi province on the Sumatran Island of Indonesia (a, b). The background of the map (c) is a digital elevation model, showing that the plots are located in the lowlands of the Jambi province. The large rectangles are the 28 different land cover types; the small squares are the locations of the 49 small plots of the 7 different land cover types. The land cover types are abbreviated as:

CLC (clear-cut land), UB (urban area), YOP (young oil palm plantation), MOP (mature oil palm plantation), PF (acacia plantation forest), RU (rubber plantation) and FO (forest).

2.2 Data

2.2.1 Meteorological data

Air temperature and relative air humidity were measured at four reference meteorological stations located in open areas within the study area (Drescher et al., 2016), with thermohygrometers (type 1.1025.55.000, Thies Clima, Göttingen, Germany) placed at 2m height. Measurements were recorded every 15 s and then averaged and stored in a DL16 Pro data logger (Thies Clima, Göttingen, Germany) as 10 min mean, from February 2013 to December 2015. We used the air temperature from the meteorological stations to compare to MODIS air temperatures (MOD07_L2). The relative air humidity was used as an input parameter for NASA's online atmospheric correction (ATCOR) parameter tool to derive parameters to correct Landsat thermal band for atmospheric effects (see Satellite data / Sect. 2.3). We also used air temperature and relative humidity (RH) from two eddy covariance flux towers located in the study area (Meijide et al., 2017): one in a young oil palm plantation (2 years old; S 01°50.127', E 103°17.737') and the other one in a mature oil palm plantation (12 years old; S 01°41.584', E 103°23.484'). At these flux towers, air temperature and relative humidity were measured above the canopy with the same instruments as in the reference meteorological stations (see Meijide et al. (2017), for a description of the methodology). At the flux tower located in the mature oil palm plantation, we also measured the surface canopy temperature between August 2014 and December 2015, which was compared to MODIS LST estimates from the same period. The canopy temperature was measured with two infrared sensors (IR100) connected to a data logger (CR3000), both from Campbell Scientific Inc. (Logan, USA). For a regional coverage we used ERA-Interim daily air temperature grids (http://apps.ecmwf.int/datasets/data/interim-full-daily/levtype=sfc/; Dee et al., 2011) from 2000 –to 2015 at 0.125° resolution to study the annual air temperature trend in this period.

2.2.2 Satellite data

- *Landsat satellite data*

We downloaded three Landsat VIS/TIR 30 m resolution surface reflectance images with low cloud cover, covering the lowland area Jambi (WRS path 125, row 61) which were acquired on different dates: on 19 June 2013 (Landsat 7 ETM+), 27 June 2013 (Landsat 8 OLI) and 25 June 2015 (Landsat 7 ETM+) (Figure 4, e & f). Like all Landsat 7 ETM+ images acquired after 31 May 2003, the images we used were affected by a scan line error causing a data loss of about 22% (http://landsat.usgs.gov/products_slcoffbackground.php).

From these images we derived 10 land surface variables which we grouped in (a) four biophysical variables (land surface temperature (LST, °C), albedo (α, unitless), normalized difference vegetation index (NDVI, unitless) and evapotranspiration (ET, mm hr^{-1})), (b) three

radiation balance variables (reflected shortwave radiation (Sw↑, W m^{-2}), outgoing longwave radiation (Lw↑, W m^{-2}), and net radiation (R_{net}, W m^{-2})), and (c) three energy partitioning variables (ground heat flux (G, W m^{-2}), sensible heat flux (H, W m^{-2}) and latent heat flux (LE, W m^{-2})) (section 2.3.1).

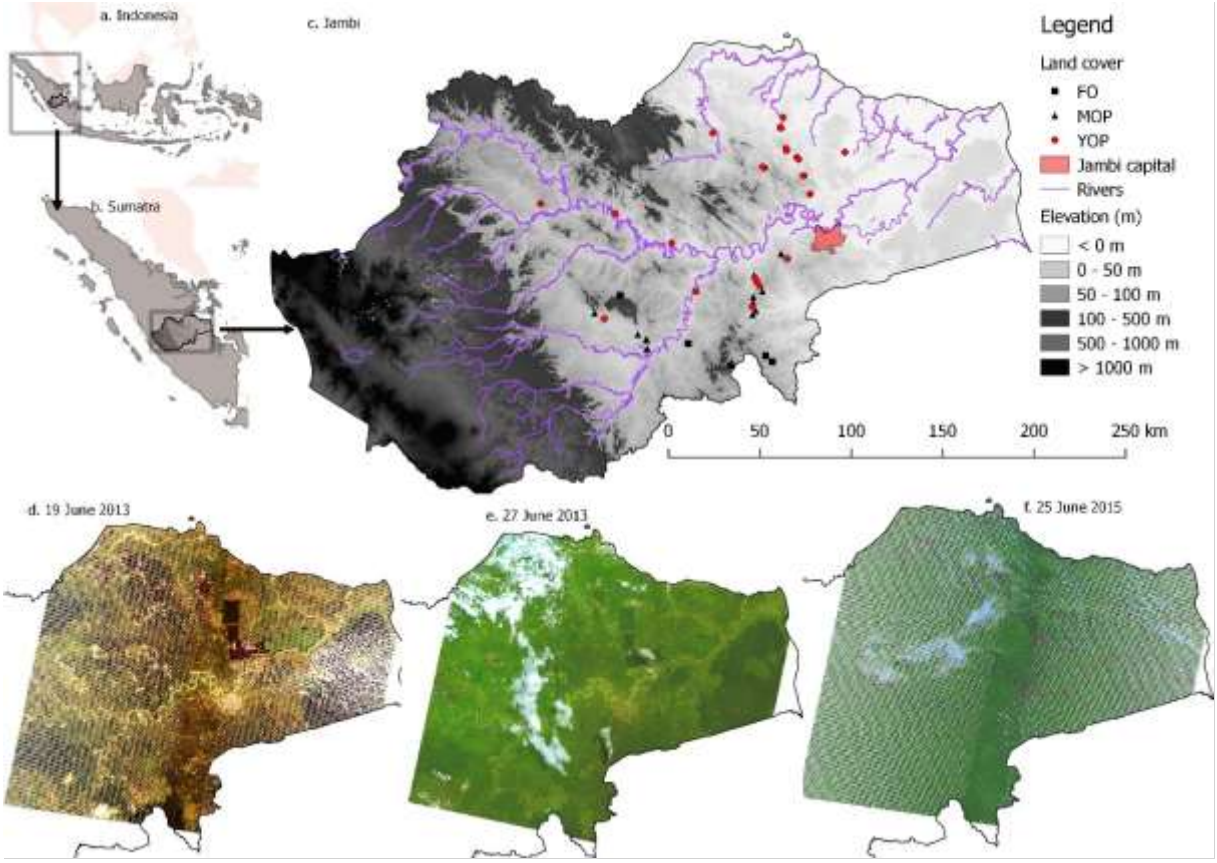

Figure 4. The study region in Jambi on Sumatra, Indonesia
a – c:The study sites are 41 plots: 5 Forest (squares), 12 Mature oil palm plantations (9 – 25 years old, triangles) and 24 young oil palm plantations (< 9 years old, round dots). YOP = young plantation, MOP = mature plantation, FO = Forest. **d – f**: satellite images covering the study area and the respective days on which they were acquired.

- *MODIS satellite data*

We also downloaded the tile h28v09 of the MODIS Terra (MOD) and Aqua (MYD) daily 1km Land Surface Temperature and Emissivity products (MOD11A1 and MYD11A1 Collection 5) and MODIS 16-day 500 m vegetation indices NDVI/EVI product (MOD13A1 Collection 5) from 05 March 2000 to 31 December 2015 for Terra data and from 8 July 2002 to 31 December 2015 for Aqua data. We downloaded other supporting satellite data such as the MODIS Atmospheric Profile product (MOD07_L2) and the MODIS Geolocation product (MOD03). All MODIS data were reprojected to WGS84, UTM zone 48 south with the MODIS Reprojection Tool (MRT). The quality of the MODIS data was examined with the provided quality flags and only pixels with the highest-quality flag were used in the analysis.

2.2.3 Fieldwork data

For this study, we used two data sets of different plot sizes. For the first data set, we delineated 28 large plots (ranging from 4 to 84 km^2) of 7 different land cover types: forest (FO), rubber (RU), acacia plantation forest (PF), young oil palm plantation (YOP), mature oil palm plantation (MOP), urban area (UB) and clear-cut areas (CLC) (Figure 3). The delineation was based on visual interpretation in combination with field observations, which were conducted between October and December 2013. The large size of the plots was necessary to make a comparison between MODIS and Landsat images. For the second data set, we selected 49 smaller plots within and outside these 28 large plots (between 50 m × 50 m and 1000 m × 1000 m) (Figure 3) which allowed us to increase the number of plots to use when analyzing Landsat images. These small plots were used to extract the LST, NDVI, albedo (α) and ET from a high resolution Landsat satellite image (see section satellite data) for the different land cover types of interest.

Most selected plots were located in the center of the image and thus not affected by the data loss; e.g. the forest plots located at the edges of the scan line error zone faced minimal data loss because they were large enough.

Furthermore, we selected 5 forests plots and a chronosequence of 44 oil palm plantations. The age of the oil palm plantations was between 0 and 25 years (survey from 2013): 10 plantations were selected from an ongoing project (CRC-990: Drescher et al. (2016)), 5 plantations were obtained from Niu et al. (2015) and (Röll et al., 2015), 9 plots were obtained from Google Earth (GE TM) and the rest of the plantations were selected during a field survey (October – December 2013) (Table 1). During the survey we asked the age of the oil palm plantation to the owners and recorded the size and location with a GPS-instrument.

For the images acquired on 19 and 27 June 2013 we used the chronosequence surveyed in 2013, for the image acquired on 25 June 2015 we adjusted the age of the oil palm plantations by adding two years to the age of the chronosequence of 2013 (Table 1).

Table 1. Overview of the study sites of the oil palm chronosequence

	Plot	Coordinates	Vegetation (2013)	Age (2013)	Age (2015)	Source
1.	FO1	2°10'17.90"S 103°21'05.00"E	Forest	> 25#	> 25#	Fieldwork 2013
2.	FO2	2°08'44.73"S 103°19'23.66"E	Forest	> 25#	> 25#	Fieldwork 2013
3.	FO3	2°11'17.22"S 103°10'05.52"E	Forest	> 25#	> 25#	Fieldwork 2013
4.	FO4	2°05'31.57"S 102°58'36.85"E	Forest	> 25#	> 25#	Fieldwork 2013
5.	FO5	1°52'33.60"S 102°40'26.54"E	Forest	> 25#	> 25#	Fieldwork 2013
6.	YOP1	1°55'38.50"S 103°15'40.40"E	Young oil palm	3	5	Niu et al. (2015); Röll. et al (2015)
7.	YOP2	1°58'50.00"S 102°36'18.40"E	Young oil palm	5	7	Niu et al. (2015); Röll. et al (2015)
8.	YOP3	1°42'48.03"S 103°25'06.14"E	Young oil palm	2	4	Fieldwork 2013
9.	YOP4	1°48'59.83"S 103°16'57.09"E	Young oil palm	1	3	Fieldwork 2013
10.	YOP5	1°25'33.15"S 103°31'12.83"E	Young oil palm	5	7	Fieldwork 2013
11.	YOP6	1°20'39.03"S 103°29'32.77"E	Young oil palm	2	4	Fieldwork 2013
12.	YOP7	1°20'43.98"S 103°29'24.22"E	Young oil palm	1	3	Fieldwork 2013
13.	YOP8	1°18'35.24"S 103°19'03.78"E	Young oil palm	1	3	Fieldwork 2013
14.	YOP9	1°18'18.82"S 103°18'32.34"E	Young oil palm	1	3	Fieldwork 2013
15.	YOP10	1°09'17.11"S 103°05'13.61"E	Young oil palm	5	7	Fieldwork 2013
16.	YOP11	1°13'53.47"S 103°24'54.25"E	Young oil palm	3	5	Fieldwork 2013
17.	YOP12	1°13'24.81"S 103°24'46.10"E	Young oil palm	5	7	Fieldwork 2013
18.	YOP13	1°05'08.30"S 103°23'59.75"E	Young oil palm	3	5	Fieldwork 2013
19.	YOP14	1°07'51.27"S 103°23'16.57"E	Young oil palm	1	3	Fieldwork 2013
20.	YOP15	1°07'58.53"S 103°23'26.15"E	Young oil palm	2	4	Fieldwork 2013
21.	YOP16	1°15'46.91"S 103°27'41.14"E	Young oil palm	5	7	Fieldwork 2013
22.	YOP17	1°16'13.68"S 103°28'08.17"E	Young oil palm	5	7	Fieldwork 2013
23.	YOP18	1°14'24.24"S 103°40'27.34"E	Young oil palm	5	7	Fieldwork 2013
24.	YOP19	1°38'40.56"S 102°54'11.76"E	Young oil palm	2	4	Fieldwork 2013
25.	YOP20	1°30'40.04"S 102°39'05.62"E	Young oil palm	1	3	Fieldwork 2013
26.	YOP22	1°50'07.62"S 103°17'44.22"E	Young oil palm	1	3	CRC* (Pompa air)
27.	YOP23	1°47'54.71"S 103°16'30.72"E	Young oil palm	3	5	Fieldwork 2013
28.	YOP24	1°51'36.17"S 103°00'48.83"E	Young oil palm	3	5	Fieldwork 2013

Table 1 continued						
	Plot	**Coordinates**	**Vegetation (2013)**	**Age (2013)**	**Age (2015)**	**Source**
29.	YOP25	1°50'49.35"S 103°17'49.70"E	Young oil palm	2	4	Google Earth
30.	YOP26	1°49'33.82"S 103°17'10.71"E	Young oil palm	4	6	Google Earth
31.	YOP27	1°54'23.98"S 103°17'00.68"E	Young oil palm	4	6	Google Earth
32.	YOP28	1°50'54.73"S 103°17'40.98"E	Young oil palm	4	6	Google Earth
33.	YOP29	1°47'03.48"S 103°17'31.79"E	Young oil palm	4	6	Google Earth
34	YOP30	1°48'54.25"S 103°16'36.31"E	Young oil palm	6	8	Google Earth
35.	YOP31	1°47'29.64"S 103°15'44.07"E	Young oil palm	6	8	Google Earth
36.	YOP32	1°46'13.23"S 103°16'32.94"E	Young oil palm	6	8	Google Earth
37.	YOP33	1°45'19.80"S 103°16'57.11"E	Young oil palm	6	8	Google Earth
38.	MOP7	1°57'43.20"S 103°15'30.30"E	Mature oil palm	18	20	Niu et al. (2015); Röll. et al (2015)
39.	MOP8	1°57'22.40"S 102°33'39.90"E	Mature oil palm	22	24	Niu et al. (2015); Röll. et al (2015)
40.	MOP9	1°56'41.50"S 103°16'41.90"E	Mature oil palm	25	27	Niu et al. (2015); Röll. et al (2015)
41.	MOP2	1°41'34.80"S 103°23'27.60"E	Mature oil palm	12	14	CRC* (PTPN6)
42.	MOP15	2°04'32.00"S 102°47'30.70"E	Mature oil palm	13	15	CRC* (BO2)
43.	MOP16	2°04'15.20"S 102°47'30.60"E	Mature oil palm	12	14	CRC* (BO3)
44.	MOP17	2°03'01.50"S 102°45'12.10"E	Mature oil palm	11	13	CRC* (BO4)
45.	MOP10	2°06'48.90"S 102°47'44.50"E	Mature oil palm	9	11	CRC* (BO5)
46.	MOP11	1°54'35.60"S 103°15'58.30"E	Mature oil palm	16	18	CRC* (HO1)
47.	MOP12	1°53'00.70"S 103°16'03.60"E	Mature oil palm	14	16	CRC* (HO2)
48.	MOP13	1°51'28.40"S 103°18'27.40"E	Mature oil palm	17	19	CRC* (HO3)
49.	MOP14	1°47'12.70"S 103°16'14.00"E	Mature oil palm	10	12	CRC* (HO4)

* CRC: CRC-990 Efforts is a research project studying the Ecological and Socioeconomic Functions of Tropical Lowland Rainforest Transformation Systems in Sumatra (Indonesia). For this research we used the plots of the CRC-990 project. PTPN6, Pompa Air, BO2, BO3, BO4, BO5, HO1, HO2, HO3, HO4 are the names of the oil palm plantation plots of the CRC-990 project. #: The age of the forest is unknown, but as they are assumed to be older than the lifecycle of oil palm plantations, a minimum age of 25 years is chosen for comparison purposes.

2.3 Processing and analysis

2.3.1 Retrieval of biophysical variables from Landsat 7 ETM+ VIS/TIR images

2.3.1.1 NDVI

NDVI was derived from the reflectances corrected for atmospheric effects in the red (ρRED, band 3 Landsat 7 ETM+) and near-infrared (ρNIR, band 4 Landsat 7 ETM+) bands, with

$$NDVI = \frac{\rho NIR - \rho RED}{\rho NIR + \rho RED}$$

2.3.1.2 Albedo

The surface albedo (α) was computed with the equation of Liang (2000) for estimating broadband albedo from Landsat surface reflectance bands, with:

$$\alpha = 0.3141\ \rho_1 + 0.1607\ \rho_3 + 0.369\ \rho_4 + 0.1160\ \rho_5 + 0.0456\ \rho_7 - 0.0057$$

where ρ_1, ρ_3, ρ_4, ρ_5 and ρ_7 are the Landsat 7 ETM+ surface reflectance bands (corrected for atmospheric effects).

2.3.1.3 Land surface temperature

- *Comparison MODIS LST to in situ measured canopy LST*

Canopy surface temperature was measured above a homogeneous mature oil palm plantation (12 years old). MODIS LST during 1½ year (mid 2014 – end 2015) was extracted from the pixel covering the location where the *in situ* canopy surface temperature was measured. LST from MODIS on the Terra and Aqua platform were used: Aqua LST in our comparison were measured in the evening hours (around 22:30, local time), Terra LST were measured during morning hours (10:30 am, local time).

- *Comparison MODIS Air temperature with locally measured air temperature*

MODIS air temperatures were extracted from the MODIS Air temperature profile product (MOD07) and compared with in situ measured air temperatures measured at a young oil palm plantation (2 years), an urban area and an open field (surrounded by forest) where the meteorological towers in Jambi were located.

- *Atmospheric correction of the thermal band*

For the atmospheric correction of the thermal radiance we used a Web-based Atmospheric parameter Correction Tool that has been developed for TM and ETM+ thermal data (Barsi et al., 2005; Coll et al., 2010). It uses atmospheric profiles from the National Centers for Environmental Prediction (NCEP) interpolated to a particular location, date and time, and the MODTRAN-4 code to calculate the atmospheric-correction parameters for the bandpass of either the TM or ETM+ thermal band for a given date and site (Coll et al., 2010).
The correction parameters τ, Rp and Rsky are derived from NASA's online atmospheric correction calculator (Barsi et al., 2003, 2005) which requires the following input: latitude and longitude, elevation, air temperature, surface pressure and relative air humidity.

The output of the online atmospheric parameter calculator is: band average atmospheric transmission (τ), effective bandpass upwelling radiance (Rp) and the effective bandpass downwelling radiance (Rsky). The calculated atmospheric parameters can be applied to a given scene to retrieve the surface temperature for the area of interest. The thermal band (L6) is corrected for atmospheric effects after Wukelic et al. (1989) and Coll et al. (2010) as:

$$\mathrm{Rc} = \frac{\mathrm{L6} - \mathrm{Rp}}{\tau} - (1 - \varepsilon\mathrm{NB})\mathrm{Rsky}$$

The input data required for the atmospheric calculator and the output parameters required for atmospheric correction and applied to the selected Landsat satellite image are summarized in Table 2.

Table 2. Input and output parameters for/from NASA's online atmospheric correction parameter calculator applied to two satellite images of the study area.

Location	**Date (yyyy-mm-dd):**	**2013-06-19**
Input	Lat	-1.966
	Lon	102.601
	GMT Time:	3:13
Input surface conditions	Surface altitude (km):	0.046
	Surface pressure (mb):	1002.90
	Surface air temperature (C):	28.35
	Surface relative humidity (%):	50.90
Output summary	Band average atmospheric transmission:	0.67
	Effective bandpass upwelling radiance:	2.68
	Effective bandpass downwelling radiance:	4.25

Band average atmospheric transmission = τ, effective bandpass upwelling radiance = Rp ($W/m^2/sr/\mu m$), effective bandpass downwelling radiance = Rsky ($W/m^2/sr/\mu m$).

- *LST retrieval from Landsat*

LST was derived following the method proposed by Bastiaanssen (2000), Bastiaanssen et al. (1998a), Coll et al. (2010) and Wukelic et al. (1989) for computing the surface temperature from the TIR band (band 6) of Landsat (Table 3). The TIR band was first converted to thermal radiance (L6, W $m^{-2}sr^{-1}\mu m^{-1}$) and then to atmospherically corrected thermal radiance (Rc, W $m^{-2}sr^{-1}\mu m^{-1}$) as described by Wukelic et al. (1989) and Coll et al. (2010), and with the atmospheric parameters obtained on NASA's online Atmospheric Correction Calculator (Barsi et al., 2003, 2005). The surface temperature (LST, K) was computed with the following equation similar to the Planck equation, as in Coll et al. (2010) and Wukelic et al. (1989):

$$\mathrm{LST} = \frac{\mathrm{k2}}{\ln\left(\frac{\varepsilon \mathrm{NB} \cdot \mathrm{k1}}{\mathrm{Rc}} + 1\right)}$$

where εNB is the emissivity of the surface obtained from the NDVI (Table 3), k1 (= 666.09 mW cm^{-2} sr^{-1} μm^{-1}) and k2 (= 1282.71 K) are sensor constants for converting the thermal radiance obtained from band 6 of Landsat 7 to surface temperature.
The surface temperature derived from Landsat thermal band was compared with the MODIS LST product that was acquired on the same day at 10:30 am local time. The Landsat LST image was first resampled to MODIS resolution to enable a pixel-to-pixel comparison, followed by extracting the average LST of 7 land cover types with the data set containing the large delineated plots (Figure 3).

Surface temperature from Landsat ETM+ is derived in a series in steps using the red (R), near-infrared (NIR) and thermal infrared (TIR) band, and follows the method described by Bastiaanssen et al. (1998a, 1998b) and summarized in Table 3.

Table 3. Steps in the retrieval of the surface temperature from Landsat 7 TIR band

Computation step	**Symbol**	**Unit**	**Formulation**
1. Conversion of the digital number (DN) of the VIS and TIR bands to spectral radiance	L_λ	W $m^{-2}sr^{-1}\mu m^{-1}$	$L_\lambda = \frac{LMAX - LMIN}{QCALMAX - QCALMIN} \times (DN - QCALMIN) + LMIN$
2. Conversion of spectral radiance bands to reflectance[#] (λ = 1, 2, 3, 4, 5, 6, 7)	ρ_λ	-	$\rho_\lambda = \frac{\pi \times L_\lambda}{ESUN_\lambda \times cos\theta \times d_r}$
3. Normalized Difference Vegetation Index	NDVI	-	$NDVI = \frac{\rho 4 - \rho 3}{\rho 4 + \rho 3}$
4. Soil Adjusted Vegetation Index	SAVI	-	$SAVI = \frac{(1 + L)(\rho 4 - \rho 3)}{(L + \rho 4 + \rho 3)}$
5. Transformed SAVI to pseudo-LAI[§]	SAVI"	-	$SAVI'' = \frac{-\ln\left(\frac{0.69 - SAVI}{0.59}\right)}{0.91}$
6. Narrowband emissivity	εNB	-	$\varepsilon NB = 0.97 + 0.0033\ SAVI''$; $SAVI'' < 3$ (a) $\varepsilon NB = 0.98$; $SAVI'' \geq 3$ (b)
7. Broadband emissivity	$\varepsilon 0$	-	$\varepsilon 0 = 0.95 + 0.01\ SAVI''$; $SAVI'' < 3$ (a) $\varepsilon 0 = 0.98$; $SAVI'' \geq 3$ (b)
8. Atmospheric correction of the thermal radiance band	Rc	W $m^{-2}sr^{-1}\mu m^{-1}$	$Rc = \frac{L6 - Rp}{\tau NB} - (1 - \varepsilon NB)Rsky$
9. Surface temperature calculation	LST	K	$LST = \frac{k2}{\ln\left(\frac{\varepsilon NB \times k1}{Rc} + 1\right)}$

Where:

DN	the digital number of each pixel of band λ	W $m^{-2}sr^{-1}\mu m^{-1}$
LMAX	calibration constant specific for each Landsat sensor (see Table 4)	W $m^{-2}sr^{-1}\mu m^{-1}$
LMIN		
QCALMAX	highest and lowest range values for rescaled radiance in DN (see Table 4)	W $m^{-2}sr^{-1}\mu m^{-1}$
QCALMIN		
$ESUN_\lambda$	the mean solar exo-atmospheric irradiance for each band (see Table 5)	W $m^{-2}\mu m^{-1}$
θ (θ = 90º- β)	solar incidence angle	angular degrees
β	sun elevation from meta data satellite image	angular degrees
d_r	the relative distance between earth and sun $d_r = 1 + 0.033 \cos (DOY \frac{2\pi}{365})$	-
DOY	the sequential time of the year The unit of the angle ($DOY \times \frac{2\pi}{365}$) is in radians.	-
ρ_4	surface reflectance of band 4 (NIR, 750 – 900 nm)	-
ρ_3	surface reflectance of band 3 (VIS Red, 630 – 690 nm)	-
L	adjustment factor to minimize the backscatter effect of soil background reflectance through the canopy (0.1)	-
τNB	band average atmospheric transmittance	-
Rp	effective bandpass upwelling radiance (or Path radiance)	W $m^{-2}sr^{-1}\mu m^{-1}$
Rsky	effective bandpass downwelling radiance	W $m^{-2}sr^{-1}\mu m^{-1}$
k1 (= 666.09)	sensor constants for converting band 6 to surface temperature	mW cm^{-2} sr^{-1} μm^{-1} K
k2 (= 1282.71)		

#: when using Landsat surface reflectance product, this step is not necessary. §The transformed SAVI is considered here to be equal to the LAI.

References: 4: Huete (1988); 5: Bulcock and Jewitt (2010); 6, 7: Bastiaanssen et al. (1998a, 1998b); 8: Wukelic et al. (1989); Coll et al. (2010).

Table 4. LMIN and LMAX values for Landsat 7 ETM+ (Landsat 7 Science User Data Handbook Chap. 11, 2002) in units W m^{-2} sr^{-1} μm^{-1} (after July 1, 2000)

	Band number	**1**	**2**	**3**	**4**	**5**	**6**	**7**	**8**
Low gain	LMAX	293,7	300,9	234,4	241,1	47,57	17,04	16,54	243,1
	LMIN	-6,2	-6,4	-5	-5,1	-1	0	-0,35	-4,7
High gain	LMAX	191,6	196,5	152,9	157,4	31,06	12,65	10,8	158,3
	LMIN	-6,2	-6,4	-5	-5,1	-1	3,2	-0,35	-4,7
	QCALMAX	255	255	255	255	255	255	255	255
	QCALMIN	1	1	1	1	1	1	1	1

Table 5. Mean solar exo-atmospheric irradiance (ESUNλ) for Landsat 7 ETM+ (Landsat 7 Science User Data Handbook, Chapter 11, 2002). Units are in W m^{-2} μm^{-1}.

	Band 1	Band 2	Band 3	Band 4	Band 5	Band 61	Band 62	Band 7
Landsat 7	1969	1840	1551	1044	225.7	1	1	82.07

- *Statistical analysis of Landsat LST retrieval*

For a comparison of the Landsat-derived LST and the MODIS LST we analyzed the statistical relationships with the coefficient of determination (R^2), the root mean square error (RMSE), the mean absolute error (MAE) and the bias:

$$\text{RMSE} = \sqrt{\frac{\sum_{i=1}^{N}(E_i - O_i)^2}{N}}$$

$$\text{Bias} = \frac{\sum_{i=1}^{N}(E_i - O_i)}{N}$$

$$\text{MAE} = \frac{\sum_{i=1}^{N}|E_i - O_i|}{N}$$

Where O_i is MODIS LST, E_i is the Landsat surface temperature and N is the number of pixels compared. Model type 2 linear regression was applied for fitting the relation between MODIS LST and Landsat LST.
We tested the relation between the biophysical variables LST (or L6 and Rc, both as pre- or intermediate products before obtaining LST), albedo (α), NDVI and ET with a correlation analysis and a multiple linear regression was applied to analyze the effects of the biophysical variables on the LST. We used the model: LST (or Rc or L6) ~ α + NDVI + ET, and used R^2 and standardized β coefficients to evaluate the strength of the biophysical variables in predicting the LST.

2.3.1.4 Evapotranspiration

We estimated ET (mm hr^{-1}) from latent heat fluxes (LE, W m^{-2}) with the Surface Energy Balance Algorithm for Land (SEBAL) (Bastiaanssen, 2000; Bastiaanssen et al., 1998a, 1998b), which were computed as the residual from sensible (W m^{-2}) and ground (W m^{-2}) heat fluxes subtracted from net radiation (Rn, W m^{-2}) as:

$$LE = Rn - G - H$$

We calculated Rn as the sum of incoming shortwave and longwave radiation, minus the reflected shortwave and longwave radiation and the emitted longwave radiation. The surface albedo, surface emissivity and surface temperature determine the amounts of incoming and reflected radiation:

$$Rn = (1 - \alpha)\, S_d\downarrow + \varepsilon_a \sigma T_a^4 - (1 - \varepsilon_0)\varepsilon_a \sigma T_a^4 - \varepsilon_0 \sigma LST^4$$

Rn is the net radiation (W m^{-2});
$S_d\downarrow$ is the incoming shortwave solar radiation (in W m^{-2}) at the surface;
α is the surface albedo (-)
ε_0: the surface emissivity (-), derived from the NDVI and is described in Table 3.
ε_a: the atmospheric emissivity (-), estimated with:

Where $S_d\downarrow$ is the incoming shortwave solar radiation (W m^{-2}) at the surface, α is the surface albedo, ε_0 is the surface emissivity (-), ε_a is the atmospheric emissivity (-), σ is the Stephan-Boltzmann constant (5.67×10^{-8} W m^{-2} K^{-4}), LST is the surface temperature (K) and T_a is the sky temperature (K). The average atmospheric emissivity (ε_a) is estimated with the model of Idso and Jackson (1969):

$$\varepsilon_a = 1 - 0.26 \times \exp\left((-7.77 \times 10^{-4}) \times (273.15 - T_a)^2\right)$$

σ: Stephan-Boltzmann constant (5.67×10^{-8} W m^{-2} K^{-4});
LST: the surface temperature (K) derived from Landsat;
T_a: is the (near surface) air temperature / sky temperature (K).

Ground heat fluxes (W m^{-2}) were derived as a fraction of Rn from an empirical relationship between LST, α, and NDVI (Bastiaanssen, 2000) as:

$$G = Rn \times \frac{LST - 273.15}{\alpha} \times (0.0038\alpha + 0.0074\alpha^2) \times (1 - 0.98NDVI^4)$$

G is the ground heat flux (W m^{-2});
Rn is the net radiation (W m^{-2});
LST: the surface temperature (K) derived from Landsat;
α is the surface albedo (-)

In SEBAL Sensible heat flux (W m^{-2}) was calculated as:

$$H = \rho Cp \frac{\Delta T}{r_{ah}} = \rho Cp \frac{a\, LST + b}{r_{ah}}$$

Where ρ is the air density (1.16 kg m^{-3}); Cp is the specific heat of air at constant pressure (1004 J kg^{-1} K^{-1}); r_{ah} is the aerodynamic resistance to heat transport (s m^{-1}); *a* and *b* are regression coefficients, which are determined by a hot extreme pixel (where LE = 0 and H is maximum) and a cold extreme pixel (where H = 0 and LE is maximum). The aerodynamic resistance to heat transport, r_{ah}, is calculated through an iterative process with air temperature measured at 2 m as input. SEBAL is described in Bastiaanssen (2000) and Bastiaanssen et al. (1998a, b).

Sensible heat flux (H, W m^{-2}) is calculated in a series of steps as:

a. z_{0m} (the particular momentum roughness length for each pixel) is derived from an empirical relation between z_{0m} and NDVI and albedo as

$$z_{0m} = e^{\left(a \times \frac{NDVI}{\alpha}\right)+b}$$

coefficients *a* and *b* are derived from the linear relation between:

$$\ln z_{0m} \sim a \times \frac{NDVI}{\alpha} + b$$

b. friction velocity (u*, m s^{-1}) at weather station ($u_{200,}$ m s^{-1}) is derived as:

$$u^* = \frac{k \times u_z}{ln\left(\frac{z}{z_{0m}}\right)}$$

c. the wind speed 200 m above the weather station ($u_{200,}$ m s^{-1}) is derived as:

$$u_{200} = u^* \frac{ln\left(\frac{200}{z_{0m}}\right)}{k}$$

k = von Karman's constant = 0.41

c. The aerodynamic resistance to heat transport r_{ah} (s m^{-1}) is calculated as:

$$r_{ah} = \frac{ln\left(\frac{z_2}{z_1}\right)}{u^* \times k}$$

d. the near surface temperature difference (dT) for each pixel is defined as:

dT = b + a LST

a and *b* are correlation coefficients which are derived by:
i. selecting hot and cold pixels (a.k.a. anchor pixels) in the LST image
ii. using an excel sheet the coefficients *a* and *b* are derived from several iterations

e. finally sensible heat (H) is estimated as:

$$H = \rho \times Cp \frac{a\ LST + b}{r_{ah}}$$

r_{ah} = aerodynamic resistance to heat transport r_{ah} (s m^{-1})
ρ = 1.16 kg m^{-3} (air density)
Cp = 1004 J kg^{-1} K^{-1} (air specific heat)

Latent heat flux (LE, W m^{-2}) is estimated as residual from Net radiation, Ground heat and sensible heat flux as:

$LE = Rn - G - H$

Instantaneous evapotranspiration (ET, mm hr^{-1}) for each pixel is estimated from LE as:

$$ET_{inst} = 3600 \frac{LE}{\lambda}$$

3600 is the time conversion from seconds to hours
λ = latent heat of vaporization (2.43×10^6 J kg^{-1})

The technical description can be found in Bastiaanssen et al. (1998a, 1998b).

2.4 Local short-term differences between different land cover types

From the created LST, NDVI, albedo and ET images we extracted the average values of the different land cover classes with the data set containing the small 49 delineated plots covering 7 different land cover types (Figure 3). The average effect of land transformation, i.e. the change from forest to another non-forest land cover type, on the surface temperature was evaluated as (see Li et al. (2015)):

$\Delta LST = LST_{non\text{-}forest} - LST_{forest}$

A negative ΔLST indicates a cooling effect and positive ΔLST indicates a warming effect of the non-forest vegetation compared with forest. The same procedure was applied in evaluating the effect of land transformation on the NDVI, albedo and ET.

The standard deviation of 2 means is calculated as the 'pooled standard deviation':

$$sd = \sqrt{\frac{(n1-1)sd1^2 + (n2-1)sd2^2}{n1+n2-2}}$$

n1: sample size population 1 (here: the number of pixels of land cover class Forest, FO)
n2: sample size population 2 (here: the number of pixels of land cover class *i* (*i* = RU, MOP, PF, YOP, CLC, UB)
sd1: standard deviation of the mean of the first population (here: Forest, FO)
sd2: standard deviation of the mean of the second population *i* (*i* = RU, MOP, PF, YOP, CLC, UB)

2.5 Relation between oil palm plantation development and biophysical variables, energy balance and energy partitioning

From the created images we extracted the average values of the different oil palm plantations. We used the average values calculated for forests as a reference and calculated the difference between the oil palm plantations and forest as:

$$\Delta_{var(\,i)} = Var(i)_{\text{oil palm}(j)} - Var(i)_{\text{forest}}$$

with

$Var(i)$ = {LST, α, NDVI, ET, Sw↑, Lw↑, RN, G, H, LE}
and

j = the age of the oil palm plantation = {0, … , 25}

The relation between the $\Delta_{var\,i}$ and age was quantified by a n-order GLM-function (n = 1,2,3, or 4), where the best fit-model was selected with the Akaike's information criterion (AIC) and an ANOVA analysis of the GL models.

To test the suitability of NDVI as a simple measure for vegetation development and changing biophysical variables we quantified the relation between LST ~ albedo + NDVI with a GLM.

2.6 Large scale and long term effects of land cover change on the surface temperature in Jambi

To analyze the long-term effects on the provincial scale we used the MODIS daily LST time series (MOD11A1 and MYD11A1) from 2000 to 2015. MOD11A1 provides LST for 10:30 and 22:30 and we used the times series between 2000 and 2015. MYD11A1 provides LST for 1:30 and 13:30 and is available from 8 July 2002; we used complete years in our analysis and therefore used the MYD11A1 time series from 2003 to 2015. We calculated the mean annual LST at four different times of the day (10:30 , 13:30, 22:30 and 1:30) between 2000 and 2015 for the lowland of Jambi from the MODIS daily LST time series (MOD11A1 and MYD11A1). First, we calculated for each pixel the average LST pixel value using only the best-quality pixels for every year. Then, from these pixels we made a composite image (n = 16, one for each year) for the province. Finally, from each composite image we calculated the mean annual lowland provincial temperature as the average of all the pixels that are enclosed by a zone delineating the lowland of the Jambi province. We performed the same analysis with the MODIS 16-day NDVI product (2000 – 2015) and the ERA daily temperature grid (2000 – 2015) to compare the annual trends of LST, NDVI and air temperature of the province. The average provincial LST and NDVI were compared with the mean LST and NDVI of a selected forest that remained undisturbed forest during the 2000 – 2015 period.

3 Results

3.1 Retrieval of biophysical variables from Landsat 7 ETM+ VIS/TIR images

3.1.1 Land surface temperature

- *Comparison of MODIS LST to in situ measured canopy LST*

Both in situ and MODIS observations are consistent, i.e. the morning temperatures (10:30 am local time vs Terra LST) were warmer than the evening temperatures (10:30 pm local time vs Aqua LST) (Figure 5). Measured canopy surface temperatures were higher compared to MODIS LST. The differences between the two sources are caused by the comparison of point measurements with pixel values, differences in spatial resolution, differences in soil contribution to the LST estimate, distance in LST measurements and particularly differences in emissivity used for temperature correction. The thermal infrared sensor measuring the surface canopy temperature of the oil palm plantation had fixed default values. MODIS emissivity is derived from 3 thermal bands and adjusted accordingly for every measurement.

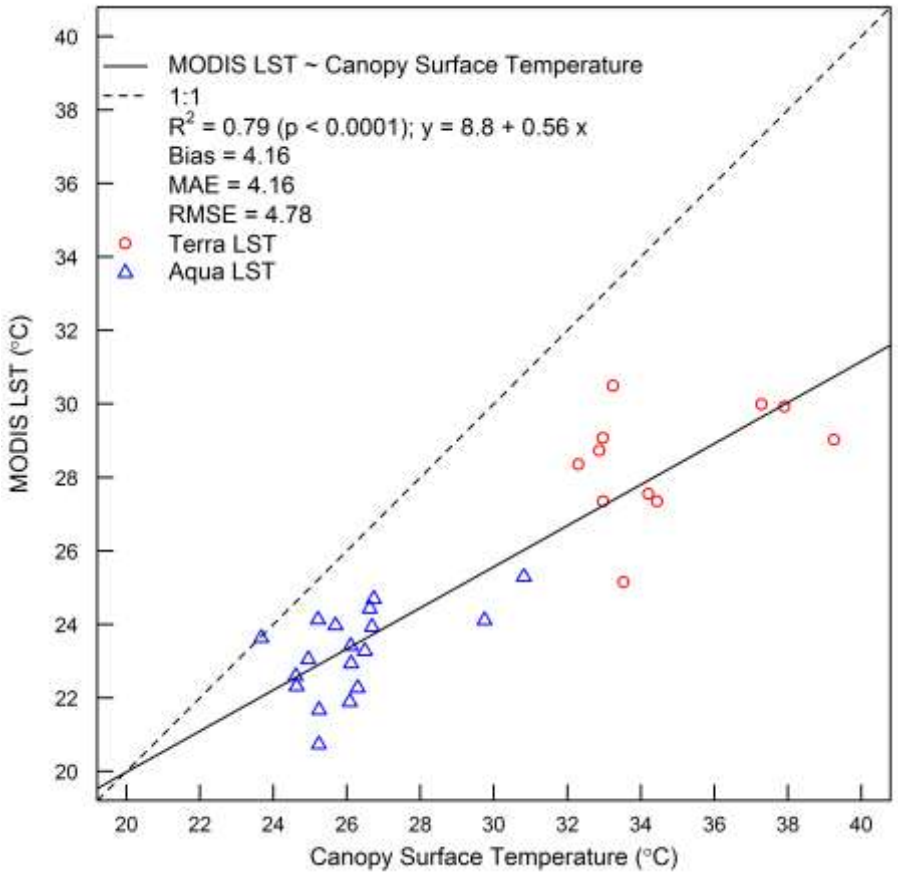

Figure 5. MODIS LST compared to in situ measured canopy surface temperature.

- *Comparison of MODIS Air temperature with locally measured air temperature*

Both in situ and MODIS observations are consistent, i.e. the morning temperatures (10:30 am, local time) were warmer than the evening temperatures (10:30 pm, local time) (Figure 6). Young oil palm plantations and urban areas have the highest air temperature during the day: both measured and observed by MODIS. Differences between the two sources are caused by the comparison of point measurements with pixel values, differences in spatial resolution and distance in LST measurements.

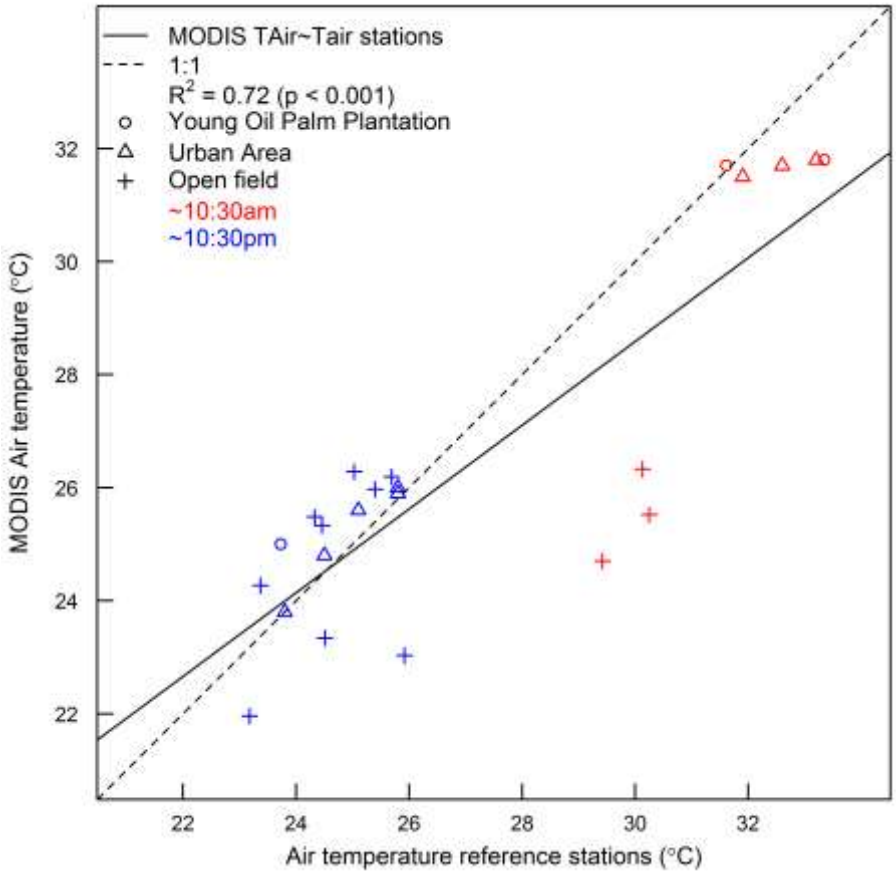

Figure 6. MODIS Air temperature compared with in situ measured air temperatures

- *Evaluating the use of Landsat and MODIS satellite data for surface temperature retrieval*

Landsat and MODIS images showed similar spatial LST patterns (Figure 7). In both images the relatively hot areas (red) correspond to the known clear-cut areas, urban areas or other sparsely vegetated areas, the relatively cool areas (blue) correspond to vegetated areas such as forest, plantation forests and mature oil palm plantations. The coarse-resolution scale of MODIS (1000 m for LST) allows a large regional coverage of the study area but does not allow to retrieve detailed information on small patches (smaller than 1 km^2). In contrast, the Landsat 7 image allows a detailed study of patches that are small enough (as small as 30 x 30 m^2) but it is affected

by the scan line error causing data loss at the edges of the image. In both MODIS and Landsat images clouds and cloud shadows were removed and therefore lead to data gaps in the images.

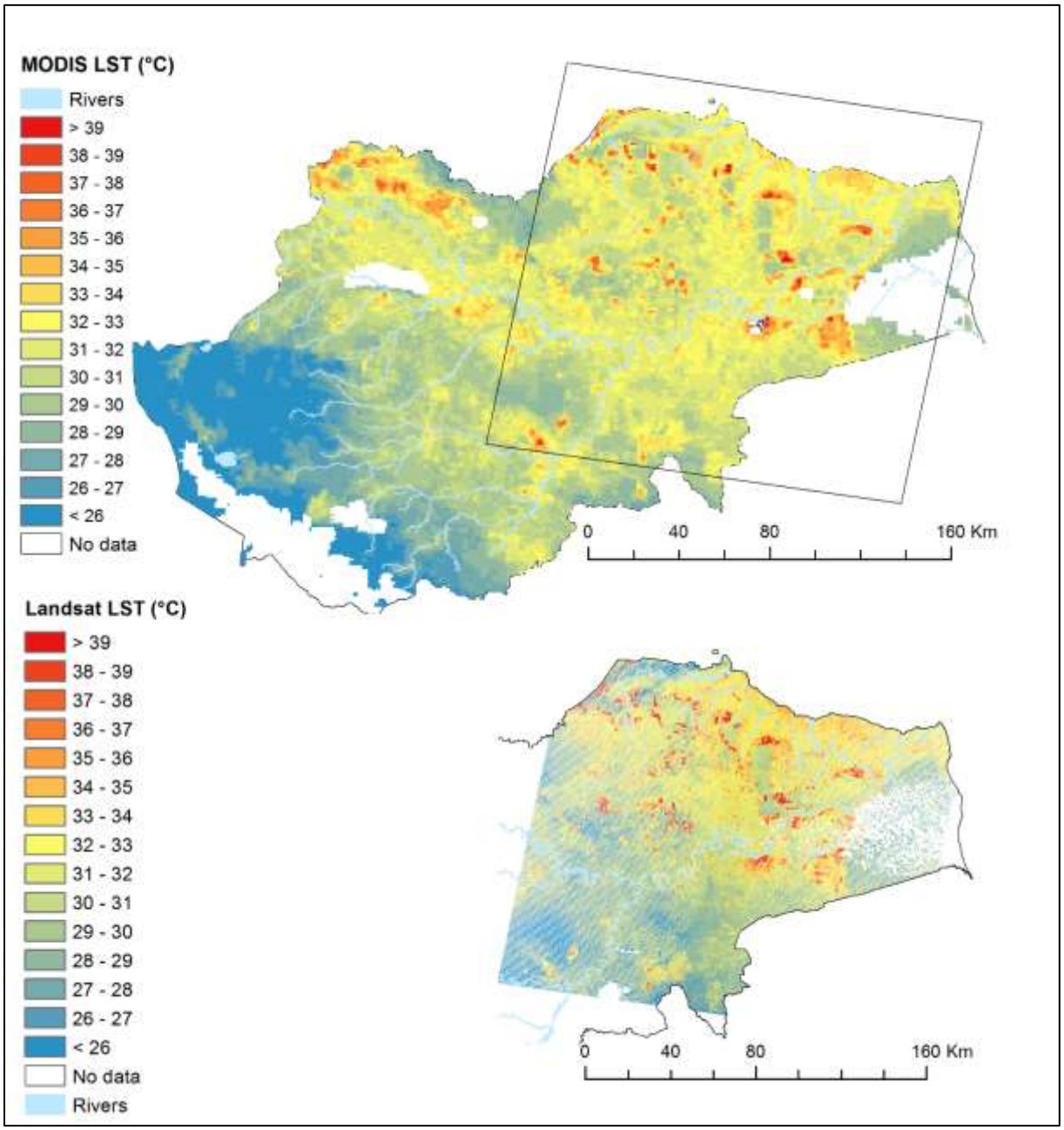

Figure 7. MODIS LST image (**a**) compared with Landsat LST image (**b**).
Cloud cover and cloud shadow cover resulted in data gaps (no data). The difference in acquisition time between the images is 15 minutes. The square in the MODIS image is the area that is covered by the Landsat tile (path 125, row 61). Both satellite images were acquired on 19 June 2013.

Landsat-derived LST correlated well with MODIS LST ($R^2 = 0.82$; $p < 0.001$;Figure 8) with a RMSE of 1.8 ºC. The seven land cover types had distinctive LSTs and the observed differences between these land cover types were consistent in both images. The non-vegetated surfaces (CLC and UB) had higher surface temperatures than the vegetated surface types (FO, YOP, MOP, PF and RU). Clear-cut land had the highest surface temperature of all compared land

cover types, followed by urban areas, whereas the vegetated land cover types had lower surface temperatures: LST_{CLC} (39.7 ± 2.0 °C) > LST_{UB} (35.8 ± 1.3 °C) > LST_{YOP} (31.0 ± 0.7 °C) > LST_{PF} (30.3 ± 0.7 °C) > LST_{MOP} (29.0 ± 0.8 °C) > LST_{RU} (27.8 ± 0.9 °C) > LST_{FO} (27.6 ± 1.4 °C) (Landsat LST, Fig. 3). The same trend was derived from the MODIS image but with higher surface temperatures, except for CLC: LST_{CLC} (37.7 ± 1.8 ºC) > LST_{UB} (36.3 ± 1.6 °C) > LST_{YOP} (31.7 ± 0.9 ºC) > LST_{MOP} (30.7 ± 0.9 ºC) > LST_{PF} (29.9 ± 0.9 ºC) > LST_{RU} (29.6 ± 0.4 ºC) > LST_{FO} (29.2 ± 0.4 ºC) (MODIS LST, Figure 8).

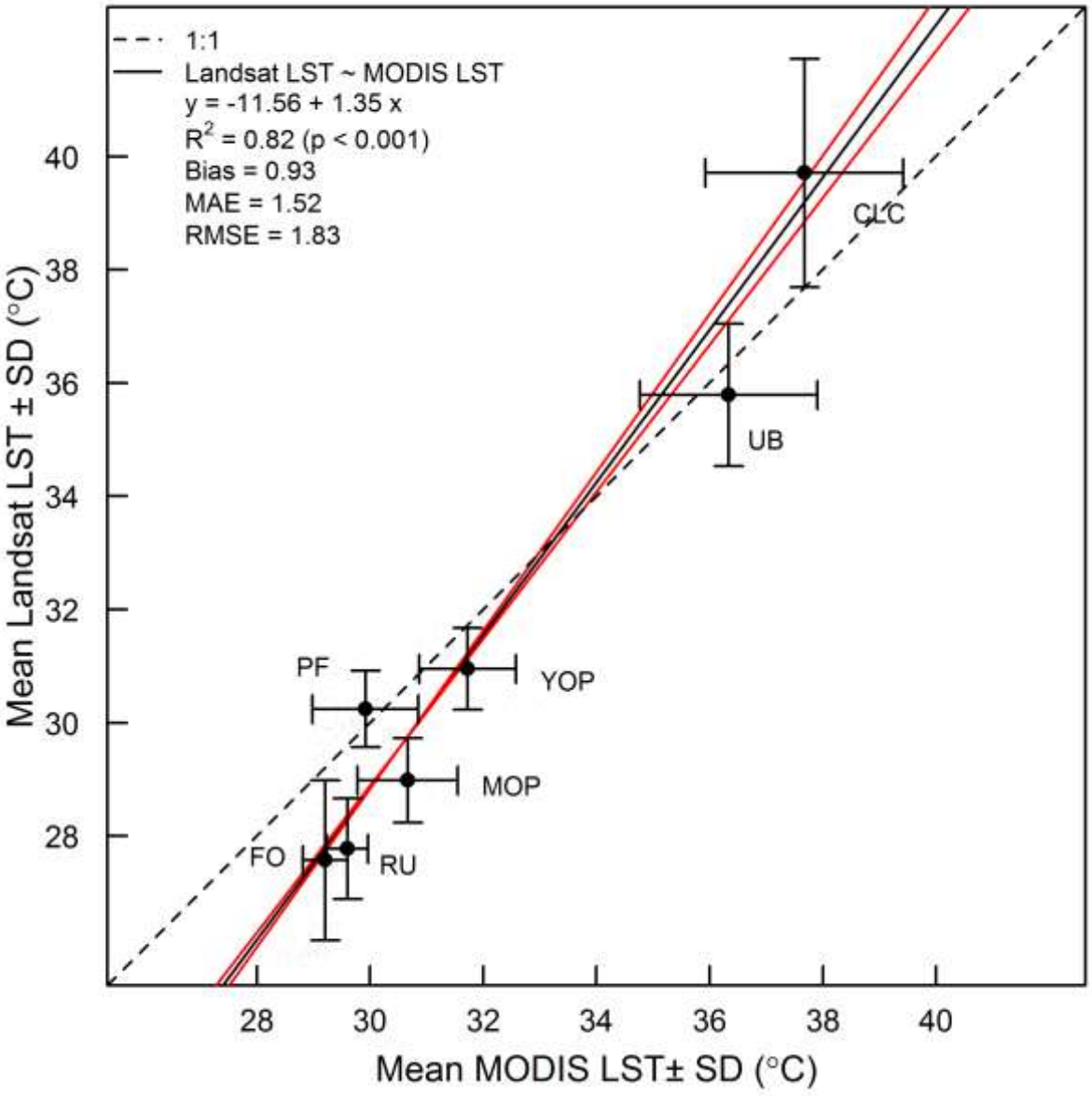

Figure 8. Average surface temperature (LST) and standard deviation (SD) of 7 land cover types derived from a Landsat thermal image compared with the mean and SD of MODIS LST.
CLC = Clear cut land, UB = Urban areas, YOP = young oil palm plantation, PF = Acacia Plantation Forest, MOP = Mature Oil palm plantation, FO = Forest, RU = Rubber plantation. The dashed line is the theoretical 1:1 line, the solid lines are the Linear Model type 2 regression line (black) and the confidence limits of the regression line (red). The Landsat and MODIS images were acquired on 19 June 2013, at 10:13 and 10:30 local time respectively. Landsat pixels (30 m) were resampled to MODIS pixel resolution (926 m) to make a pixel to pixel comparison between the two sources possible.

3.1.2 Evapotranspiration

We calculated u^* and r_{ah} for a young and mature oil palm plantation (Table 6). These were calculated from meteorological measurement on these locations. Because the satellite image was acquired outside the time period in which meteorological measurements were made, we selected dates and times that had similar conditions on the day the image was acquired. We used incoming shortwave radiation as a main criteria (> 690 Wm^{-2} and < 720 Wm^{-2}, between 10.00 and 11:00 am local time). u^* and r_{ah} derived from the satellite image show a certain level of agreement with the u^* and r_{ah} calculated from meteorological data.

We tested different combinations of 5 hot and 5 cold pixels, that could serve as anchor pixels, and then compared the effects of anchor pixel selection on the ET output. Our comparison showed that the anchor pixels we selected showed an overall effect on the magnitude of ET of less than 10% and had no effect on the ranking of the ET by land use type (Figure 9).

We calculated *LE* and *H* for a young and mature oil palm plantation (Table 6). These were calculated from flux measurements on these locations. Because the satellite image was acquired outside the time period in which meteorological measurements were made, we selected dates and times that had similar conditions on the day the image was acquired. *LE* and *H* derived from the satellite image show some agreement with the *LE* and *H* calculated from meteorological data.

Table 6. u^*, r_{ah}, LE and H measured at a young and mature oil palm plantation

	Young Oil Palm Plantation (YOP)		**Mature oil Palm Plantation (MOP)**	
	Lower limit§	Upper limit§	Lower limit§	Upper limit§
u^* (m s^{-1})	0.40 ± 0.15	0.47 ± 0.18	0.12 ± 0.02	0.37 ± 0.11
r_{ah} (s m^{-1})	24.14 ± 11.80	26.92 ± 12.17	22.93 ± 5.20	54.97 ± 7.13
LE (W m^{-2})	215.77 ± 61.05	226.22 ± 68.29	413.67 ± 109.54	441.00 ± 109.76
H (W m^{-2})	138.34 ± 50.85	140.57 ± 51.32	90.11 ± 32.64	97.25 ± 33.56

§ The table shows 2 values for u^*, r_{ah}, LE and H. These values were calculated for the lower (> 690 W m^{-2}) and upper (< 720 W m^{-2})limit of incoming solar radiation we selected to match conditions on the day the satellite image was acquired.

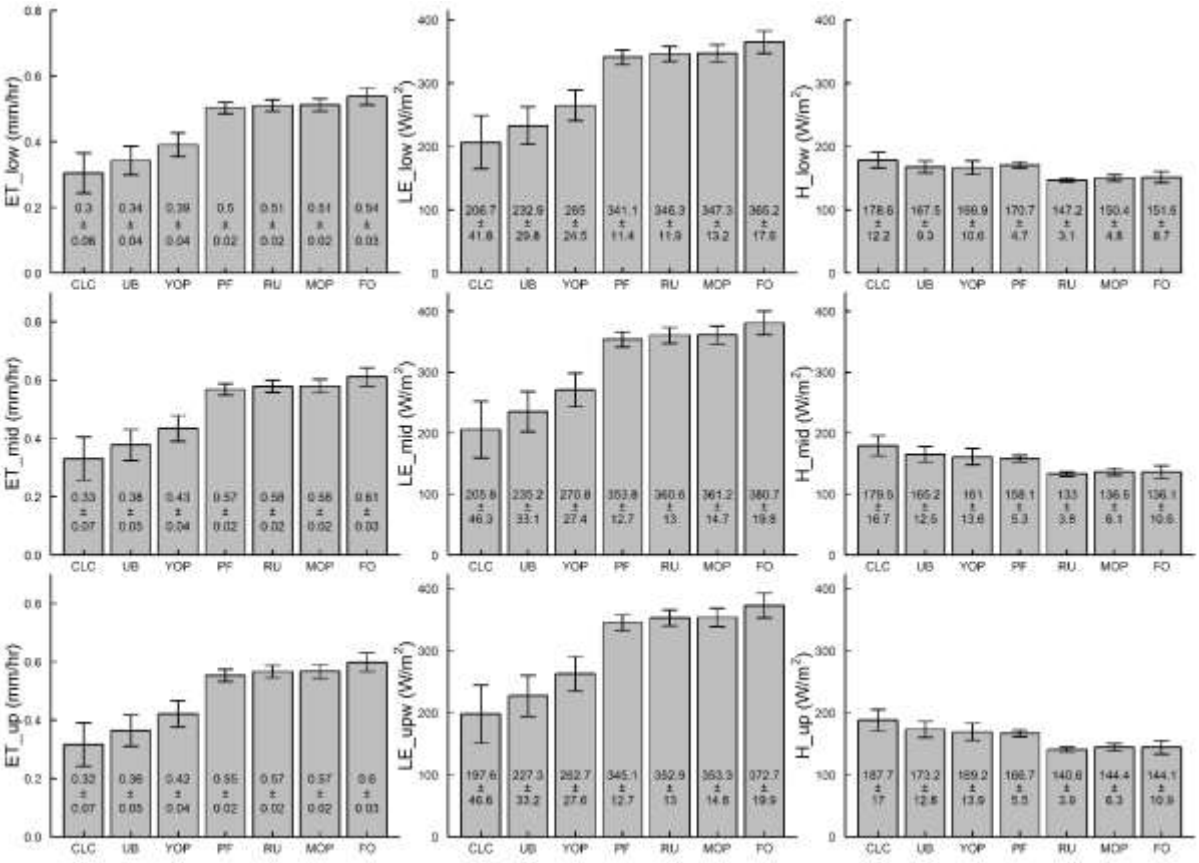

Figure 9. ET, LE and H derived with SEBAL for the image acquired on 19 June 2013

3.1.3 Surface energy balance, energy partitioning and biophysical variables derived from Landsat

The processing of the satellite data resulted in 10 images per date that quantified the land surface variables and their spatial patterns in the lowlands of Jambi covering different landscapes (Figure 10). Areas with higher surface temperatures (Figure 10a) show patterns that correspond to areas with lower vegetation (Figure 10c) and areas with lower surface temperatures show patterns that correspond to areas with more vegetation cover. The patterns of the biophysical variables, energy partitioning and energy balance variables correspond to the amount of vegetation cover (NDVI). Areas with higher surface temperatures show correspondingly lower LE partitioning ((Figure 10j), higher H partitioning (Figure 10i), lower ET rates (Figure 10d), lower G (Figure 10h) and lower LWout (Figure 10f). Vegetated areas also show patterns of higher net radiation ((Figure 10g).

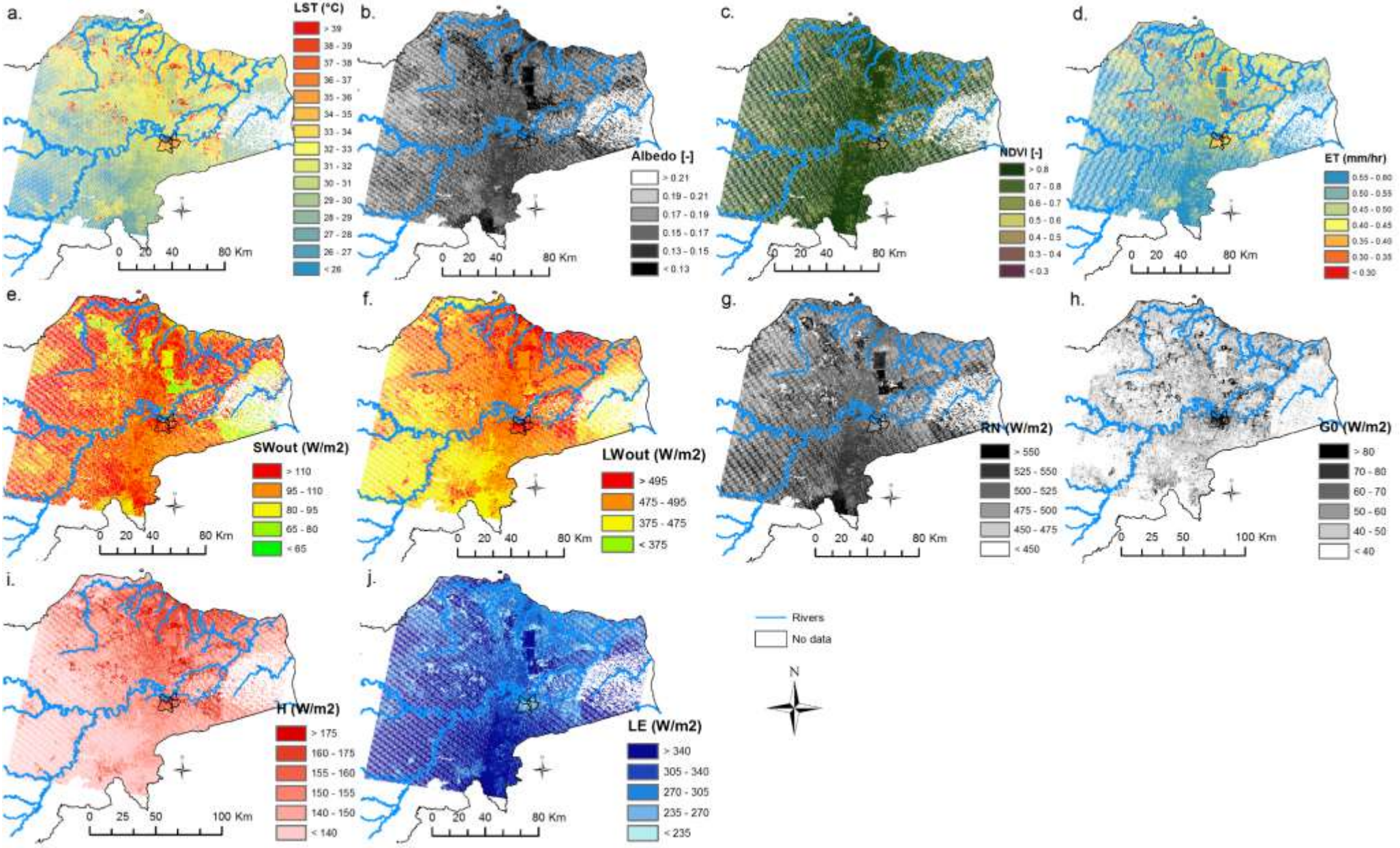
a.
LST (°C)
> 39
38 - 39
37 - 38
36 - 37
35 - 36
34 - 35
33 - 34
32 - 33
31 - 32
30 - 31
29 - 30
28 - 29
27 - 28
26 - 27
< 26
0 20 40 80 Km
b.
Albedo [-]
> 0.21
0.19 - 0.21
0.17 - 0.19
0.15 - 0.17
0.13 - 0.15
< 0.13
0 20 40 80 Km
c.
NDVI [-]
> 0.8
0.7 - 0.8
0.6 - 0.7
0.5 - 0.6
0.4 - 0.5
0.3 - 0.4
< 0.3
0 20 40 80 Km
d.
ET (mm/hr)
0.55 - 0.60
0.50 - 0.55
0.45 - 0.50
0.40 - 0.45
0.35 - 0.40
0.30 - 0.35
< 0.30
0 20 40 80 Km
e.
SWout (W/m2)
> 110
95 - 110
80 - 95
65 - 80
< 65
0 20 40 80 Km
f.
LWout (W/m2)
> 495
475 - 495
375 - 475
< 375
0 20 40 80 Km
g.
RN (W/m2)
> 550
525 - 550
500 - 525
475 - 500
450 - 475
< 450
0 20 40 80 Km
h.
G0 (W/m2)
> 80
70 - 80
60 - 70
50 - 60
40 - 50
< 40
0 25 50 100 Km
i.
H (W/m2)
> 175
160 - 175
155 - 160
150 - 155
140 - 150
< 140
0 25 50 100 Km
j.
LE (W/m2)
> 340
305 - 340
270 - 305
235 - 270
< 235
0 20 40 80 Km
Rivers
No data
N

Figure 10. Biophysical variables, surface energy balance and energy partitioning derived from a Landsat satellite image acquired on 19 June 2013. a. Surface temperature (LST, °C); b. Albedo (α, unitless); c. Normalized Difference Vegetation Index (NDVI, unitless); d. Evapotranspiration (ET, mm hr^{-1}); e. Reflected shortwave radiation ($S_w\uparrow$, W m^{-2}); f. Outgoing longwave radiation ($L_w\uparrow$, W m^{-2}); g. Net radiation (Rn, W m^{-2}); h. Ground heat flux (G, W m^{-2}); i. Sensible heat flux (H, W m^{-2}); j. Latent heat flux (LE, W m^{-2}). No data areas occur due to cloud cover, cloud shadow and to the scan line error of the Landsat 7 image. This image was acquired at 10:13 am local time.

3.2 Local short-term differences between different land cover types

The ΔLST between RU, MOP, PF, YOP, UB and CLC land cover types and FO were all positive, meaning that the other land cover types were warmer than forests (Figure 11, a). RU and MOP were 0.4 ± 1.5 and 0.8 ± 1.2 °C warmer than forest, respectively. PF and YOP were much warmer than forests (ΔLST_{PF-FO} = 2.3 ± 1.1; ΔLST_{YOP-FO} = 6.0 ± 1.9 °C). The largest ΔLSTs were between forest and the non-vegetated land cover types, i.e. UB (ΔLST = 8.5 ± 2.1 °C) and CLC (ΔLST = 10.9 ± 2.6 °C). The LST differences were significant ($p < 0.05$, post hoc Tukey's HSD test), except between RU and FO ($p = 0.78$, post hoc Tukey's HSD test (Table 7 & Table 8).

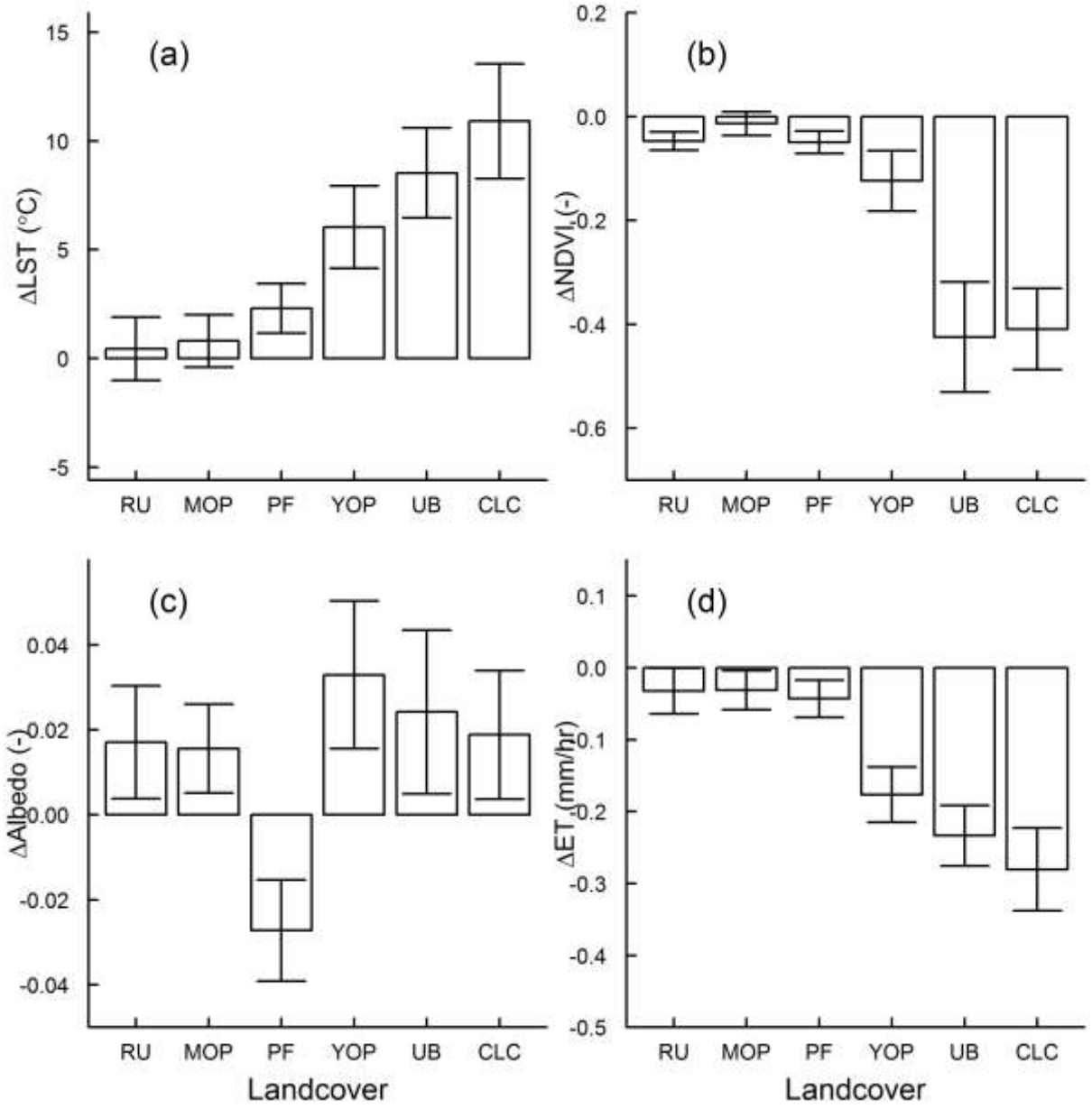

Figure 11. Differences (mean ± SD) in biophysical variables.
a. surface temperature (ΔLST), b. normalized difference vegetation index (ΔNDVI), c. albedo (ΔAlbedo) and d. evapotranspiration (ΔET) between other land covers (RU, MOP, PF, YOP, UB and CLC) and forest (FO) in the Jambi province, derived from a Landsat LST image acquired on 19 June 2013 at 10:13 local time.

Table 7. ANOVA statistics

		Df	Sum Sq.	Mean Sq.	F value	Pr(>F)
LST	Group	6	657323	109554	26240	***
	Residuals	41583	173612	4		
Albedo	Group	6	17.0	2.84	11492	***
	Residuals	41583	10.3	0.00		
NDVI	Group	6	1197	200	32402	***
	Residuals	41583	256	0		
ET	Group	6	464	77.3	41141	***
	Residuals	41583	78	0.0		

*** : $p = 2 \times 10^{-16}$

Similar differences were found for the ΔNDVI between forest and the other land covers (Figure 11b). The negative ΔNDVI indicates that the non-forest land cover types had lower NDVI than the forest. ΔNDVI between FO and RU, MOP, PF and YOP were small (between – 0.01 ± 0.02 ($\Delta NDVI_{MOP - FO}$) and – 0.12 ± 0.06 ($\Delta NDVI_{YOP - FO}$)). The largest ΔNDVIs were between forest and the non-vegetated land cover types, i.e. UB and CLC (ΔNDVI = – 0.42 ± 0.11 and – 0.41 ± 0.08, respectively). All ΔNDVIs were significant ($p < 0.05$, post hoc Tukey's HSD test).

The difference in albedo (Δalbedo) between forest and the other land covers was very small (Figure 11c), with ΔAlbedo values between – 0.03 ± 0.01 ($\Delta albedo_{PF - FO}$) and 0.03 ± 0.02 ($\Delta albedo_{YOP - FO}$). These differences were significant ($p < 0.05$, post hoc Tukey's HSD test). PF had a lower albedo than forest ($\Delta Aalbedo_{PF - FO}$ = – 0.03 ± 0.01), while the other land cover types had a higher albedo than forest.

All compared land covers had lower ET than forest. RU, MOP and PF had slightly lower ET than FO (ΔET_{RU-FO} = – 0.03 ± 0.04, ΔET_{MOP-FO} = – 0.03 ± 0.03 mm hr^{-1}, ΔET_{PF-FO} = – 0.04 ± 0.03 mm hr^{-1}) (Figure 11d). YOP, UB and CLC had much lower ET values than forests: ΔET_{YOP-FO} = – 0.18 ± 0.04 mm/hr, ΔET_{UB-FO} = – 0.23 ± 0.04 mm hr^{-1}, ΔET_{CLC-FO} = – 0.26 ± 0.06 mm hr^{-1}).

The ΔETs were significant ($p < 0.05$, post hoc Tukey's HSD test). The SEBAL-based LE estimates were within the variability range of LE measurements from eddy covariance measurements under similar meteorological conditions (see Ch. 3.1.2).

Table 8. Post-hoc Tukey HSD test statistics

		Land cover					
L6		**UB**	**FO**	**MOP**	**YOP**	**PF**	**CLC**
	FO	0.00000					
	MOP	0.00000	0.00000				
	YOP	0.00000	0.00000	0.00000			
	PF	0.00000	0.00000	0.00000	0.00000		
	CLC	0.00000	0.00000	0.00000	0.00000	0.00000	
	RU	0.00000	***0.79912***	***0.90144***	0.00000	0.00000	0.00000
Rc		**UB**	**FO**	**MOP**	**YOP**	**PF**	**CLC**
	FO	0.00000					
	MOP	0.00000	0.00000				
	YOP	0.00000	0.00000	0.00000			
	PF	0.00000	0.00000	0.00000	0.00000		
	CLC	0.00000	0.00000	0.00000	0.00000	0.00000	
	RU	0.00000	***0.83540***	***0.91619***	0.00000	0.00000	0.00000
LST		**UB**	**FO**	**MOP**	**YOP**	**PF**	**CLC**
	FO	0.00000					
	MOP	0.00000	0.00000				
	YOP	0.00000	0.00000	0.00000			
	PF	0.00000	0.00000	0.00000	0.00000		
	CLC	0.00000	0.00000	0.00000	0.00000	0.00000	
	RU	0.00000	0***.78391***	0***.89703***	0.00000	0.00000	0.00000
NDVI		**UB**	**FO**	**MOP**	**YOP**	**PF**	**CLC**
	FO	0.00000					
	MOP	0.00000	0.00000				
	YOP	0.00000	0.00000	0.00000			
	PF	0.00000	0.00000	0.00000	0.00000		
	CLC	0.00000	0.00000	0.00000	0.00000	0.00000	
	RU	0.00000	0.00099	0.05903	0.00000	1***.00000***	0.00000
Albedo		**UB**	**FO**	**MOP**	**YOP**	**PF**	**CLC**
	FO	0.00000					
	MOP	0.00000	0.00000				
	YOP	0.00000	0.00000	0.00000			
	PF	0.00000	0.00000	0.00000	0.00000		
	CLC	0.00000	0.00000	0.00000	0.00000	0.00000	
	RU	0.04009	0.00000	***0.99443***	0.00000	0.00000	***0.99009***
ET		**UB**	**FO**	**MOP**	**YOP**	**PF**	**CLC**
	FO	0.00000					
	MOP	0.00000	0.00000				
	YOP	0.00000	0.00000	0.00000			
	PF	0.00000	0.00000	0.00000	0.00000		
	CLC	0.00000	0.00000	0.00000	0.00000	0.00000	
	RU	0.00000	0.00000	***1.00000***	0.00000	***0.62621***	0.00000

Albedo had a weaker influence on the LST ($\rho = 0.25$, $p < 0.05$) (Table 9) than NDVI and ET. As the thermal radiance band (L6) and the atmospherically corrected thermal band (Rc) were the basis for the LST calculation, the high correlation between L6 and NDVI ($\rho = -0.87$, $p < 0.05$) and between L6 and ET ($\rho = -0.98$, $p < 0.05$) resulted in a high correlation between LST and NDVI ($\rho = -0.88$) and between LST and ET ($\rho = -0.98$). The analysis showed that albedo, NDVI and ET were all significant predictors of LST ($F_{(3, 41586)} = 1 \times 10^6$, $p < 0.05$). ET was the strongest predictor of LST (standardized $\beta = -1.11$, $p < 0.05$). Albedo (standardized $\beta = -0.19$, $p < 0.05$) and NDVI (standardized $\beta = -0.19$, $p < 0.05$) were weaker predictors of LST.

Table 9. Statistical analysis between biophysical variables (albedo (α), NDVI and ET) and Sspectral radiance band (L6), corrected thermal band (Rc) and Landsat land surface temperature (LST).

Model		**ρ**	**R^2**	**β**	**Stand. β**	**Model fit (R^2)**	**F-statistics**
	α	0.26	0.05	-2.94	-0.19		F (3, 41586) =
L6 ~ α + NDVI + ET	**NDVI**	-0.87	0.10	0.23	0.11	0.99	1.10×106, ***
	ET	-0.98	1.13	-4.00	-1.16		
	α	0.25	0.05	-4.88	-0.20		F (3, 41586) =
Rc ~ α + NDVI + ET	**NDVI**	-0.88	0.04	0.16	0.05	0.99	1.79×106 , ***
	ET	-0.98	1.00	-6.21	-1.10		
	α	0.25	0.05	-34.01	-0.19		F(3, 41586) =
LST ~ α + NDVI + ET	**NDVI**	-0.88	0.05	1.30	0.05	0.99	2.3×106, ***
	ET	-0.98	1.00	-43.53	-1.11		

***: $p = 2\times10^{-16}$

LM: Multiple linear regression analysis between LST (or L6 or Rc) and three biophysical variables: Aalbedo (α), NDVI and ET. ρ is the correlation coefficient. R^2 is the R square of the components; β is the regression coefficient of the component; stand. β is the standardized β; Model fit (R^2) is the overall model fit of the multiple linear regression.

A separate analysis (Table 10) showed that ET was a strong predictor of LST for each land cover type in this study and that NDVI and albedo were minor predictors of LST.

Table 10. The relation LST-Albedo-NDVI-ET separated by land cover type.

	Rc			LST		
FO	**α**	**NDVI**	**ET**	**α**	**NDVI**	**ET**
ρ	-0.31	-0.48	-0.96	-0.30	-0.48	-0.96
R^2	0.09	0.06	0.96	0.09	0.06	0.97
β	-4.67	1.42	-6.36	-33.86	10.38	-46.43
Stand. β	-0.31	0.13	-1.01	-0.31	0.126	-1.01
Modelfit (R^2)	0.99			0.99		
RU	**α**	**NDVI**	**ET**	**α**	**NDVI**	**ET**
ρ	0.20	-0.48	-0.89	0.20	-0.48	-0.89
R^2	0.12	0.18	1.29	0.12	0.18	1.29
β	-5.59	1.34	-6.50	-40.89	9.74	-47.47
Stand. β	-0.57	0.37	-1.45	-0.57	0.37	-1.45
Modelfit (R^2)	0.99			0.99		
PF	**α**	**NDVI**	**ET**	**α**	**NDVI**	**ET**
ρ	0.26	-0.30	-0.98	0.26	-0.30	-0.98
R^2	0.07	0.06	1.12	0.07	0.06	1.12
β	-2.87	0.87	-6.22	-20.74	6.26	-44.55
Stand. β	-0.28	0.19	-1.15	-0.28	0.19	-1.146
Modelfit (R^2)	0.99			0.99		
MOP	**α**	**NDVI**	**ET**	**α**	**NDVI**	**ET**
ρ	-0.15	-0.41	-0.95	-0.15	-0.41	-0.95
R^2	0.05	0.11	1.07	0.05	0.11	1.07
β	-5.32	1.42	-6.51	-38.50	10.36	-47.26
Stand. β	-0.30	0.27	-1.12	-0.302	0.27	-1.13
Modelfit (R^2)	0.99			0.99		
YOP	**α**	**NDVI**	**ET**	**α**	**NDVI**	**ET**
ρ	-0.71	-0.58	-0.93	-0.72	-0.58	-0.92
R^2	0.25	0.12	0.87	0.26	0.12	0.86
β	-5.55	0.85	-6.79	-39.11	6.06	-47.52
Stand. β	-0.36	0.21	-0.93	-0.36	0.21	-0.94
Modelfit (R^2)	0.99			0.99		
UB	**α**	**NDVI**	**ET**	**α**	**NDVI**	**ET**
ρ	-0.44	-0.72	-0.89	-0.44	-0.72	-0.89
R^2	0.20	0.02	0.77	0.19	0.02	0.78
β	-6.95	-0.08	-6.40	-47.69	-0.51	-44.22
Stand. β	-0.45	-0.03	-0.87	-0.45	-0.03	-0.87
Modelfit (R^2)	0.99			0.99		
CLC	**α**	**NDVI**	**ET**	**α**	**NDVI**	**ET**
ρ	-0.13	-0.68	-0.98	-0.13	-0.68	-0.98
R^2	0.03	0.05	1.02	0.03	0.04	1.01
β	-6.21	0.35	-7.10	-42.87	1.97	-47.66
Stand. β	-0.20	0.07	-1.05	-0.21	0.06	-1.04
Modelfit (R^2)	0.99			0.99		

All metrics were highly significant ($p = 2\times10^{-16}$).

Abbreviations: FO = Forest, RU = Rubber, PF = Acacia Plantation Forest, MOP = Mature Oil Palm, YOP = Young Oil palm, CLC = Clear cut land, UB = Urban Areas

3.3 Development of biophysical variables during the oil palm rotation cycle

The age of the oil palm plantations in the chronosequence we used for the satellite images of 19 June and 27 June 2013 was between 0 and 25 years and between 3 and 19 years in the chronosequence we used for the image that was acquired 2 years later on 25 June 2015 (Figure 12). Young oil palm plantations are characterized by higher surface temperatures, higher albedo, lower NDVI and lower ET while mature oil palm plantations show the opposite trend and are characterized by lower surface temperatures, lower albedo, higher NDVI and higher ET (Figure 12).

Oil palm plantations have higher LST than forests which results in positive ΔLST between oil palm plantations and forest (Figure 12a). The difference between forest and recently established plantation can be as high as 11 °C. The surface temperatures decrease as the oil palm plantations grow older and the differences between forest temperatures become smaller. The smallest differences between oil palm plantations and forest are reached in the mature phase of the plantations when they reach near-forest temperatures, 6 – 8 years after establishment. The decreasing surface temperature trend is still observed 2 years later (25 June 2015) and shows that the differences become smaller when the plantations become older.

Oil palm plantations have a higher albedo than forests which gives positive Δα between oil palm plantations and forest (Figure 12b). In the first year Δα can be as large as 0.04 and decreases linearly during the development of the oil palm plantation, a trend that is consistent for all three dates.

Oil palm plantations have lower NDVI than forests which results in negative ΔNDVI between oil palm plantations and forest (Figure 12c). ΔNDVI is largest between oil palm plantations in the early and young stage of the oil palm plantations and forests (ΔNDVI: 0.5 – 0.4) and the difference becomes smaller as the plantations mature (Figure 12c) which can be observed for all three dates. The smallest ΔNDVI between oil palm plantations and forest are reached 4 – 5 years after planting.

Oil palm plantations have lower ET in the young phase (Figure 12d). The ΔET between forest and oil palm plantations are the largest in the initial and young stage of the oil palm plantations (< 5 years) (ΔET: 0.16 – 0.32 mm hr^{-1}). The differences become smaller when the plantations become older with the smallest differences in the mature oil palm phase (ΔET between 0.04 and 0.01 mm hr^{-1}).

The decreasing trend of the differences between the biophysical variables of forests and oil palm plantations can be described by a 1st, 2nd, 3rd or 4th order function which are summarized in Table 11 (Section 3.5). The ΔLST, ΔNDVI and ΔLST trend can be described by a 2nd, 3rd and 4th order function whereas Δα can be described by a linear function (Table 11).

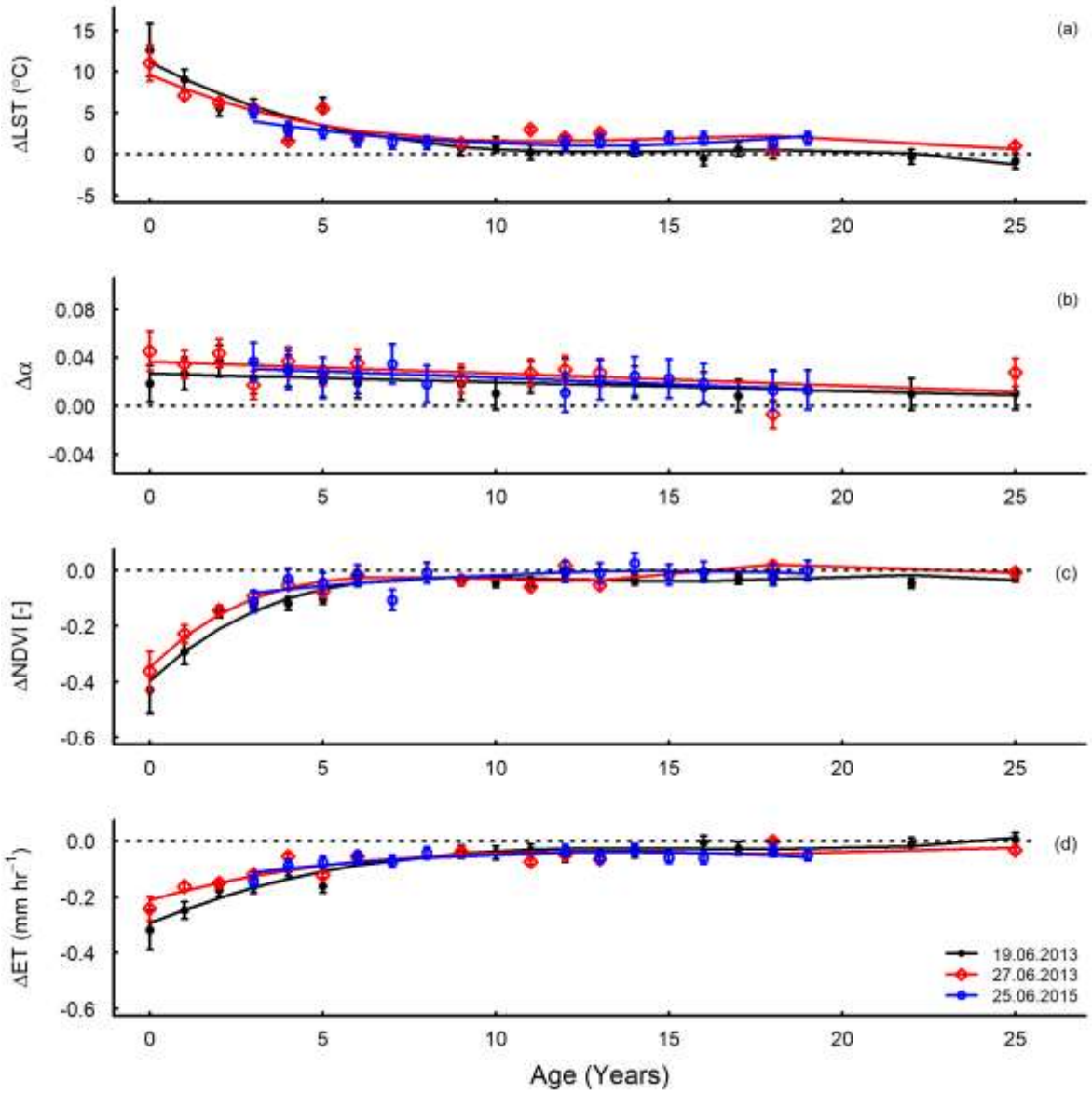

Figure 12. Development of the biophysical variables, ΔLST, Δα, ΔNDVI and ΔET, during the rotation cycle of oil palm plantations extracted from three different date satellite images.
a. ΔLST (°C); b. Δα (unitless); c. ΔNDVI (unitless); d. ΔET (mm hr^{-1}). The development of the biophysical variables is expressed as deviation from the average value of forests e.g. ΔLST = $LST_{Oil\ palm} - LST_{Forest}$. Black line/filled circles: 19 June 2013, red line/open diamonds: 27 June 2013, blue line/open circles: 25 June 2015. A n-order GLM-function was fitted through the points to fit the trend.

3.4 Development of radiation balance during the oil palm rotation cycle

Young oil palm plantations are further characterized by a higher reflection of solar radiation (SW↑), higher emission of thermal longwave radiation (LW↑) and lower Net radiation (RN) compared to mature oil palm plantations and forests (Figure 13).

Δ SW↑ is higher in the first years and decreases linearly with the development of the plantations, a trend which is observed for all 3 dates (Figure 13a).

ΔLW↑ is also higher for young oil palm plantations with ΔLW↑ that are 3 – 4 times larger than ΔLW↑ between mature oil palm plantations and forests (Figure 13b). ΔLW↑ also has a consistent decreasing trend for all 3 dates.

ΔRN becomes smaller with increasing age of the plantations (Figure 13c). The largest ΔRN are observed for the youngest oil palm plantation phase (ΔRN = 75 – 100 W m^{-2} between 0 and 2 years old) and are 4 – 5 times larger than ΔRN in the mature phase.

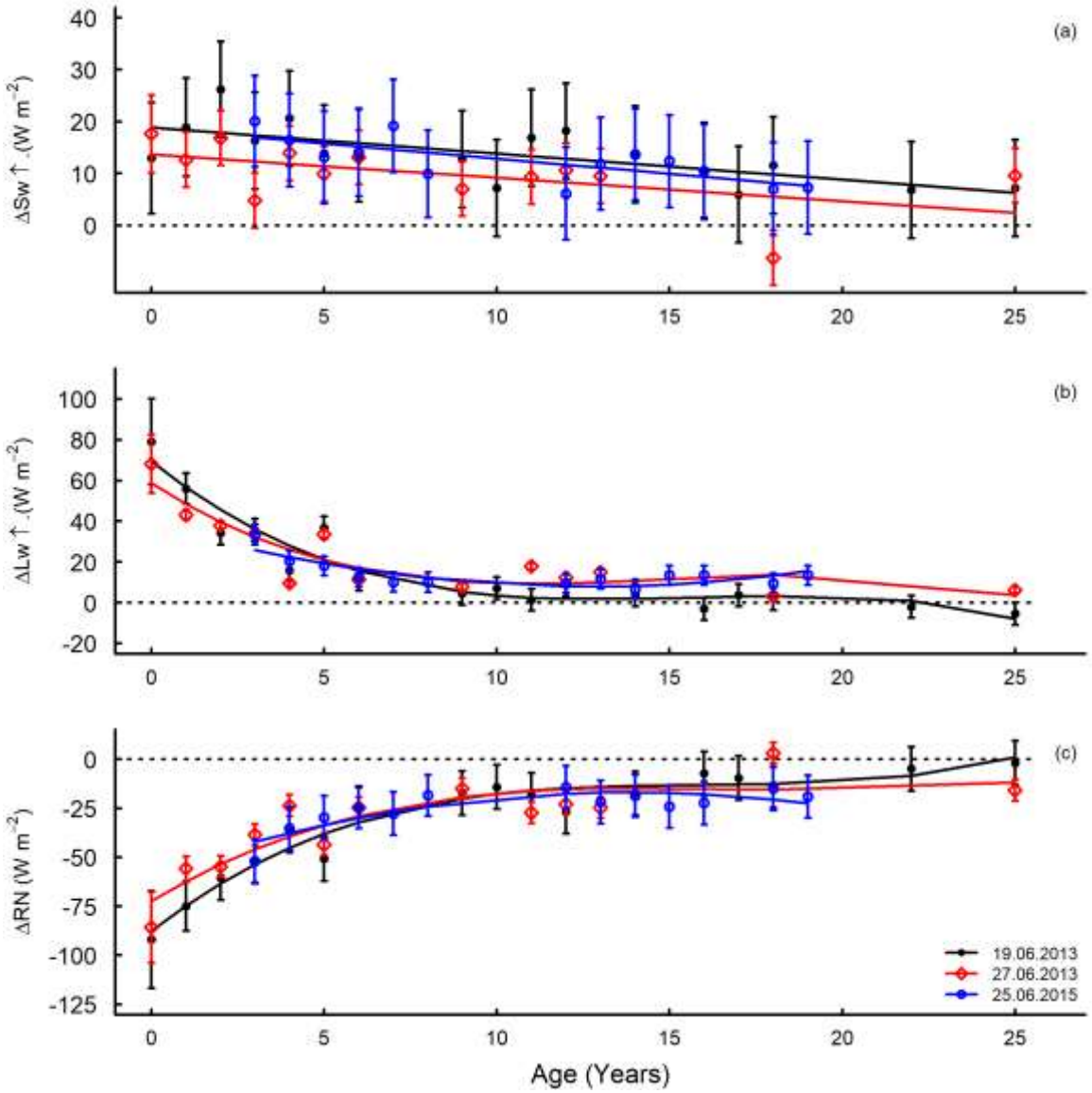

Figure 13. Development of the radiation balance variables, ΔSw↑, ΔLw↑ and ΔRN, during the rotation cycle of oil palm plantations extracted from three different date images.
a. $\Delta Sw\uparrow = Sw\uparrow_{Oil\ palm} - Sw\uparrow_{Forest}$; b. $\Delta Lw\uparrow = Lw\uparrow_{Oil\ palm} - Sw\uparrow_{Forest}$; c. $\Delta RN = RN_{Oil\ palm} - RN_{Forest}$. A n-order GLM-function was fitted through the points to fit the trend. Black line/filled circles: 19 June 2013, red line/open diamonds: 27 June 2013, blue line/open circles: 25 June 2015.

3.5 Development of energy partitioning during the oil palm rotation cycle

Differences in energy partitioning between young oil palm plantations and mature oil palm plantations and forests also show consistent trends (Figure 14). G and H fluxes of young oil palm plantations are larger than those of forests and mature oil palm plantations which gives positive ΔG and ΔH that become smaller with increasing age (Figure 14 a & b). LE fluxes show an opposite trend to the G and H fluxes: LE fluxes of young oil palm plantations are lower than LE fluxes of forests. The ΔLE are negative in the young oil palm stage and the differences become less with increasing age (Figure 14c).

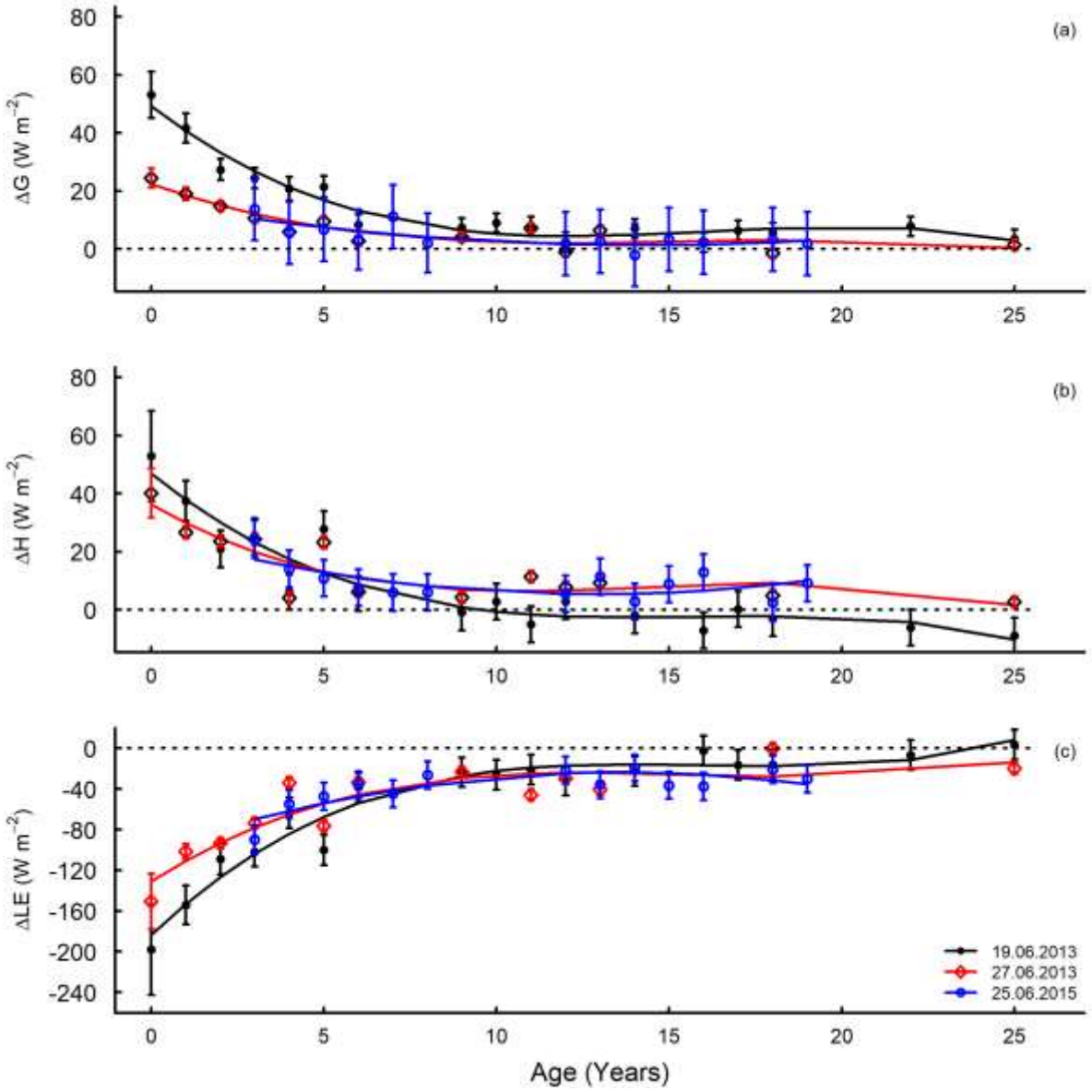

Figure 14. Development of the energy partitioning variables, ΔG, ΔH and ΔLE, during the rotation cycle of oil palm plantations extracted from three different date images.
a. $\Delta G = G_{Oil\ palm} - G_{Forest}$; b. $\Delta H = H_{Oil\ palm} - H_{Forest}$; c. $\Delta LE = LE_{Oil\ palm} - LE_{Forest}$. A n-order GLM-function was fitted through the points to fit the trend. Black line/filled circles: 19 June 2013, red line/open diamonds: 27 June 2013, blue line/open circles: 25 June 2015.

The change of the differences of the biophysical variables (Figure 12), energy balance (Figure 13) and energy partitioning variables (Figure 14) can be described by different models (Table 11). Δα and ΔSW↑ trends can be described by a linear equations and the other trends are described by a second, third or fourth order equation.

Table 11. Trends of the Δbiophysical variables, ΔRadiation balance and Δenergy partitioning variables quantified by n-order functions.

Variable	**Date**	**Equation**
ΔLST	19 June 2013	$y = -2.18\ x^3 + 0.14\ x^2 - 0.003\ x + 11.16$; $R^2 = 0.92$; $p < 0.05$
	27 June 2013	$y = -1.79\ x^3 + 0.13\ x^2 - 0.003\ x + 9.61$; $R^2 = 0.81$; $p < 0.05$
	25 June 2015	$y = -0.79\ x^2 + 0.03\ x + 6.06$; $R^2 = 0.71$; $p < 0.05$
Δα	19 June 2013	$y = -0.001\ x + 0.03$; $R^2 = 0.48$; $p < 0.05$
	27 June 2013	$y = -0.001\ x + 0.04$; $R^2 = 0.3$; $p > 0.05$
	25 June 2015	$y = -0.001\ x + 0.03$; $R^2 = 0.54$; $p < 0.05$
ΔNDVI	19 June 2013	$y = 0.12\ x^4 - 0.01\ x^3 + 0.001\ x^2 - 0.00001\ x - 0.4$; $R^2 = 0.95$; $p < 0.05$
	27 June 2013	$y = 0.12\ x^4 - 0.02\ x^3 + 0.001\ x^2 - 0.00002\ x - 0.35$; $R^2 = 0.96$; $p < 0.05$
	25 June 2015	$y = 0.02\ x^2 - 0.001\ x - 0.13$; $R^2 = 0.49$; $p < 0.05$
ΔET	19 June 2013	$y = 0.05\ x^3 - 0.003\ x^2 + 0.0001\ x - 0.29$; $R^2 = 0.95$; $p < 0.05$
	27 June 2013	$y = 0.03x^3 - 0.002\ x^2 + 0\ x - 0.21$; $R^2 = 0.82$; $p < 0.05$
	25 June 2015	$y = 0.02\ x^2 - 0.0007\ x - 0.16$; $R^2 = 0.68$; $p < 0.05$
ΔSW↑	19 June 2013	$y = -0.5\ x + 18.88$; $R^2 = 0.48$; $p < 0.05$
	27 June 2013	$y = -0.45\ x + 13.68$; $R^2 = 0.3$; $p > 0.05$
	25 June 2015	$y = -0.6\ x + 18.71$; $R^2 = 0.54$; $p < 0.05$
ΔLW↑	19 June 2013	$y = -13.65\ x^3 + 0.89\ x^2 - 0.02\ x + 69.49$; $R^2 = 0.92$; $p < 0.05$
	27 June 2013	$y = -11.07\ x^3 + 0.79\ x^2 - 0.02\ x + 58.83$; $R^2 = 0.81$; $p < 0.05$
	25 June 2015	$y = -4.88\ x^2 + 0.19\ x + 38.86$; $R^2 = 0.71$; $p < 0.05$
ΔRN	19 June 2013	$y = 13.72\ x^3 - 0.85\ x^2 + 0.02\ x - 87.6$; $R^2 = 0.95$; $p < 0.05$
	27 June 2013	$y = 10.57\ x^3 - 0.63\ x^2 + 0.01\ x - 72.22$; $R^2 = 0.79$; $p < 0.05$

Table 11 (continued)		
	25 June 2015	$y = 5.92\ x^2 - 0.21\ x - 57.85$; $R^2 = 0.73$; $p < 0.05$
ΔG	19 June 2013	$y = -9.18\ x^3 + 0.6\ x^2 - 0.01\ x + 49.21$; $R^2 = 0.96$; $p < 0.05$
	27 June 2013	$y = -4.22\ x^3 + 0.28\ x^2 - 0.01\ x + 22.44$; $R^2 = 0.84$; $p < 0.05$
	25 June 2015	$y = -2.06\ x^2 + 0.07\ x + 16.05$; $R^2 = 0.56$; $p < 0.05$
ΔH	19 June 2013	$y = -9.54\ x^3 + 0.61\ x^2 - 0.01\ x + 46.81$; $R^2 = 0.88$; $p < 0.05$
	27 June 2013	$y = -6.84\ x^3 + 0.5\ x^2 - 0.01\ x + 36.23$; $R^2 = 0.77$; $p < 0.05$
	25 June 2015	$y = -3.17\ x^2 + 0.12\ x + 25.75$; $R^2 = 0.46$; $p < 0.05$
ΔLE	19 June 2013	$y = 32.44\ x^3 - 2.06\ x^2 + 0.04\ x - 183.62$; $R^2 = 0.95$; $p < 0.05$
	27 June 2013	$y = 21.62\ x^3 - 1.41\ x^2 + 0.03\ x - 130.89$; $R^2 = 0.82$; $p < 0.05$
	25 June 2015	$y = 11.15\ x^2 - 0.41\ x - 99.64$; $R^2 = 0.68$; $p < 0.05$

3.6 Relation NDVI and LST

NDVI is a stronger predictor of the LST than albedo for the relationship between LST, Albedo and NDVI for different land use types on all three dates (stand. β NDVI = -0.88, -0.89, -0.72 against stand. β albedo = -0.005, 0.07 and -0.10, for 19 June 2013, 27 June 2013 and 25 June 2015 respectively, $p < 0.05$) (Table 12). The models quantifying the LST–albedo–NDVI relations for different land use types derived from the images of 19 June and 25 June 2013 had better fits (R^2adj. = 0.78 and 0.85) than derived for the image 0f 25 June 2015 (R^2adj. = 0.48). NDVI is also a stronger predictor of the LST than albedo for the LST–albedo–NDVI relationship of oil palm plantations on all three dates (stand. β NDVI = -0.88, -0.76, -0.62 against stand. β albedo = -0.005, 0.006 and 0.26, $p< 0.05$) (Table 12).

Table 12. GLM-regression between LST, albedo and NDVI

LST ~ Albedo + NDVI			
	Different LU types		
	19 June 2013	**27 June 1013**	**25 June 2015**
Model	-0.84 α - 21.14 NDVI + 47.39	11.95 α - 23.28 NDVI + 45.69	-15.67 α - 16.82 NDVI + 44.76
R^2-adj.	0.78	0.85	0.48
p	< 0.05	< 0.05	< 0.05
Beta coeff α	- 0.005	0.07	- 0.10
Beta coeff NDVI	- 0.88	- 0.89	- 0.72
	Only oil palm		
	19 June 2013	**27 June 1013**	**25 June 2015**
Model	-1.75 α - 27.10 NDVI + 51.90	1.13 α - 20.66 NDVI + 46.57	38.47 α - 17.16 NDVI + 36.90
R^2-adj.	0.77	0.58	0.53
p	< 0.05	< 0.05	< 0.05
Beta coeff α	- 0.005	0.006	0.26
Beta coeff NDVI	- 0.88	- .76	- 0.62

When only analyzing the LST-NDVI relationship there is an inverse linear relationship between LST and NDVI of different land use types (R^2adj. = 0.78, 0.85 and 0.47, on 19 June 2013, 27 June 2013 and 25 June 2015, respectively) (Figure 15). The land use types with the lowest NDVI have the highest surface temperatures and the land use types with higher NDVI have lower surface temperatures on all three dates.

The models quantifying the LST–NDVI relation for oil palm plantations had slightly lower fits (R^2adj. = 0.77, 0.58 and 0.53) than derived for all land use types (Figure 15, right panels). The NDVI-LST relation for oil palm plantations is also linearly inverse where younger oil palm plantations, with lower NDVI have higher surface temperatures, and older and mature oil palm plantations with higher NDVI, have lower surface temperatures.

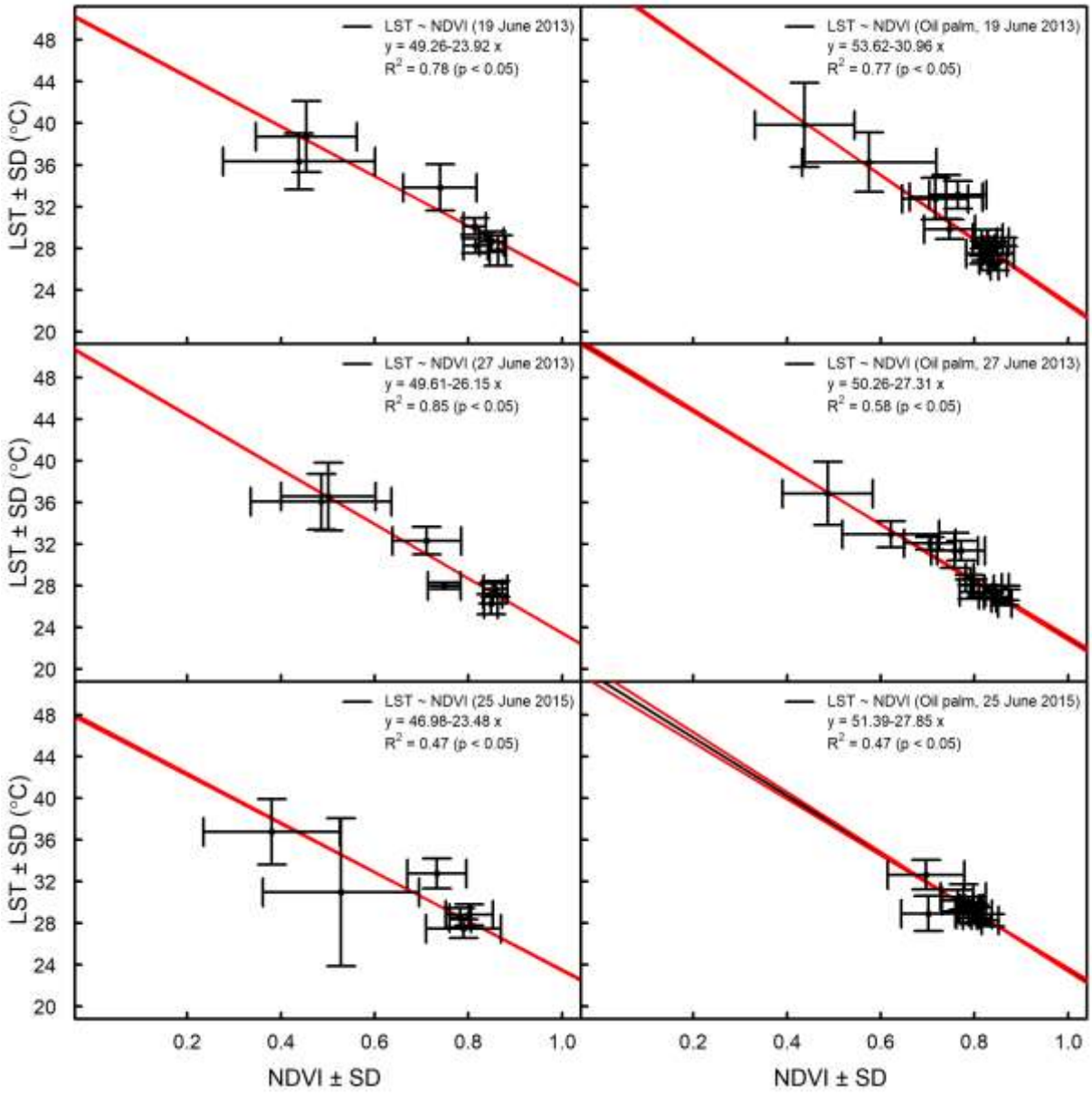

Figure 15. Relation NDVI – LST extracted for 3 different dates : 19 June 2013, 27 June 2013 and 25 June 2015.
Left panels : relation between NDVI and LST of different land use types; right panels: relation between NDVI and LST of oil palm plantations.

3.7 Large scale and long term effects of land transformations at the province level from 2000 – 2015

The average annual LST of Jambi was characterized by a fluctuating but increasing trend during daytime (Figure 16 a, b) between 2000 and 2015. The average morning LST (10:30) increased by 0.07 ºC per year ($R^2 = 0.59$; $p < 0.001$), while the midday afternoon LST (13:30 local time) increased by 0.13 °C per year ($R^2 = 0.35$; $p = 0.02$) between 2003 and 2015. While the daytime LST showed a clear increase, the night and evening LST (22:30 and 01:30, Figure 16c, d) trends showed a small decrease of – 0.02 °C ($R^2 = 0.29$; $p = 0.02$) and – 0.01 °C ($R^2 = 0.05$; $p = 0.50$) per year, respectively. The observed LST trends resulted in a total LST increase of 1.05 °C and 1.56 °C in the morning (10:30) and afternoon (13:30), respectively, and a total decrease of the LST of 0.3 °C (22:30) and 0.12 °C (01:30) at night over the period from 2000 to 2015 in Jambi.

To separate the effect of land use change from global climate warming, we used a site constantly covered by forest over that period (from the forest sites we used in this study) as a reference that was not directly affected by land cover changes. That site showed smaller changes in LST than the entire province: only the mean morning LST (10:30) had a significant but small trend with an increase of 0.03 °C per year ($R^2 = 0.21$, $p < 0.05$) resulting in a total LST increase of 0.45 °C between 2000 and 2015 (Figure 16a). This LST warming is much smaller than the overall warming at provincial level of 1.05 °C. The LST time series at other times showed no significant trends: the mean afternoon LST (13:30) increased by -0.05 °C per year ($R^2 = 0.01$, $p = 0.31$) (Figure 16b), and the night and evening LST by 0.01°C per year (Figure 16 c, d, $p = 0.19$ and $p = 0.60$, respectively).

The mean annual NDVI in Jambi decreased by 0.002 per year, resulting in a total NDVI decrease of 0.03 ($R^2 = 0.34$; $p = 0.01$; Fig. 5e). The NDVI of the forest showed a small but not significant increase of 0.001 per year ($R^2 = 0.04$, $p = 0.23$) (Figure 16e) fluctuating around an NDVI of 0.84.

The mean annual midday air temperature (at 13:00, local time, Figure 16f) and the mean annual night air temperature (at 01:00, local time) increased every year by 0.05 °C and 0.03 °C, respectively, resulting in a total air temperature increase of 0.75 °C ($R^2 = 0.66$, $p < 0.001$) and 0.45 °C ($R^2 = 0.32$, $p = 0.01$) between 2000 and 2015 (Figure 16f).

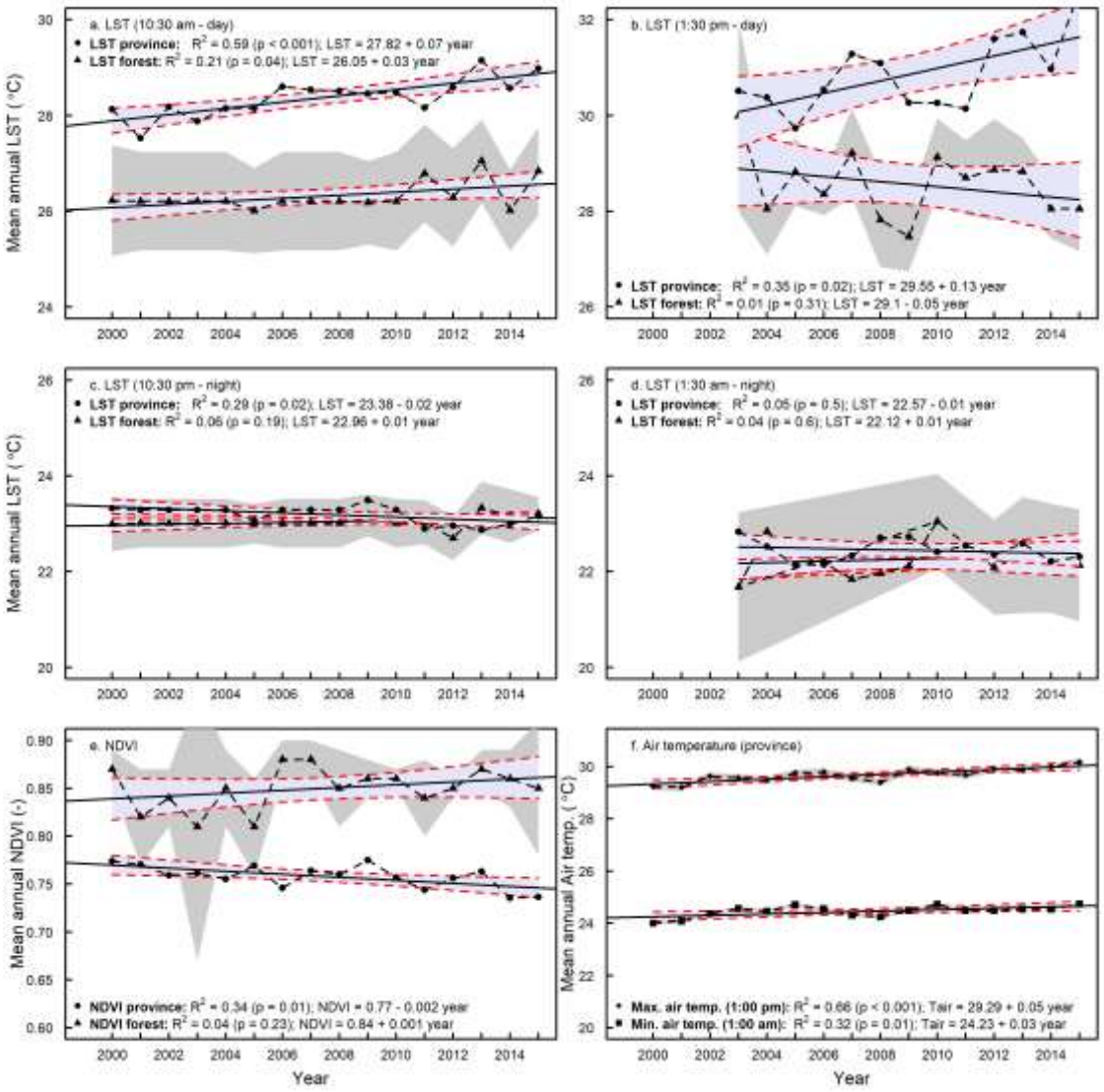

Figure 16. Long term NDVI, LST and air temperature analysis.
Mean annual LST (**a – d**), mean annual NDVI (**e**) and mean annual air temperature trends (**f**) in the Jambi province between 2000 and 2015 derived from MODIS LST (**a** 10:30, **b** 13:30, **c** 22:30 and **d** 01:30, local time), MODIS NDVI and ERA Interim daily air temperature (1:00 and 13:00, local time) data sets, respectively. Grey-shaded areas are the confidence intervals of the means; blue-shaded areas are the confidence intervals of the regression lines. MODIS LST time series for 13:30 and 01:30 were available from the middle of 2002; for this reason we used the complete years from 2003 to 2015.

- *Large scale and long term seasonality analysis*

The relationships in the dry season are stronger than for the wet season as we have much more usable data during the dry season. There are significant differences between LST of the dry and wet season. At 10:30 am the LST increased 0.09 ± 0.02 °C per year during the dry season, while the increase during the wet season was lower (0.06 ± 0.02 °C per year) (Figure 17). Around

1:30 pm the LST increased 0.08 ± 0.03 °C per year, against 0.03 ± 0.02 °C increase per year during the wet season. At 10:30 pm the LST increased 0.03 ± 0.01 °C per year in the dry season, compared to a LST increase of 0.02 ± 0.01 °C in the wet season. At 1:30 am, the LST increased 0.05 ± 0.02 °C in the dry season, while the LST during the wet season increased 0.05 ± 0.03 °C. The increase of the LST at 1:30 pm, 10:30 pm and 1:30 am in the wet season was not significant ($p = 0.12$, $p = 0.06$ and $p= 0.11$, respectively). The significant increase of the LST during the dry season at all 4 times of observations suggests that the warming is more pronounced during the dry season compared to the wet season, which is reasonable as we have more incoming radiation during the dry season. Nevertheless, we prefer to pool the data from the dry and the wet season in order to get more statistically robust relationships.

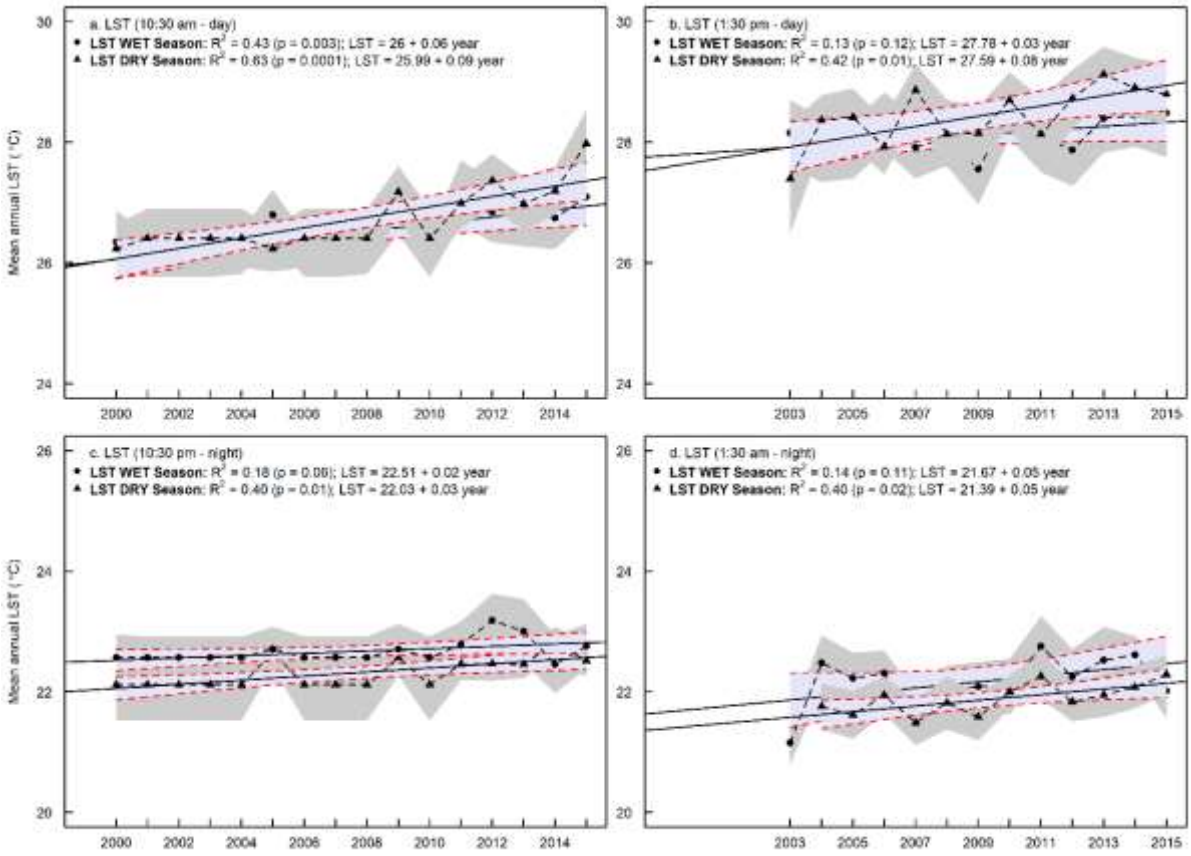

Figure 17. Long term seasonality LST analysis.
Mean annual LST (a – d), in the Jambi province between 2000 and 2015 derived from MODIS LST (5a. 10:30 am, 5b. 1:30 pm, 5c. 10:30 pm and 5d. 1:30 am, local time) in the wet and dry season. Grey-shaded areas are the confidence intervals of the means, blue-shaded areas are the confidence intervals of the regression lines. MODIS LST time series for 1:30 pm and 1:30 am were available from the mid of 2002; for this reason we used the complete years from 2003 till 2015. Wet season: All months except June – September/October; Dry season: June – September/October.

The analysis of the MODIS LST data did not show any anomalous LST that could be attributed to forest fires. This is caused by the mask we applied in selecting the best quality pixels which probably also removed pixels covered by smoke. A seasonality analysis was not possible with Landsat data because there is not enough data.

From Clough et al. (2016) we used the observed LULC for a part of the Jambi province.

Table 13. Land use change (1990) – 2000 – 2010

	Area (km^2)			Cover (%)			Change (%)
LULC	**1990**	**2000**	**2011**	**1990**	**2000**	**2011**	**2011-2000**
other	57.83	34.34	52.41	3.3	2.0	3.0	1.03
bush	84.94	263.86	346.99	4.8	15.1	19.7	4.72
OP	204.22	426.51	504.22	11.6	24.3	28.7	4.40
RU	525.90	666.87	668.67	30.0	38.0	38.1	0.06
FO	881.93	361.45	182.53	50.3	20.6	10.4	-10.22
Total	1754.82	1753.03	1754.82	100	100	100	

Table 14. Contribution of land cover change to total LST increase

	Increase 2000 – 2010*)	ΔLST**) (°C)	Contribution to LST (°C)	Remark
RU	0.001	0.4	0.00	1)
MOP	0.022	0.8	0.02	2)
PF	0.000	2.3	0.00	3)
YOP	0.022	6.0	0.13	4)
UB	0.005	8.5	0.04	5)
CLC	0.029	10.9	0.31	6)
Total	0.079		0.51	
Total observed change	0.102			
Missing	0.024			7)

Remarks/explanation:
*) units in fraction of the land cover, which is calculated as the observed change (%, Table 13) divided by 100
**) warming effect from Figure 11
1) From the observed changes, but seems to be very underestimated, we assume the remaining rubber is mixed with forests as Jungle Rubber
2) MOP = we assume half of the plantations to be mature
3) PF is not included because the area increase is not known
4) YOP = we assume half of the plantations to be young
5) We assume half of “other” to be urban areas (this assumption is already an overestimation)
6) We assume 50% of the bush to be degraded areas and barren and 50% of the class other to be clear cut land
7) 50% of class "bush" is not included, because this class was not part of our study

4 Discussion

Evaluating the use of Landsat and MODIS satellite data for surface temperature retrieval: Landsat compared to MODIS

In this study we retrieved the surface temperature from a Landsat image and compared this with MODIS LST. The results showed a good agreement between both LSTs (Figure 8), which is comparable to other studies and thus gives confidence in our analysis. Bindhu et al. (2013) found also a close relationship between MODIS LST and Landsat LST by using the same aggregation resampling technique as our method and found a R^2 of 0.90, a slope of 0.90, and an intercept of 25.8 °C for LST, compared to our R^2 of 0.8, slope of 1.35 and intercept of –11.58 °C (Figure 8). Zhang and He (2013) validated Landsat LST with MODIS LST and also found good agreements (RMSD 0.71 – 1.87 ºC) between the two sensors, whereas we found a RMSE of 1.71 ºC. Nevertheless, there still are differences and slope versatility between the two satellite sources. These differences are typically caused by differences between the MODIS and Landsat sensors in terms of (a) different sensor properties e.g. spatial and radiometric resolution and sensor calibration; (b) geo-referencing and differences in atmospheric corrections (Li et al., 2004); and (c) emissivity corrections i.e. the use of approximate equations to derive the emissivity from the NDVI from Landsat's red and NIR bands. Li et al. (2004) and Vlassova et al. (2014) identified these same factors in their comparison of ASTER LST with MODIS LST and Landsat LST with MODIS LST, respectively. Vlassova et al. (2014) found good agreements between MODIS and Landsat LST and obtained higher LSTs with MODIS than with Landsat, which they attributed to the delay of 15 minutes in acquisition time between MODIS and Landsat. MODIS LST is measured 15 minutes later and our results showed that MODIS LSTs were indeed higher than Landsat LST. The comparison of MODIS LST with locally measured canopy surface temperatures during the overpass time of MODIS also showed agreement (Figure 5). The slope was possibly related to differences in instrumentation and emissivity corrections and to scale issues; this comparison could corroborate the quality check of MODIS LST. As the MODIS LST product is proven to be accurate within 1 ºC (Silvério et al., 2015; Wan et al., 2004) and has been intensively validated, the use of MODIS LST was a proper way to assess the quality of our Landsat LST.

The errors from the different sources (such as atmospheric correction, emissivity correction, resampling Landsat to MODIS resolution) are difficult to quantify. When we tested the impact of atmospheric correction and emissivity errors on the LST from Landsat retrieval we found that (a) the overall patterns across different land use types did not change, (b) emissivity was the most important factor, although the effects on LST retrieval were small and (c) errors related to atmospheric correction parameters were small because there were minor differences between the default atmospheric correction (ATCOR) parameters and the ATCOR parameters derived with actual local conditions (RH, air pressure and air temperature). Following the method of Coll et al. (2009) and Jiang et al. (2015) we show that the use of the online atmospheric correction parameter calculator is a good option provided that RH, air temperature and air pressure measurements are available. We additionally compared locally measured air temperatures with MODIS air temperature and found a good agreement (Figure 6), which

served as a verification that we used a correct air temperature for the atmospheric correction parameter calculator. Overall, our comparison of Landsat LST with MODIS LST and against ground observations suggests that we are able to retrieve meaningful spatial and temporal patterns of LST in the Jambi province.

LST patterns across different land use and land cover (LULC) types

The land cover types in our study covered a range of land surface types that develop after forest conversion. This is the first study in this region that includes oil palm and rubber as land use types that develop after forest conversion. The coolest temperatures were at the vegetated land cover types while the warmest surface temperatures were on the non-vegetated surface types like urban areas and bare land. Interestingly, the oil palm and rubber plantations were only slightly warmer than the forests whereas the young oil palm plantations had clearly higher LST than the other vegetated surfaces. For other parts of the world, Lim et al. (2005, 2008), Fall et al. (2010) and Weng et al. (2004) also observed cooler temperatures for forests and the highest surface temperatures for barren and urban areas.
In Indonesia, land transformation is often not instantaneous from forest to oil palm or rubber plantation, but can be associated with several years of bare or abandoned land in-between (Sheil et al., 2009). Oil palm plantations typically have a rotation cycle of 25 years, resulting in repeating patterns with young plantations (Dislich et al., 2016). Given the large LST differences between forests and bare soils or young oil palm plantations that we observed, a substantial warming effect of land transformation at regional scale is expected.

Drivers of local differences between different land cover types

All the land cover types (except acacia plantation forests) had a higher albedo than forest, indicating that these land cover types absorbed less incoming solar radiation than forests. Nevertheless, these land cover types were warmer than forests, suggesting that the albedo was not the dominant variable explaining the LST. Indeed, the statistical analysis showed that the correlation between ET and LST was higher than the correlation between albedo and LST. The ΔETs were significant, highlighting that despite their higher albedo, all land cover types had higher LSTs than forests related to lower ET rates than forests. In contrast, forests that absorb more solar radiation because of the lower albedo have lower LST because of the higher ET they exhibit, hereby identifying evaporative cooling as the main determinant of regulating the surface temperature of all vegetation cover types (Li et al., 2015).

Both observational and modeling studies carried out in other geographic regions and with other trajectories support our observations. Observational studies in the Amazonia by Lawrence and Vandecar (2015) on the conversion of natural vegetation to crop or pasture land showed a surface warming effect. Salazar et al. (2015) provided additional evidence that conversion of forest to other types of land use in the Amazonia caused significant reductions in precipitation and increases in surface temperatures.
Alkama and Cescatti (2016) and earlier studies by Loarie et al. (2011a, 2011b) showed that tropical deforestation may increase the LST. Croplands in the Amazonian regions were also

warmer than forests through the reduction of ET (Ban-Weiss et al., 2011; Feddema et al., 2005) and that the climatic response strongly depends on changes in energy fluxes rather than on albedo changes (Loarie et al., 2011a, 2011b). A study by (Silvério et al., 2015) indeed found that tropical deforestation changes the surface energy balance and water cycle and that the magnitude of the change strongly depends on the land uses that follow deforestation. They found that the LST was 6.4 ºC higher over croplands and 4.3 ºC higher over pasture lands compared to the forest they replaced, as a consequence of energy balance shifts. (Ban-Weiss et al., 2011; Davin and de Noblet-Ducoudré, 2010) added that in addition to the reduction of ET, the reduction of surface roughness most likely enhanced the substantial local warming.

Also for non-Amazonian regions, the replacement of forests by crops caused changes comparable with our observations. In temperate Argentina, Houspanossian et al. (2013) found that the replacement of dry forests by crops resulted in an increase of albedo but still forests exhibited cooler canopies than croplands. The cooler canopies were a result of a higher aerodynamic conductance that enhanced the capacity of tree canopies to dissipate heat into the atmosphere, and to both latent and sensible heat fluxes operating simultaneously to cool forest canopies.

In a global analysis Li et al. (2015) showed that tropical forests generally have a low albedo, but still the net energy gain caused by solar energy absorption is offset by a greater latent heat loss via higher ET and that in the tropical forests the high ET cooling completely offsets the albedo warming. For China, this cooling effect was also shown by Peng et al. (2014) who compared LST, albedo and ET of plantation forests, grassland and cropland with forests.

Our findings are also supported by modeling studies. (Beltrán-Przekurat et al., 2012) found for the southern Amazon that conversion of wooded vegetation to soybean plantations caused an increase of the LST due to decreased latent heat and increased sensible heat fluxes. Climate models also show the same warming trends and land surface modeling also projects an increase in surface temperatures following deforestation in the Brazilian Cerrado (Beltrán-Przekurat et al., 2012; Loarie et al., 2011b). In a global analysis, Pongratz et al. (2006) showed a LST increase of forest to cropland or pasture transitions, which was driven by a reduced roughness length and an increased aerodynamic resistance, and that the temperature response is intensified in forest to clear/bare land transitions (1.2 – 1.7 ºC increase). Similar to observational studies, the modeling results of Bathiany et al. (2010) show that ET is the main driver of temperature changes in tropical land areas.

We point here that our study included a ground heat flux, but did not take into account the storage of heat in the soil and the release of stored heat out of the soil during the daily cycle, and the Landsat satellite image was obtained under cloud-free conditions with high shortwave radiation input and low fraction of diffuse radiation. Therefore, the LST retrieved on cloud-free days might be overestimated compared to cloudy days, as the differences in LST between land uses are supposed to be lower when diffuse radiation increases.

The use of a chronosequence of oil palm plantations

In this study we used a chronosequence to study biophysical variables, radiation balance and energy partitioning and their relation with the succession of oil palm plantations. To our knowledge this is the first chronosequence study in this region for oil palm plantations in combination with satellite data. This approach allowed us to study the temporal dynamics of the oil palm plantation development across multiple timescales (Walker et al., 2010). As oil palm plantations follow the same trajectory, this approach is appropriate to study plant succession at decadal time-scales when there is evidence that sites of different ages follow the same trajectory and it provided us the opportunity to study the development of the oil palm plantations over time periods that are longer than direct observations would permit (Walker et al., 2010). Although the satellite data are limited to one-time-of-day measurements, the advantage of using satellite data is that the data are spatially continuous (Moran and Jackson et al. 1989) and the use of the chronosequence in combination with satellite data from 3 different dates enabled us to study the dynamically changing oil palm plantation in multiple ways. The two images that were acquired within 8 days difference (19 June and 27 June 2013) and which were acquired with 2 different sensors (ETM+ and OLI, respectively), allowed us to study the biophysical variables within a short difference in time and can serve as a repeated measurement using different sensors. The use of the satellite image that was acquired 2 years later (25 June 2015) allowed us to study the temporal development of the oil palm plantations and thus allowed a multi date comparison of the biophysical variables.

The oil palm plantations we sampled were all, except one, small scale holder plantations which have smaller areas than the commercial plantations which can sometimes be as large as 10 km^2. One oil palm plantation (12 years old in 2013) from which we sampled a plot and which we used in our chronosequence belongs to a large commercial company. Excluding this plot in the analysis did not have any effects on the observed trends and analysis and we decided to include it in all the analyses. Given that in this mature plantation one meteorological tower is located from which we also used the measurements for our comparison and validation purposes justifies the inclusion of this oil palm plantation in our chronosequence.

The age of the oil palm plantations in the chronosequence we used in combination with the images acquired on 19 June and 27 June 2013 ranged from 0 to 25 years. In the chronosequence that was used with the image acquired on 25 June 2015 the age ranged from 3 to 19 years because we did not conduct a new field survey to include newly established oil palm plantations so that oil palm plantations, between 0 and 2 years are missing in the 2015 chronosequence. Furthermore, oil palm plantations that were under clouds, in cloud shadows or in the scan line gap of the satellite image were also removed from the analysis which was for example the case for oil plantations older than 19 years.

The development of surface biophysical variables in a dynamically changing oil pam vegetation: the effect of oil palm age

Young oil palm plantations are characterized by a higher surface temperature, higher albedo, lower NDVI and lower ET than forests and mature oil palm plantations. Due to their higher albedo they also reflect more incoming solar radiation than forest and mature oil palm plantations (Figure 13a). Despite reflecting more solar radiation, young oil palm plantations have a higher surface temperature which is caused by a lower evaporative cooling effect that dominates the albedo warming effect in tropical regions. This mechanism was already identified in an earlier part of the research (Sabajo et al., 2017) and applied to the young oil palm plantations, the present study confirms that recently established and young oil palm plantations are characterized by reduced evapotranspiration, lower NDVI, higher albedo and higher surface temperatures than mature oil palm plantations and forests. These differences in biophysical variables, in combination with differences in radiation balance and energy partitioning between young, mature oil palm plantations and forests are also reflected in energy partitioning differences: H partitioning is favored above LE partitioning in young plantations whereas this pattern is the reverse in mature oil palm plantations and forests.

Studies in the region confirmed the cooler temperatures of forests compared to oil palm plantations. Forests in Malaysia with mean diurnal temperature of 26.33 °C were cooler than mature and young oil palm plantations (Luskin and Potts, 2011) and forests on Borneo were 6.5 °C cooler than oil palm plantations (Hardwick et al 2015). In Malaysia mature and young oil palm plantations were on average respectively between 2.03 and 2.34 °C and between 2.97 and 4.03 °C warmer than forests and clear cut land was 6.86 °C warmer than forests (Luskin and Potts, 2011) whereas in our study clear cut land, as represented by the initial stage of oil palm plantation , was between 9 and 10°C warmer than forest.

Analogue to research in other geographical or climatological regions e.g. Liu and Randerson (2008), we also found that the increase in surface temperature during the first years of the oil palm plantations cause outgoing longwave radiation to increase and as a consequence lower net radiation during the first years of the oil palm plantation phase.

Field studies and measurements in the same study area of the present study by Meijide et al. (2017) also show the effects of oil palm age on surface biophysical variables, water and energy fluxes in oil palm plantations. Meijide et al. (2017) found a small difference in albedo between a 1-year and a 12-year old oil palm plantation (0.15 ± 0.02 vs. 0.14 ± 0.01, for 1-year and 12-year old, respectively) whereas our results show the same small differences between these two plantations i.e. 0.03 ± 0.01, for the 1 and 12-year old plantation (Figure 12a).
Furthermore Meijide et al. (2017) found that the 1-year old oil palm plantation had less ET (918 ± 46 mm yr^{-1}), higher H and lower LE than a 12-years old mature oil palm plantation. Direct quantitative comparison between Meijide et al. (2017) and our results cannot be made directly, but the consistent trends observed in our research show that ET and LE are lower and H is higher in the young palm phase than in the mature phase, whereas in the mature phase ET and the energy partitioning is reversed. We compared our LE and H for a 1-year and 12-year old oil

palm plantation with LE and H calculated from meteorological data and found that they were in agreement (Sabajo et al., 2017).

For YOP measured LE fluxes were between 215.17 ± 61.05 and 226.22 ± 68.29 W m^{-2} whereas the satellite derived LE for YOP were 288.25 ± 16.80 and 255.13 ± 19.57 Wm^{-2} (for 19 June 2013 and 25 June 2015, respectively). Measured LE fluxes in MOP were between 413.67 ± 109.54 and 441.00 ± 109.76 W m^{-2} whereas we found satellite derived LE fluxes between 355.25 ± 5.09, 251.55 ± 1.97 and 313.83 ± 9.40 (for 19 June 2013, 27 June 2013 and 25 June 2015, respectively).
Measured H fluxes in YOP were between 138.34 ± 50.85 and 140.57 ± 51.32 W m^{-2} (Meijide et al., 2017) whereas our satellite derived H fluxes were between 145.57 ± 8.29, 67.98 ± 4.85 W m^{-2} (for 19 June 2013 and 25 June 2015, respectively). In MOP Meijide et al. (2017) measured H fluxes between 90.11 ± 32.64 and 97.25 ± 33.56 W m^{-2} whereas we found satellite derived H fluxes of 134.71 ± 2.26, 53.75 ± 1.01 and 52.27 ± 5.71 W m^{-2} (for 19 June 2013, 27 June 2013 and 25 June 2015, respectively).

In another research in the same study area a wider range of oil palm plantations with different ages between 2 and 25 years was used with results that also showed that the transpiration in oil palm plantation was different between plantations of different ages (Röll et al., 2015). ET was the lowest in the youngest oil palm plantation (2 years old: 0.2 mm day^{-1}) and increased with age to a relatively constant ET of 1.3 mm day^{-1} (Röll et al., 2015). The findings of the field studies of Meijide et al. (2017) and Röll et al. (2015) are consistent with our findings but we must point out that in the present study we included the same oil palm plantations (Table 1) of their studies and show that our remote sensing based findings are in agreement with the field results.

Even though our multi date analysis and comparison of biophysical variables, radiation balance and energy partitioning of different aged oil palm plantations showed a consistent age related trend that is in agreement with empirical research, we mention that the H fluxes might be overestimated, and the LE fluxes might be underestimated in young oil palm plantations. This could be the case for partial cover canopies because in partial cover canopies LST is actually composed of the temperatures of the plants, soil and shaded areas which result in measurements of the LST that are dominated by the soil surface rather than by the transpiring vegetation (Moran et al., 1989).

LST-NDVI relationship: the effect of oil palm age

Using NDVI as an indicator of vegetation abundance Weng et al. (2004) (for the US) and Yue et al. (2007) for China, found that areas with a high mean NDVI had a lower LST than areas with a low mean NDVI, therefore suggesting that vegetation abundance is an important factor in controlling the LST through higher ET rates.
For different land use types and for oil palm plantations we found a negative relation between NDVI and LST which is in agreement with Goetz (1997) who, for grasslands in the United States, found a close negative relation between the NDVI and the LST. For different sensors

among which TM, Goetz (1997) found consistent inverse relationships between the NDVI and LST. We show that this relationship also applies to ETM+ and OLI images. Our LST-NDVI analysis which show patterns of vegetated areas with high NDVI having lower surface temperatures and areas with lower NDVI such as urban areas and clear-cut land have higher surface temperatures are consistent on all 3 dates. This pattern is also consistent for oil palm plantations, where young oil palm plantations with lower NDVI have higher surface temperatures and older and mature plantations with higher NDVI have lower surface temperatures (Figure 15). The LST-NDVI relation for oil palm plantations derived from the image acquired on 25 June 2015 shows a smaller range of the NDVI and LST because the all plantations are 2 years older in this image and age range was between 3 and 19 years. This smaller age range was due to not having conducted a new survey to include newly established oil palm plantations and due to the mask we applied mask to removed cloud and cloud shadows pixels which also removed some oil palm plantations.
In an earlier part of this research it was shown that ET is the main determinant of the LST (Sabajo et al., 2017). We excluded the albedo because our analysis already showed that NDVI was more correlated to LST than albedo to LST. As ET is higher in vegetated areas the high correlation between LST and NDVI, the consistent inverse LST-NDVI correlations found for oil palm plantations in this research support our assumption that the LST-NDVI relationship could serve as a direct measure to study the development of oil palm plantations and serve as a substitute for the LST-ET relationship.

Large scale consequences of land transformations at the province level from 2000 – 2015

The increases of the mean surface temperature in Jambi were stronger during the morning (10:30) and afternoon (13:30 than during the evening (22:30) and night (01:30). Given that our results show a decrease of the NDVI in the same period, suggests that the observed increased trend of the day time LST can be attributed to the land cover changes that occurred. Our assumption that the observed decreasing NDVI trend is caused by land conversions is supported by two different studies which reported that in Jambi, between 2000 and 2011 (Drescher et al., 2016) and between 2000 and 2013 (Clough et al., 2016), the forest area decreased and that the largest increases were for rubber, oil palm, and agricultural and tree crop areas. The class 'other land use types', which includes urban areas, showed a minor increase (around 1%), suggesting that the decrease in NDVI was most likely caused by forest cover loss and not by urban expansion (Table 13 and Table 14). The same observations on LULC change in Indonesia were also done by Lee et al. (2011), Margono et al. (2012, 2014) and Luskin et al. (2014). Luskin et al. (2014) showed that in Jambi, during the period 2000 – 2010, forests decreased by 17% while oil palm and rubber area increased by 85% and 19%, respectively.

Given these trends in LULC changes, the observed LST trends were most likely caused by gradual decrease of forest cover loss at the expense of agriculture and croplands. Our assumptions are supported by findings of (Silvério et al., 2015), Costa et al. (2007), Oliveira et al. (2013), Spracklen et al. (2012) and Salazar et al. (2015) that indicate that land use transitions in deforested areas likely have a strong influence on regional climate. Alkama and Cescatti (2016) show that biophysical effects of forest cover changes can substantially affect the local

climate by altering the average temperature, which is consistent with our observations and can be related to the observed land use change in the Jambi province. As Indonesia has undergone high rates of forest cover loss from 2000 to 2012 (Margono et al., 2014), these findings support our assumptions that the observed LST increase in the Jambi province was most likely caused by the observed land use changes.

To separate the effect of global warming from land-use-change-induced warming, we considered areas with permanent and large enough forests as a reference where changes are mainly because of global warming. We find that LST of forests shows either no significant trends (at 13:30, 22:30, 01:30 h) or just a clearly smaller increase of 0.03 °C per year at 10:30. The difference between the LST trend of the province and of the forest at 10:30 was 0.04 °C per year, resulting in a ΔLST of 0.6 °C between the province and forest in the period 2000 and 2015. We point out that our MODIS analysis has a larger proportion of data from the dry season compared from the wet season, as there were more cloud-free conditions during the dry season. Thus, our reported warming effect reflects cloud-free conditions. During cloudy conditions, particularly in the wet season, the warming effect is expected to be lower. The seasonality analysis showed that the relationships in the dry season are stronger than for the wet season (Figure 17), which suggests that the warming is more pronounced during the dry season compared to the wet season, which is reasonable as we have more incoming radiation during the dry season.

With the warming effects we found between forest and other land cover types (ΔLST, Figure 11a) and the observed land cover changes by Clough et al. (2016) and Drescher et al. (2016) (Table 13 and Table 14), we estimated the contribution of all land cover types (except forest) to the ΔLST of the province between 2000 and 2015 to be 0.51°C out of the observed 0.6°C, which also supports our assumption that the LST increase in Jambi was for 85% driven by land cover changes (Table 13 and Table 14), with clear-cut areas having a large contribution as they have the largest warming effect.

The observed small but significant increase in LST of forests of 0.03 °C per year at 10:30 reflects a LST change independent of land cover changes, as the forest remained unchanged over that time period. A potential driver of that LST increase is the general global air temperature trend because of changes in radiative forcing or border effects (advection from warmer land uses), which is similar to the 1994 - 2014 time series analysis of Kayet et al. (2016), who showed a LST increase for all land cover types ranging from wasted land, agriculture land, open forest, dense forest, water bodies and built-up areas.

The observed trends of the provincial air temperature (Figure 16f) were significant, suggesting that a general warming due to global and regional effects contributes to the observed warming at the provincial level during day and nighttime, but that it is smaller than the land cover change induced effects (Table 13 and Table 14) at the provincial level (Figure 16a & b).
In our long-term analysis on the regional effects of land use change we observed an increase in the mean LST and mean air temperature in the 2000 - 2015 period, concurrent with a decrease of the NDVI. The warming observed from MODIS LST data and from the air temperature

obtained from the independent ERA-Interim reanalysis in the Jambi province are most likely caused by the observed decrease of the forest area and an increase of oil palm, rubber and other cash crop areas in the same period, with other effects such as radiative forcing changes and additional natural effects playing a smaller role. Given the plans of the Indonesian government to expand oil palm production with a projected additional demand of 1 to 28 Mha in 2020 (Wicke et al., 2011), the strong warming effect we show for Jambi may serve as an indication of future LST changes for other regions of Indonesia that will undergo land transformations towards oil palm plantations.

A recent study by (Tölle et al., 2017) showed that for Southeast Asia, land use change at large scale may not only increase surface temperature but also impact other aspects of local and regional weather and climate, including in regions remote from the original landscape disturbance. Their results also indicate that land clearings can amplify the response to climatic extreme events such as El Niño Southern Oscillation (ENSO). The observed effects of land use change on the biophysical variables may have implications for ecosystem services in the Jambi province beyond a pure warming effect. The high precipitation in this region in combination with the reduced vegetation cover of bare land and young oil palm plantations impose risks of soil erosion caused by surface run off. Less water infiltration into the soil, thereby decreasing the soil water storage, may lead to low water availability in the dry season (Dislich et al., 2016; Merten et al., 2016). High surface temperatures in combination with low water availability may make the vegetation and the surroundings more vulnerable to fires.

In assessing the climatic effects of LULCC on local and regional climatic effects we have considered the warming effects of the major land use types that develop after forest conversion which included the effects of clear cut land, young oil palm and mature oil palm plantations. Our survey however shows that along the oil palm rotation cycle different warming effects were observed which suggests that different effects should be taken into account in evaluating the climatic effects of the dynamically changing vegetation. Quantifying the climatic impacts of oil palm plantations and the dynamically changing nature of oil palm plantations is therefore challenging because information on the age class distribution of large scale commercial and small scale holders and information on the spatial heterogeneity within the oil palm cultivation due to different size, shapes and location is lacking. We therefore suggest modeling approaches to assess the climatic effects during the oil palm rotation cycle.

Applications

Even though the results show that in the mature phase the biophysical variables, radiation balance and energy partitioning of oil palm plantations seem to reach near-forest conditions mature oil palm plantation will never reach the stability of forest conditions (Luskin and Pots, 2011) because biophysical forcings that occur with land alterations will disappear if the land reverts to pre-conditions (Zhao and Jackson, 2013). Given that oil palm is an important and well established economic source in Indonesia it is highly possible that oil palm plantations will not be reverted back to the pre-condition state of forests. Our results suggest the potential of including management practices in drastically reducing the adverse and harsh conditions that

occur after clearing and land preparation for the new oil palm rotation cycle. Due to the rotation nature of oil palm cultivation, the knowledge on the harsh environmental conditions in the initial years should be considered when establishing new plantations or when re-initiating a new oil palm rotation cycle. Luskin and Potts (2011) for example, suggested to introduce a variable retention method in the management which leaves mature palm trees during the initial conversion and convert the rest after 5 – 10 years after the crop has started, thereby creating a patch work of different age plantations, reducing the patch and field size and increasing the total habitat variety and complementarity in the landscape. Initial results of ongoing biodiversity enrichment in the study area (Gérard et al., 2017; Teuscher et al., 2016) to include tree islands in the plantations show that including them is a way of increasing the biodiversity does not affect yield significantly (Gérard et al., 2017). The results are however in the initial phase and need to be work out to an operational level. Although their research was designed as a biodiversity enrichment experiment, including tree islands can also have positive effects on the microclimate and serve as a buffering function within the plantation, especially during initial phases where an effect known as the oasis effect caused by advection of sensible heat from the surrounding warmer areas (Hao et al., 2016; Potchter et al., 2008) increases the evapotranspiration in the vegetated area, in our case the tree islands, and causes more cooling which can occur during the day and night.

We must point out that oil palm cultivation is not only the domain of the professional large scale farming by trained agronomists but also the domain of small scale holders who, independently or under the assistance of extension services try to make a living out of the palm oil cultivation and that oil palm is not the only type of agricultural land use in the province. We focused on the expansion of oil palm plantations because this is the land use type that had the largest expansion in Jambi. But also other types of land use changes occurred in Jambi, which we included in this research but did not focus on in much detail (e.g. rubber and acacia plantations) or did not include and did not focus on at all in this research (e.g. other types of agricultural land use). In achieving or introducing new management practices in oil palm cultivation all stakeholders should be reached and informed. But the findings of our research can also be applied to other types of land use e.g. the rubber and acacia forest plantations which also have a rotation and harvest cycle after the trees become mature and unproductive or ready for harvest.

5 Conclusion

We evaluated the use of Landsat and MODIS satellite data to derive the surface temperature as sources of reliable surface temperature estimation for Jambi. The comparison of LST from both sources with each other, supported with comparison of MODIS LST with field measured canopy LST and with comparison of MODIS air temperature and field measured air temperature shows that we were able to derive reliable surface temperature estimates for Jambi. As expected, vegetated land use types had lower surface temperatures than non-vegetated or sparsely vegetated land use types. Age differences, as observed between young and mature oil palm plantations, were reflected in differences in LST between these types of vegetation.

From the biophysical variables we derived from satellite data and the analysis of the biophysical impacts of deforestation we found a local warming effect after forests are transformed to cash or tree croplands (oil palm, rubber, acacia) in the Jambi province of Sumatra. The warming effect after forest conversion results from the reduced evaporative cooling, which was identified as the main determinant of regulating the surface temperature and which can be explained as follows: (a) reduction of ET decreases surface cooling, (b) reduced surface roughness reduces air mixing in the surface layer and thus vertical heat fluxes, (c) changes in albedo change the net radiation, and (d) changes in energy partitioning in sensible and latent heat and heat storage. The effect is an increase of the mean temperatures that leads to warming effects in all tropical climatic zones (Alkama and Cescatti, 2016). Our analysis enabled us to identify the mechanisms that explain the surface temperature changes caused by alterations of biophysical variables and supported our hypothesis that in regulating the LST there are cooling and warming processes that determine the LST. This process is dependent on the vegetation cover because locations where the albedo warming effect is dominated by the evaporative cooling effect had lower LST.

In assessing the long-term effects of land transformation on regional scale, we saw that the effects of land cover changes that occurred between 2000 and 2015 are reflected back in an increase of the LST in Jambi in the same time period. The increase was accompanied by a decrease of the NDVI and an increase of the air temperature in Jambi. The warming effect induced by land cover change clearly exceeded the global warming effect.

Furthermore, we studied the relation between the age and biophysical variables, radiation balance and energy partitioning during the rotation cycle of oil palm plantations. Our results show that the change of the biophysical variables is caused by an increase in vegetation cover as the plantations mature, which confirm the hypothesis that as the oil palm plantation develops there is a consistent age dependent relationship between the age of oil palm plantations and the surface biophysical variables. The previously identified mechanisms that regulate the local climate are applicable in regulating the local climate and the changes in biophysical variables in during the rotation cycle of oil palm plantations and are summarized in Figure 18. The development of the vegetation cover itself in time causes the changes and shifts of the biophysical variables, radiation balance and energy partitioning. The initial conditions of oil palm plantations are extreme and become less extreme and develop to near forest conditions as the plantations matures.

There is a strong consistent inverse relation between the NDVI and the LST of oil palm plantations. NDVI and LST can be directly derived from remote sensing data and can be used to replace ET estimations from remote sensing when the required information for ET processing is missing. The NDVI-LST relation that was found for oil palm plantations can facilitate an easier analysis of the oil palm plantations.

This is the first to include the oil palm and rubber expansion in Indonesia. In Indonesia, smallholders take 40% of the land under oil palm cultivation for their account (Dislich et al., 2016). Because the landscape in Jambi is characterized by a small-scale smallholder-dominated mosaic, including rubber and oil palm monocultures (Clough et al., 2016), studies using medium- to coarse-resolution data are not able to capture the small-scale changes and processes at the small-scale level. By using high-resolution Landsat data we were able to include the effects of land use change on biophysical variables and the underlying processes of the small-scale holder agriculture. Understanding the effects of land cover change on the biophysical variables may support policies regarding conservation of the existing forests, planning and expansion of the oil palm plantations and possible afforestation measures.
Knowledge of biophysical variables, radiation balance and energy partitioning during the rotation cycle of oil palm can be used to including new management practices that could reduce the extreme environmental and microclimatic conditions in the initial phase of the oil palm plantations and also to other types of plantations.

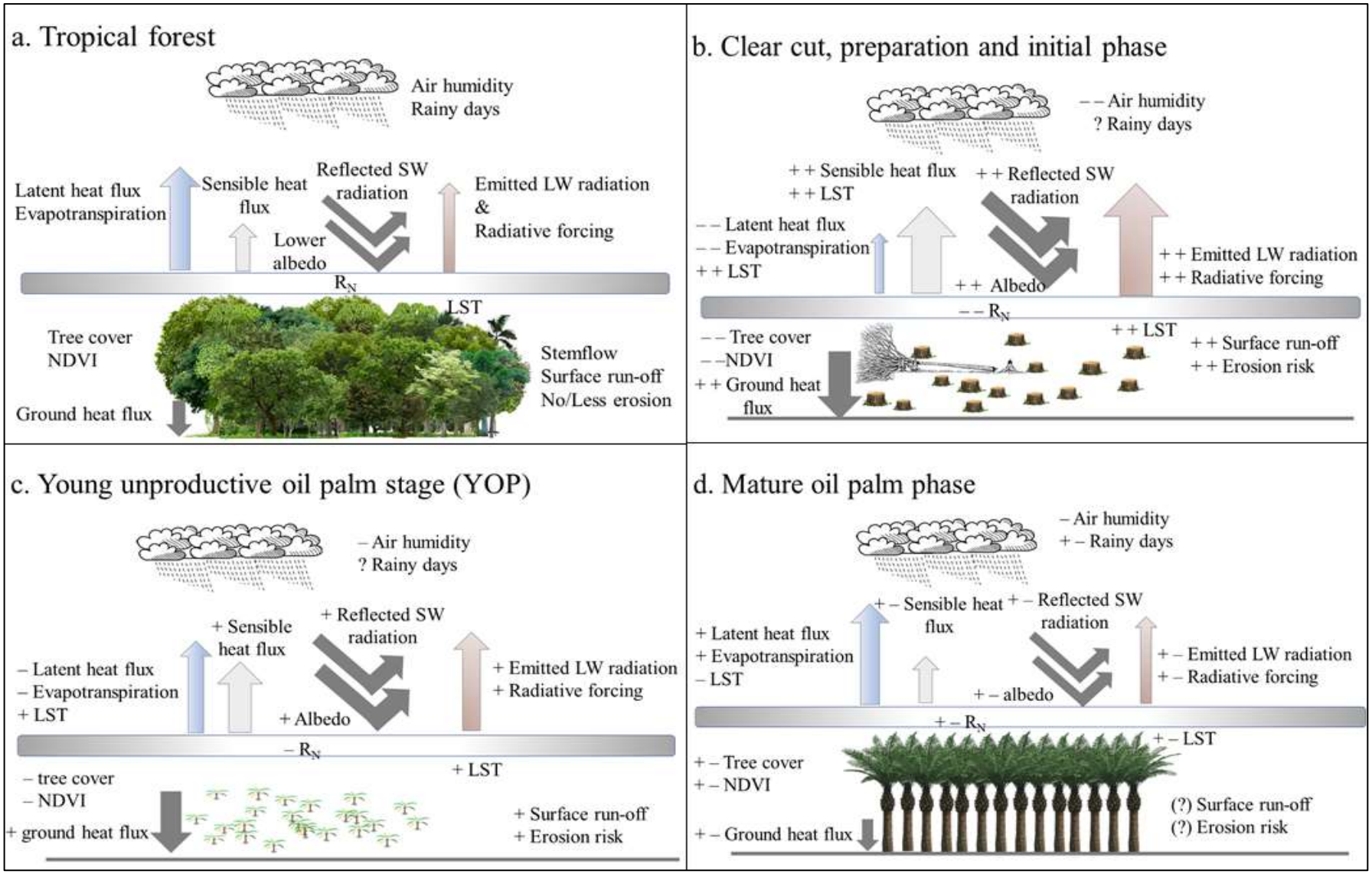

Figure 18. Summarizing / descriptive figure.

Acknowledgements

I thank the supervisors for their supervision, both on location and from distance.
This research was funded by the Erasmus Mundus Joint Doctorate Programme Forest and Nature for Society (EMJD FONASO). Additional funding was provided by the German Research Foundation (DFG) through the CRC 990 “EFForTS, Ecological and Socioeconomic Functions of Tropical Lowland Rainforest Transformation Systems (Sumatra, Indonesia)” (subproject A03). I therefor thank both EMJD-FONASO and DFG/CRC 990 for making this research possible. Administrative procedures, assistance and guidance during my stay in Indonesia was done by the CRC-office in Bogor and in Jambi, to whom I also express my gratitude. During the field work I was assisted by Huta Julu Bagus Putra, a.k.a. Monang, whose assistance was of great value because without his assistance and translation I would not be able to collect the field information or make the necessary appointments. Furthermore I thank everyone who contributed, scientifically and non-scientifically, in any way to achieve this result.

References

Alkama, R. and Cescatti, A.: Biophysical climate impacts of recent changes in global forest cover, Science, 351(6273), 600–604, doi:10.1126/science.aac8083, 2016.

Arneth, A.: Uncertain future for vegetation cover, Nature, 524, 44, 2015.

Awal, M. A. and Wan Ishak, W. .: Measurement of Oil Palm LAI by manual and LAI-2000 Method, Asian J. Sci. Res., 1(1), 49–56, doi:10.3923/ajsr.2008.49.56, 2008.

Ban-Weiss, G. A., Bala, G., Cao, L., Pongratz, J. and Caldeira, K.: Climate forcing and response to idealized changes in surface latent and sensible heat, Environ. Res. Lett., 6(3), 034032, doi:10.1088/1748-9326/6/3/034032, 2011.

Barsi, J. A., Barker, J. L. and Schott, J. R.: An Atmospheric Correction Parameter Calculator for a Single Thermal Band Earth-Sensing Instrument, Geosci. Remote Sens. Symp. 2003 IGARSS 03 Proc. 2003 Inst. Electr. Electron. Eng. IEEE Int., 5, 3014–3016 vol.5, doi:10.1109/IGARSS.2003.1294665, 2003.

Barsi, J. A., Schott, J. R., Palluconi, F. D. and Hook, S. J.: Validation of a web-based atmospheric correction tool for single thermal band instruments, Proc SPIE Earth Obs. Syst. X, 5882, doi:10.1117/12.619990, 2005.

Bastiaanssen, W. G. .: SEBAL-based sensible and latent heat fluxes in the irrigated Gediz Basin, Turkey, J. Hydrol., 229(1–2), 87–100, doi:10.1016/S0022-1694(99)00202-4, 2000.

Bastiaanssen, W. G. M., Menenti, M., Feddes, R. A. and Holtslag, A. A. M.: A remote sensing surface energy balance algorithm for land (SEBAL) - 1. Formulation, J. Hydrol., 212(1–4), 198–212, doi:10.1016/s0022-1694(98)00253-4, 1998a.

Bastiaanssen, W. G. M., Pelgrum, H., Wang, J., Ma, Y., Moreno, J. F., Roerink, G. J. and van der Wal, T.: A remote sensing surface energy balance algorithm for land (SEBAL).: Part 2: Validation, J. Hydrol., 212–213, 213–229, doi:10.1016/S0022-1694(98)00254-6, 1998b.

Bathiany, S., Claussen, M., Brovkin, V., Raddatz, T. and Gayler, V.: Combined biogeophysical and biogeochemical effects of large-scale forest cover changes in the MPI earth system model, Biogeosciences, 7(5), 1383–1399, doi:10.5194/bg-7-1383-2010, 2010.

Beltrán-Przekurat, A., Pielke Sr, R. A., Eastman, J. L. and Coughenour, M. B.: Modelling the effects of land-use/land-cover changes on the near-surface atmosphere in southern South America, Int. J. Climatol., 32(8), 1206–1225, doi:10.1002/joc.2346, 2012.

Bindhu, V. M., Narasimhan, B. and Sudheer, K. P.: Development and verification of a non-linear disaggregation method (NL-DisTrad) to downscale MODIS land surface temperature to the spatial scale of Landsat thermal data to estimate evapotranspiration, Remote Sens. Environ., 135, 118–129, doi:10.1016/j.rse.2013.03.023, 2013.

Boisier, J. P., de Noblet-Ducoudré, N. and Ciais, P.: Historical land-use-induced evapotranspiration changes estimated from present-day observations and reconstructed land-cover maps, Hydrol. Earth Syst. Sci., 18(9), 3571–3590, doi:10.5194/hess-18-3571-2014, 2014.

Bonan, G. B.: Forests and Climate Change: Forcings, Feedbacks, and the Climate Benefits of Forests, Science, 320(5882), 1444–1449, doi:10.1126/science.1155121, 2008.

Bridhikitti, A. and Overcamp, T. J.: Estimation of Southeast Asian rice paddy areas with different ecosystems from moderate-resolution satellite imagery, Agric. Ecosyst. Environ., 146(1), 113–120, doi:10.1016/j.agee.2011.10.016, 2012.

Bright, R. M., Zhao, K., Jackson, R. B. and Cherubini, F.: Quantifying surface albedo and other direct biogeophysical climate forcings of forestry activities, Glob. Change Biol., 21(9), 3246–3266, doi:10.1111/gcb.12951, 2015.

Bulcock, H. H. and Jewitt, G. P. W.: Spatial mapping of leaf area index using hyperspectral remote sensing for hydrological applications with a particular focus on canopy interception, Hydrol. Earth Syst. Sci., 14(2), 383–392, doi:10.5194/hess-14-383-2010, 2010.

Carlson, K. M., Curran, L. M., Asner, G. P., Pittman, A. M., Trigg, S. N. and Marion Adeney, J.: Carbon emissions from forest conversion by Kalimantan oil palm plantations, Nat. Clim. Change, 3(3), 283–287, doi:10.1038/nclimate1702, 2013.

Clough, Y., Krishna, V. V., Corre, M. D., Darras, K., Denmead, L. H., Meijide, A., Moser, S., Musshoff, O., Steinebach, S., Veldkamp, E., Allen, K., Barnes, A. D., Breidenbach, N., Brose, U., Buchori, D., Daniel, R., Finkeldey, R., Harahap, I., Hertel, D., Holtkamp, A. M., Hörandl, E., Irawan, B., Jaya, I. N. S., Jochum, M., Klarner, B., Knohl, A., Kotowska, M. M., Krashevska, V., Kreft, H., Kurniawan, S., Leuschner, C., Maraun, M., Melati, D. N., Opfermann, N., Pérez-Cruzado, C., Prabowo, W. E., Rembold, K., Rizali, A., Rubiana, R., Schneider, D., Tjitrosoedirdjo, S. S., Tjoa, A., Tscharntke, T. and Scheu, S.: Land-use choices follow profitability at the expense of ecological functions in Indonesian smallholder landscapes, Nat. Commun., 7, doi:10.1038/ncomms13137, 2016.

Coll, C., Wan, Z. and Galve, J. M.: Temperature-based and radiance-based validations of the V5 MODIS land surface temperature product, J. Geophys. Res., 114(D20102), doi:10.1029/2009JD012038, 2009.

Coll, C., Galve, J. M., Sanchez, J. M. and Caselles, V.: Validation of Landsat-7/ETM+ Thermal-Band Calibration and Atmospheric Correction With Ground-Based Measurements, IEEE Trans. Geosci. Remote Sens., 48(1), 547–555, doi:10.1109/TGRS.2009.2024934, 2010.

Corley, R. H. V. and Tinker, P. B.: The oil palm, 5th ed., Blackwell Publishing Ltd., Oxford., 2015.

Costa, M. H., Yanagi, S. N. M., Souza, P. J. O. P., Ribeiro, A. and Rocha, E. J. P.: Climate change in Amazonia caused by soybean cropland expansion, as compared to caused by pastureland expansion, Geophys. Res. Lett., 34(7), doi:10.1029/2007GL029271, 2007.

Dale, V. H., Efroymson, R. A. and Kline, K. L.: The land use-climate change-energy nexus, Landsc. Ecol., 26(6), 755–773, doi:10.1007/s10980-011-9606-2, 2011.

Davin, E. L. and de Noblet-Ducoudré, N.: Climatic Impact of Global-Scale Deforestation: Radiative versus Nonradiative Processes, J. Clim., 23(1), 97–112, doi:10.1175/2009JCLI3102.1, 2010.

Dee, D. P., Uppala, S. M., Simmons, A. J., Berrisford, P., Poli, P., Kobayashi, S., Andrae, U., Balmaseda, M. A., Balsamo, G., Bauer, P., Bechtold, P., Beljaars, A. C. M., van de Berg, L., Bidlot, J., Bormann, N., Delsol, C., Dragani, R., Fuentes, M., Geer, A. J., Haimberger, L., Healy, S. B., Hersbach, H., Hólm, E. V., Isaksen, L., Kållberg, P., Köhler, M., Matricardi, M., McNally, A. P., Monge-Sanz, B. M., Morcrette, J.-J., Park, B.-K., Peubey, C., de Rosnay, P., Tavolato, C., Thépaut, J.-N. and Vitart, F.: The ERA-Interim reanalysis: configuration and performance of the data assimilation system, Q. J. R. Meteorol. Soc., 137(656), 553–597, doi:10.1002/qj.828, 2011.

Dislich, C., Keyel, A. C., Salecker, J., Kisel, Y., Meyer, K. M., Auliya, M., Barnes, A. D., Corre, M. D., Darras, K., Faust, H., Hess, B., Klasen, S., Knohl, A., Kreft, H., Meijide, A., Nurdiansyah, F., Otten, F., Pe'er, G., Steinebach, S., Tarigan, S., Tölle, M. H., Tscharntke, T. and Wiegand, K.: A review of the ecosystem functions in oil palm plantations, using forests as a reference system, Biol. Rev., doi:10.1111/brv.12295, 2016.

Drescher, J., Rembold, K., Allen, K., Beckschäfer, P., Buchori, D., Clough, Y., Faust, H., Fauzi, A. M., Gunawan, D., Hertel, D., Irawan, B., Jaya, I. N. S., Klarner, B., Kleinn, C., Knohl, A., Kotowska, M. M., Krashevska, V., Krishna, V., Leuschner, C., Lorenz, W., Meijide, A., Melati, D., Nomura, M., Pérez-Cruzado, C., Qaim, M., Siregar, I. Z., Steinebach, S., Tjoa, A., Tscharntke, T., Wick, B., Wiegand, K., Kreft, H. and Scheu, S.: Ecological and socio-economic functions across tropical land use systems after rainforest conversion, Philos. Trans. R. Soc. Lond. B Biol. Sci., 371(1694), doi:10.1098/rstb.2015.0275, 2016.

Evrendilek, F., Berberoglu, S., Karakaya, N., Cilek, A., Aslan, G. and Gungor, K.: Historical spatiotemporal analysis of land-use/land-cover changes and carbon budget in a temperate peatland (Turkey) using remotely sensed data, Appl. Geogr., 31(3), 1166–1172, 2011.

Fall, S., Niyogi, D., Gluhovsky, A., Pielke, R. A., Kalnay, E. and Rochon, G.: Impacts of land use land cover on temperature trends over the continental United States: assessment using the North American Regional Reanalysis, Int. J. Climatol., 30(13), 1980–1993, doi:10.1002/joc.1996, 2010.

FAO: Global Forest Resources Assessment 2010: main report, Food and Agriculture Organization of the United nations, Rome., 2010.

Feddema, J. J., Oleson, K. W., Bonan, G. B., Mearns, L. O., Buja, L. E., Meehl, G. A. and Washington, W. M.: The Importance of Land-Cover Change in Simulating Future Climates, Science, 310(5754), 1674–1678, doi:10.1126/science.1118160, 2005.

Gérard, A., Wollni, M., Hölscher, D., Irawan, B., Sundawati, L., Teuscher, M. and Kreft, H.: Oil-palm yields in diversified plantations: Initial results from a biodiversity enrichment experiment in Sumatra, Indonesia, Agric. Ecosyst. Environ., 240, 253–260, doi:https://doi.org/10.1016/j.agee.2017.02.026, 2017.

Gerritsma, W. and Soebagyo, F. X.: An analysis of the growth of leaf area of oil palms in Indonesia, Exp. Agric., 35(03), 293–308, 1999.

Goetz, S. J.: Multi-sensor analysis of NDVI, surface temperature and biophysical variables at a mixed grassland site, Int. J. Remote Sens., 18(1), 71–94, doi:10.1080/014311697219286, 1997.

Hao, X., Li, W. and Deng, H.: The oasis effect and summer temperature rise in arid regions - case study in Tarim Basin, Sci. Rep., 6, 35418, 2016.

Hardwick, S. R., Toumi, R., Pfeifer, M., Turner, E. C., Nilus, R. and Ewers, R. M.: The relationship between leaf area index and microclimate in tropical forest and oil palm plantation: Forest disturbance drives changes in microclimate, Agric. For. Meteorol., 201(0), 187–195, doi:10.1016/j.agrformet.2014.11.010, 2015.

Hoffmann, W. A. and Jackson, R. B.: Vegetation–Climate Feedbacks in the Conversion of Tropical Savanna to Grassland, J. Clim., 13(9), 1593–1602, doi:10.1175/1520-0442(2000)013<1593:VCFITC>2.0.CO;2, 2000.

Houspanossian, J., Nosetto, M. and Jobbágy, E. G.: Radiation budget changes with dry forest clearing in temperate Argentina, Glob. Change Biol., 19(4), 1211–1222, doi:10.1111/gcb.12121, 2013.

Huete, A. .: A soil-adjusted vegetation index (SAVI), Remote Sens. Environ., 25(3), 295–309, doi:10.1016/0034-4257(88)90106-X, 1988.

Idso, S. B. and Jackson, R. D.: Thermal radiation from the atmosphere, J. Geophys. Res., 74(23), 5397–5403, doi:10.1029/JC074i023p05397, 1969.

Jiang, Y., Fu, P. and Weng, Q.: Assessing the Impacts of Urbanization-Associated Land Use/Cover Change on Land Surface Temperature and Surface Moisture: A Case Study in the Midwestern United States, Remote Sens., 7(4), 4880–4898, doi:10.3390/rs70404880, 2015.

Jung, M., Reichstein, M., Margolis, H. A., Cescatti, A., Richardson, A. D., Arain, M. A., Arneth, A., Bernhofer, C., Bonal, D., Chen, J. Q., Gianelle, D., Gobron, N., Kiely, G., Kutsch, W., Lasslop, G., Law, B. E., Lindroth, A., Merbold, L., Montagnani, L., Moors, E. J., Papale, D., Sottocornola, M., Vaccari, F. and Williams, C.: Global patterns of land-atmosphere fluxes of carbon dioxide, latent heat, and sensible heat derived from eddy covariance, satellite, and meteorological observations, J. Geophys. Res.-Biogeosciences, 116, doi:10.1029/2010jg001566, 2011.

Kayet, N., Pathak, K., Chakrabarty, A. and Sahoo, S.: Spatial impact of land use/land cover change on surface temperature distribution in Saranda Forest, Jharkhand, Model. Earth Syst. Environ., 2(3), 1–10, doi:10.1007/s40808-016-0159-x, 2016.

Koh, L. P., Miettinen, J., Liew, S. C. and Ghazoul, J.: Remotely sensed evidence of tropical peatland conversion to oil palm, Proc. Natl. Acad. Sci., 108(12), 5127–5132, 2011.

Kongsager, R. and Reenberg, A.: Contemporary land-use transitions: The global oil palm expansion., [online] Available from: www.globallandproject.org, 2012.

Lawrence, D. and Vandecar, K.: Effects of tropical deforestation on climate and agriculture, Nat. Clim. Change, 5(1), 27–36, doi:10.1038/nclimate2430, 2015.

Lee, X., Goulden, M. L., Hollinger, D. Y., Barr, A., Black, T. A., Bohrer, G., Bracho, R., Drake, B., Goldstein, A., Gu, L., Katul, G., Kolb, T., Law, B. E., Margolis, H., Meyers, T., Monson, R., Munger, W., Oren, R., Paw U, K. T., Richardson, A. D., Schmid, H. P., Staebler, R., Wofsy, S. and Zhao, L.: Observed increase in local cooling effect of deforestation at higher latitudes, Nature, 479(7373), 384–387, doi:10.1038/nature10588, 2011.

van Leeuwen, T. T., Frank, A. J., Jin, Y., Smyth, P., Goulden, M. L., van der Werf, G. R. and Randerson, J. T.: Optimal use of land surface temperature data to detect changes in tropical forest cover, J. Geophys. Res., 116(G02002), doi:10.1029/2010JG001488, 2011.

Li, F., Jackson, T. J., Kustas, W. P., Schmugge, T. J., French, A. N., Cosh, M. H. and Bindlish, R.: Deriving land surface temperature from Landsat 5 and 7 during SMEX02/SMACEX, Remote Sens. Environ., 92(4), 521–534, doi:10.1016/j.rse.2004.02.018, 2004.

Li, Y., Zhao, M., Motesharrei, S., Mu, Q., Kalnay, E. and Li, S.: Local cooling and warming effects of forests based on satellite observations, Nat. Commun., 6 [online] Available from: http://dx.doi.org/10.1038/ncomms7603, 2015.

Liang, S.: Narrowband to broadband conversions of land surface albedo I: Algorithms, Remote Sens. Environ., 76(2), 213–238, doi:10.1016/S0034-4257(00)00205-4, 2000.

Lim, Y.-K., Cai, M., Kalnay, E. and Zhou, L.: Observational evidence of sensitivity of surface climate changes to land types and urbanization, Geophys. Res. Lett., 32(22), doi:10.1029/2005GL024267, 2005.

Lim, Y.-K., Cai, M., Kalnay, E. and Zhou, L.: Impact of Vegetation Types on Surface Temperature Change, J. Appl. Meteorol. Climatol., 47(2), 411–424, doi:10.1175/2007JAMC1494.1, 2008.

Liu, H. and Randerson, J. T.: Interannual variability of surface energy exchange depends on stand age in a boreal forest fire chronosequence, J. Geophys. Res. Biogeosciences, 113(G101006), doi:10.1029/2007JG000483, 2008.

Loarie, S. R., Lobell, D. B., Asner, G. P., Mu, Q. and Field, C. B.: Direct impacts on local climate of sugar-cane expansion in Brazil, Nat. Clim. Change, 1(2), 105–109, doi:10.1038/nclimate1067, 2011a.

Loarie, S. R., Lobell, D. B., Asner, G. P. and Field, C. B.: Land-Cover and Surface Water Change Drive Large Albedo Increases in South America, Earth Interact., 15(7), 1–16, doi:10.1175/2010EI342.s1, 2011b.

Longobardi, P., Montenegro, A., Beltrami, H. and Eby, M.: Deforestation Induced Climate Change: Effects of Spatial Scale, PLoS ONE, 11(4), e0153357, doi:10.1371/journal.pone.0153357, 2016.

Luskin, M. S. and Potts, M. D.: Microclimate and habitat heterogeneity through the oil palm lifecycle, Basic Appl. Ecol., 12(6), 540–551, doi:10.1016/j.baae.2011.06.004, 2011.

Luskin, M. S., Christina, E. D., Kelley, L. C. and Potts, M. D.: Modern Hunting Practices and Wild Meat Trade in the Oil Palm Plantation-Dominated Landscapes of Sumatra, Indonesia, Hum. Ecol., 42(1), 35–45, doi:10.1007/s10745-013-9606-8, 2014.

Mahmood, R., Pielke, R. A., Hubbard, K. G., Niyogi, D., Dirmeyer, P. A., McAlpine, C., Carleton, A. M., Hale, R., Gameda, S., Beltrán-Przekurat, A., Baker, B., McNider, R., Legates, D. R., Shepherd, M., Du, J., Blanken, P. D., Frauenfeld, O. W., Nair, U. S. and Fall, S.: Land cover changes and their biogeophysical effects on climate, Int. J. Climatol., 34(4), 929–953, doi:10.1002/joc.3736, 2014.

Margono, B. A., Turubanova, S., Zhuravleva, I., Potapov, P., Tyukavina, A., Baccini, A., Goetz, S. and Hansen, M. C.: Mapping and monitoring deforestation and forest degradation in Sumatra (Indonesia) using Landsat time series data sets from 1990 to 2010, Environ. Res. Lett., 7(034010), doi:10.1088/1748-9326/7/3/034010, 2012.

Margono, B. A., Potapov, P. V., Turubanova, S., Stolle, F. and Hansen, M. C.: Primary forest cover loss in Indonesia over 2000-2012, Nat. Clim Change, 4(8), 730–735, doi:10.1038/nclimate2277, 2014.

Marlier, M. E., DeFries, R., Pennington, D., Nelson, E., Ordway, E. M., Lewis, J., Koplitz, S. N. and Mickley, L. J.: Future fire emissions associated with projected land use change in Sumatra, Glob. Change Biol., 21(1), 345–362, doi:10.1111/gcb.12691, 2015.

Meijide, A., Röll, A., Fan, Y., Herbst, M., Niu, F., Tiedemann, F., June, T., Rauf, A., Hölscher, D. and Knohl, A.: Controls of water and energy fluxes in oil palm plantations: Environmental variables and oil palm age, Agric. For. Meteorol., 239, 71–85, doi:10.1016/j.agrformet.2017.02.034, 2017.

Meijide, A., Badu, C. S., Moyano, F., Tiralla, N., Gunawan, D. and Knohl, A.: Impact of forest conversion to oil palm and rubber plantations on microclimate and the role of the 2015 ENSO event, Agric. For. Meteorol., 252, 208–219, doi:https://doi.org/10.1016/j.agrformet.2018.01.013, 2018.

Merten, J., Röll, A., Guillaume, T., Meijide, A., Tarigan, S., Agusta, H., Dislich, C., Dittrich, C., Faust, H., Gunawan, D., Hein, J., Hendrayanto, Knohl, A., Kuzyakov, Y., Wiegand, K. and Hölscher, D.: Water scarcity and oil palm expansion: social views and environmental processes, Ecol. Soc., 21(2), doi:10.5751/ES-08214-210205, 2016.

Miettinen, J., Shi, C. and Liew, S. C.: Deforestation rates in insular Southeast Asia between 2000 and 2010, Glob. Change Biol., 17(7), 2261–2270, doi:10.1111/j.1365-2486.2011.02398.x, 2011.

Miettinen, J., Hooijer, A., Wang, J., Shi, C. and Liew, S. C.: Peatland degradation and conversion sequences and interrelations in Sumatra, Reg. Environ. Change, 12(4), 729–737, doi:10.1007/s10113-012-0290-9, 2012.

Mildrexler, D. J., Zhao, M. and Running, S. W.: A global comparison between station air temperatures and MODIS land surface temperatures reveals the cooling role of forests, J. Geophys. Res., 116(G03025), doi:10.1029/2010JG001486, 2011.

Miyamoto, M.: Forest conversion to rubber around Sumatran villages in Indonesia: Comparing the impacts of road construction, transmigration projects and population, For. Policy Econ., 9(1), 1–12, doi:10.1016/j.forpol.2005.01.003, 2006.

Moran, M. S., Jackson, R. D., Raymond, L. H., Gay, L. W. and Slater, P. N.: Mapping surface energy balance components by combining landsat thematic mapper and ground-based meteorological data, Remote Sens. Environ., 30(1), 77–87, doi:https://doi.org/10.1016/0034-4257(89)90049-7, 1989.

Niu, F., Röll, A., Hardanto, A., Meijide, A., Köhler, M., Hendrayanto and Hölscher, D.: Oil palm water use: calibration of a sap flux method and a field measurement scheme, Tree Physiol., 35(5), 563–573, 2015.

Nosetto, M. D., Jobbágy, E. G. and Paruelo, J. M.: Land-use change and water losses: the case of grassland afforestation across a soil textural gradient in central Argentina, Glob. Change Biol., 11(7), 1101–1117, doi:10.1111/j.1365-2486.2005.00975.x, 2005.

Obidzinski, K., Andriani, R., Komarudin, H. and Andrianto, A.: Environmental and Social Impacts of Oil Palm Plantations and their Implications for Biofuel Production in Indonesia, Ecol. Soc., 17(1), doi:10.5751/ES-04775-170125, 2012.

Oliveira, L. J. C., Costa, M. H., Soares-Filho, B. S. and Coe, M. T.: Large-scale expansion of agriculture in Amazonia may be a no-win scenario, Environ. Res. Lett., 8(024021), doi:10.1088/1748-9326/8/2/024021, 2013.

Paterson, R. R. M., Kumar, L., Taylor, S. and Lima, N.: Future climate effects on suitability for growth of oil palms in Malaysia and Indonesia, Sci. Rep., 5, 14457, 2015.

Peng, S.-S., Piao, S., Zeng, Z., Ciais, P., Zhou, L., Li, L. Z. X., Myneni, R. B., Yin, Y. and Zeng, H.: Afforestation in China cools local land surface temperature, Proc. Natl. Acad. Sci., 111(8), 2915–2919, doi:10.1073/pnas.1315126111, 2014.

Pongratz, J., Bounoua, L., DeFries, R. S., Morton, D. C., Anderson, L. O., Mauser, W. and Klink, C. A.: The Impact of Land Cover Change on Surface Energy and Water Balance in Mato Grosso, Brazil, Earth Interact., 10(19), 1–17, doi:10.1175/EI176.1, 2006.

Potchter, O., Goldman, D., Kadish, D. and Iluz, D.: The oasis effect in an extremely hot and arid climate: The case of southern Israel, J. Arid Environ., 72(9), 1721–1733, doi:10.1016/j.jaridenv.2008.03.004, 2008.

Röll, A., Niu, F., Meijide, A., Hardanto, A., Hendrayanto, Knohl, A. and Hölscher, D.: Transpiration in an oil palm landscape: effects of palm age, Biogeosciences, 12(19), 5619–5633, doi:10.5194/bg-12-5619-2015, 2015.

Sabajo, C. R., le Maire, G., June, T., Meijide, A., Roupsard, O. and Knohl, A.: Expansion of oil palm and other cash crops causes an increase of the land surface temperature in the Jambi province in Indonesia, Biogeosciences, 14(20), 4619–4635, doi:10.5194/bg-14-4619-2017, 2017.

Salazar, A., Baldi, G., Hirota, M., Syktus, J. and McAlpine, C.: Land use and land cover change impacts on the regional climate of non-Amazonian South America: A review, Glob. Planet. Change, 128, 103–119, doi:10.1016/j.gloplacha.2015.02.009, 2015.

Salazar, A., Katzfey, J., Thatcher, M., Syktus, J., Wong, K. and McAlpine, C.: Deforestation changes land–atmosphere interactions across South American biomes, Glob. Planet. Change, 139, 97–108, doi:10.1016/j.gloplacha.2016.01.004, 2016.

Sheil, D., Casson, A., Meijaard, E., Van Noordwjik, M., Gaskell, J., Sunderland-Groves, J., Wertz, K. and Kanninen, M.: The impacts and opportunities of oil palm in Southeast Asia: What do we know and what do we need to know?, Center for International Forestry Research (CIFOR), Bogor, Indonesia, Bogor, Indonesia. [online] Available from: doi: 10.17528/cifor/002792, 2009.

Silvério, D. V., Brando, P. M., Macedo, M. N., Beck, P. S. A., Bustamante, M. and Coe, M. T.: Agricultural expansion dominates climate changes in southeastern Amazonia: the overlooked

non-GHG forcing, Environ. Res. Lett., 10(104015), doi:10.1088/1748-9326/10/10/104015, 2015.

Snyder, W. C., Wan, Z., Zhang, Y. and Feng, Y.-Z.: Classification-based emissivity for land surface temperature measurement from space, Int. J. Remote Sens., 19(14), 2753–2774, doi:10.1080/014311698214497, 1998.

Sobrino, J. A., Jiménez-Muñoz, J. C. and Paolini, L.: Land surface temperature retrieval from LANDSAT TM 5, Remote Sens. Environ., 90(4), 434–440, doi:10.1016/j.rse.2004.02.003, 2004.

Sobrino, J. A., Jiménez-Muñoz, J. C., Zarco-Tejada, P. J., Sepulcre-Cantó, G. and de Miguel, E.: Land surface temperature derived from airborne hyperspectral scanner thermal infrared data, Remote Sens. Environ., 102(1–2), 99–115, doi:10.1016/j.rse.2006.02.001, 2006.

Sobrino, J. A., Jimenez-Muoz, J. C., Soria, G., Romaguera, M., Guanter, L., Moreno, J., Plaza, A. and Martinez, P.: Land Surface Emissivity Retrieval From Different VNIR and TIR Sensors, IEEE Trans. Geosci. Remote Sens., 46(2), 316–327, doi:10.1109/TGRS.2007.904834, 2008.

Spracklen, D. V., Arnold, S. R. and Taylor, C. M.: Observations of increased tropical rainfall preceded by air passage over forests, Nature, 489(7415), 282–285, doi:10.1038/nature11390, 2012.

Teuscher, M., Gérard, A., Brose, U., Buchori, D., Clough, Y., Ehbrecht, M., Hölscher, D., Irawan, B., Sundawati, L., Wollni, M. and Kreft, H.: Experimental Biodiversity Enrichment in Oil-Palm-Dominated Landscapes in Indonesia, Front. Plant Sci., 7, 1538, doi:10.3389/fpls.2016.01538, 2016.

Tölle, M. H., Engler, S. and Panitz, H.-J.: Impact of Abrupt Land Cover Changes by Tropical Deforestation on Southeast Asian Climate and Agriculture, J. Clim., 30(7), 2587–2600, doi:10.1175/JCLI-D-16-0131.1, 2017.

Verstraeten, W. W., Veroustraete, F. and Feyen, J.: Estimating evapotranspiration of European forests from NOAA-imagery at satellite overpass time: Towards an operational processing chain for integrated optical and thermal sensor data products, Remote Sens. Environ., 96(2), 256–276, doi:10.1016/j.rse.2005.03.004, 2005.

Vlassova, L., Perez-Cabello, F., Nieto, H., Martín, P., Riaño, D. and de la Riva, J.: Assessment of Methods for Land Surface Temperature Retrieval from Landsat-5 TM Images Applicable to Multiscale Tree-Grass Ecosystem Modeling, Remote Sens., 6, 4345–4368, doi:10.3390/rs6054345, 2014.

Voogt, J. A. and Oke, T. R.: Effects of urban surface geometry on remotely-sensed surface temperature, Int. J. Remote Sens., 19(5), 895–920, doi:10.1080/014311698215784, 1998.

Walker, L. R., Wardle, D. A., Bardgett, R. D. and Clarkson, B. D.: The use of chronosequences in studies of ecological succession and soil development, J. Ecol., 98(4), 725–736, doi:10.1111/j.1365-2745.2010.01664.x, 2010.

Wan, Z., Zhang, Y., Zhang, Q. and Li, Z.-L.: Quality assessment and validation of the MODIS global land surface temperature, Int. J. Remote Sens., 25(1), 261–274, doi:10.1080/0143116031000116417, 2004.

Wang, J., Pan, F., Soininen, J., Heino, J. and Shen, J.: Nutrient enrichment modifies temperature-biodiversity relationships in large-scale field experiments, Nat. Commun., 7, 13960, doi:10.1038/ncomms13960, 2016.

Weng, Q.: Thermal infrared remote sensing for urban climate and environmental studies: Methods, applications, and trends, ISPRS J. Photogramm. Remote Sens., 64(4), 335–344, doi:10.1016/j.isprsjprs.2009.03.007, 2009.

Weng, Q., Lu, D. and Schubring, J.: Estimation of land surface temperature–vegetation abundance relationship for urban heat island studies, Remote Sens. Environ., 89(4), 467–483, doi:10.1016/j.rse.2003.11.005, 2004.

Wicke, B., Sikkema, R., Dornburg, V. and Faaij, A.: Exploring land use changes and the role of palm oil production in Indonesia and Malaysia, Land Use Policy, 28(1), 193–206, doi:10.1016/j.landusepol.2010.06.001, 2011.

Wukelic, G. E., Gibbons, D. E., Martucci, L. M. and Foote, H. P.: Radiometric calibration of Landsat Thematic Mapper thermal band, Remote Sens. Environ., 28(0), 339–347, doi:10.1016/0034-4257(89)90125-9, 1989.

Yue, W., Xu, J., Tan, W. and Xu, L.: The relationship between land surface temperature and NDVI with remote sensing: application to Shanghai Landsat 7 ETM+ data, Int. J. Remote Sens., 28(15), 3205–3226, doi:10.1080/01431160500306906, 2007.

Zhang, Z. and He, G.: Generation of Landsat surface temperature product for China, 2000–2010, Int. J. Remote Sens., 34(20), 7369–7375, doi:10.1080/01431161.2013.820368, 2013.

Zhao, K. and Jackson, R. B.: Biophysical forcings of land-use changes from potential forestry activities in North America, Ecol. Monogr., 84(2), 329–353, doi:10.1890/12-1705.1, 2013.

Zhou, X. and Wang, Y.-C.: Dynamics of Land Surface Temperature in Response to Land-Use/Cover Change, Geogr. Res., 49(1), 23–36, doi:10.1111/j.1745-5871.2010.00686.x, 2011.

Zulkifli, H., Halimah, M., Chan, K. W., Choo, Y. M. and Basri, M. W.: Life cycle assessment for oil palm fresh fruit bunch production from continued land use for oil palm planted mineral soil (Part 2), J. Oil Palm Res., 22, 887–894, 2010.

Annexes

A1. Satellite data and weather condition parameters

Table A1.1 Satellite data and weather condition parameters

	19 June 2013	**27 June 2013**	**25 June 2015**
Rp	2.68	4.74	4.77
TNB	0.67	0.43	0.40
Rsky	4.25	6.94	6.85
Sun elevation	52.72899385	53.63797454	53.25271790
Sensor	LE7	LC8	LE7
sza	0.6505501773		0.641361064
dr	0.96776103	0.9677683	0.967206363
Swin calculated with SEBAL	705.349698		423.772863
eA	0.860761367		0.857811014
Lwin (W m^{-2})	403.287806		399.352201
U_st	0.256096747		0.305285137
U_{200} (m s^{-1})	3.87651001		5.32900002
Local time	10:13	10:19	10:17
Tair	28.35+273.15	28.90+273.15	27.87+273.15
Ux = u_{1m}	1.0 m/s (PeKa)		1.9
Applied filters	-	-	T < 292
Tower measurements			
Cumulative rain 7 days	Max 2 mm	Max 2.5 mm	Max. 0.5 mm
Atcor input			
Local time (UTM)	3:13	3:19	3:17
Input (lat / lon)	-1.966 / 102.601	-1.966 / 102.601	-1.693 / 103.391
Surface altitude (km)	0.046	0.049	0.051
Surface pressure (mb)	1002.900	1007.050	1005.300
Surface temperature (°C)	28.350	28.900	27.870
Surface relative humidity (%)	50.900	75.425	75.550
Atcor output			
Band average atmospheric transmission	0.67	0.43	0.40
Effective bandpass upwelling radiance (W m^{-2} sr-1 μm^{-1})	2.68	4.74	4.77
Effective bandpass downwelling radiance (W m^{-2} sr-1 μm^{-1})	4.25	6.94	6.85

A2. Rainfall analysis

All images had a dry period of at least 7 days prior to the images were taken

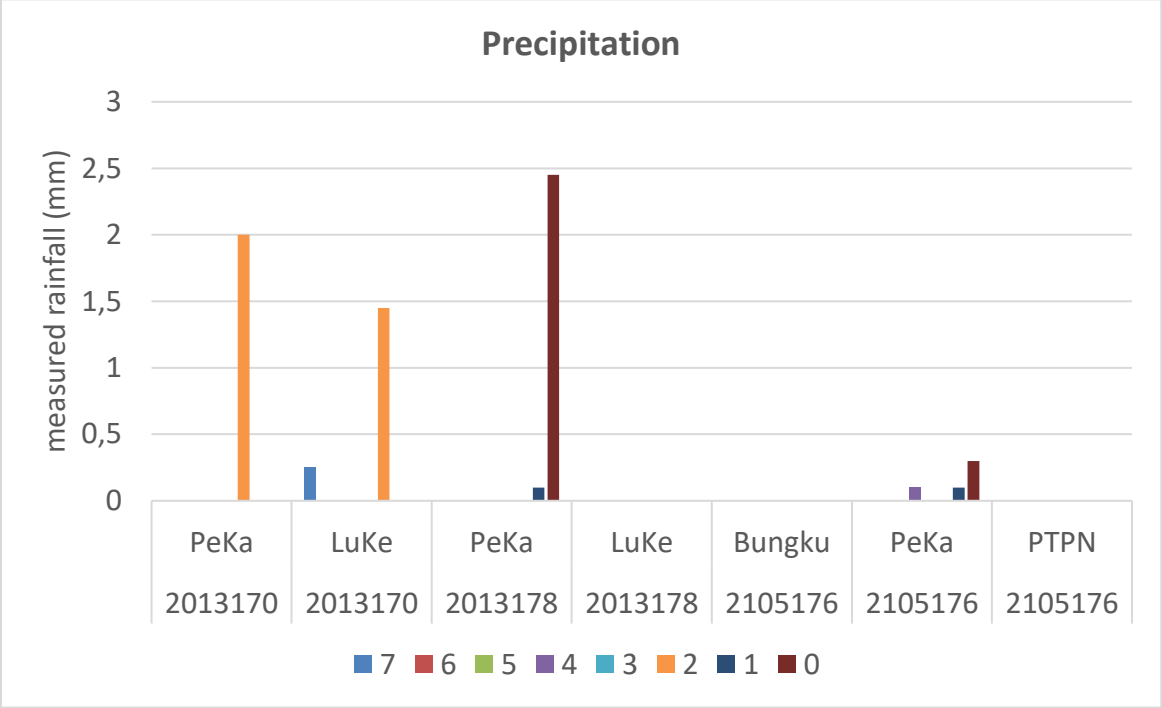

Fig. A2.1 Rainfall analysis 7 days prior to the satellite image acquisition.

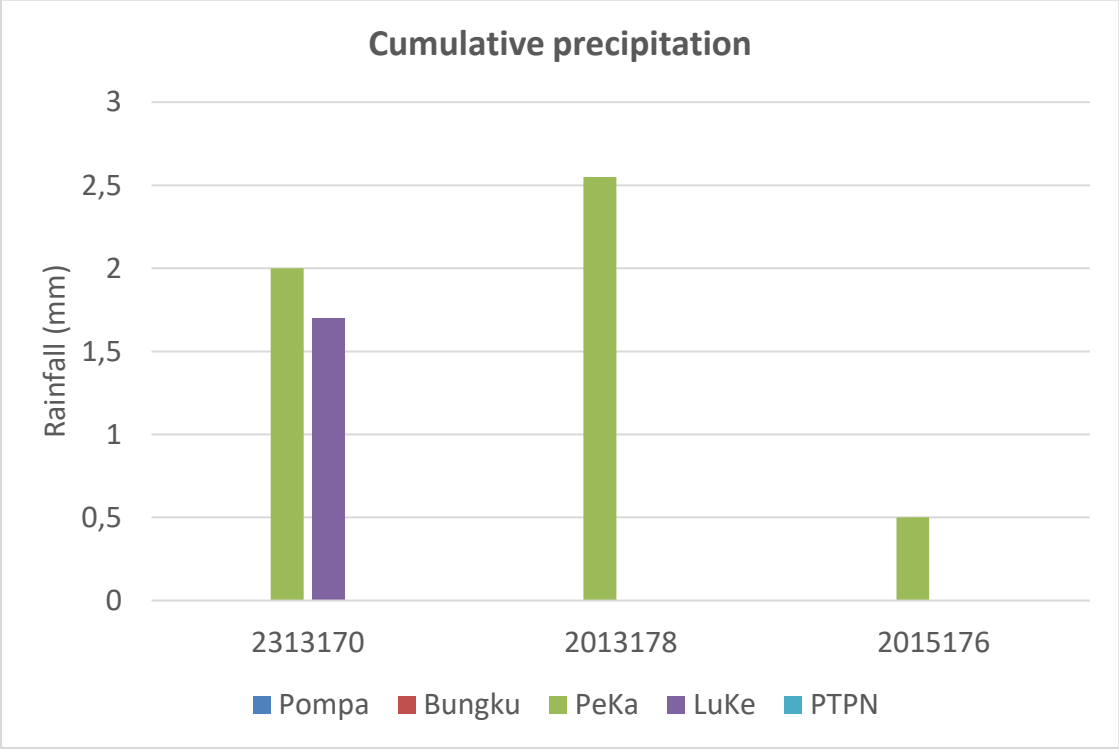

Fig. A2.2 Cumulative rainfall analysis 7 days prior to the satellite image acquisition.

A3. Mean LST, NDVI, Albedo and NDVI for 7 land cover types

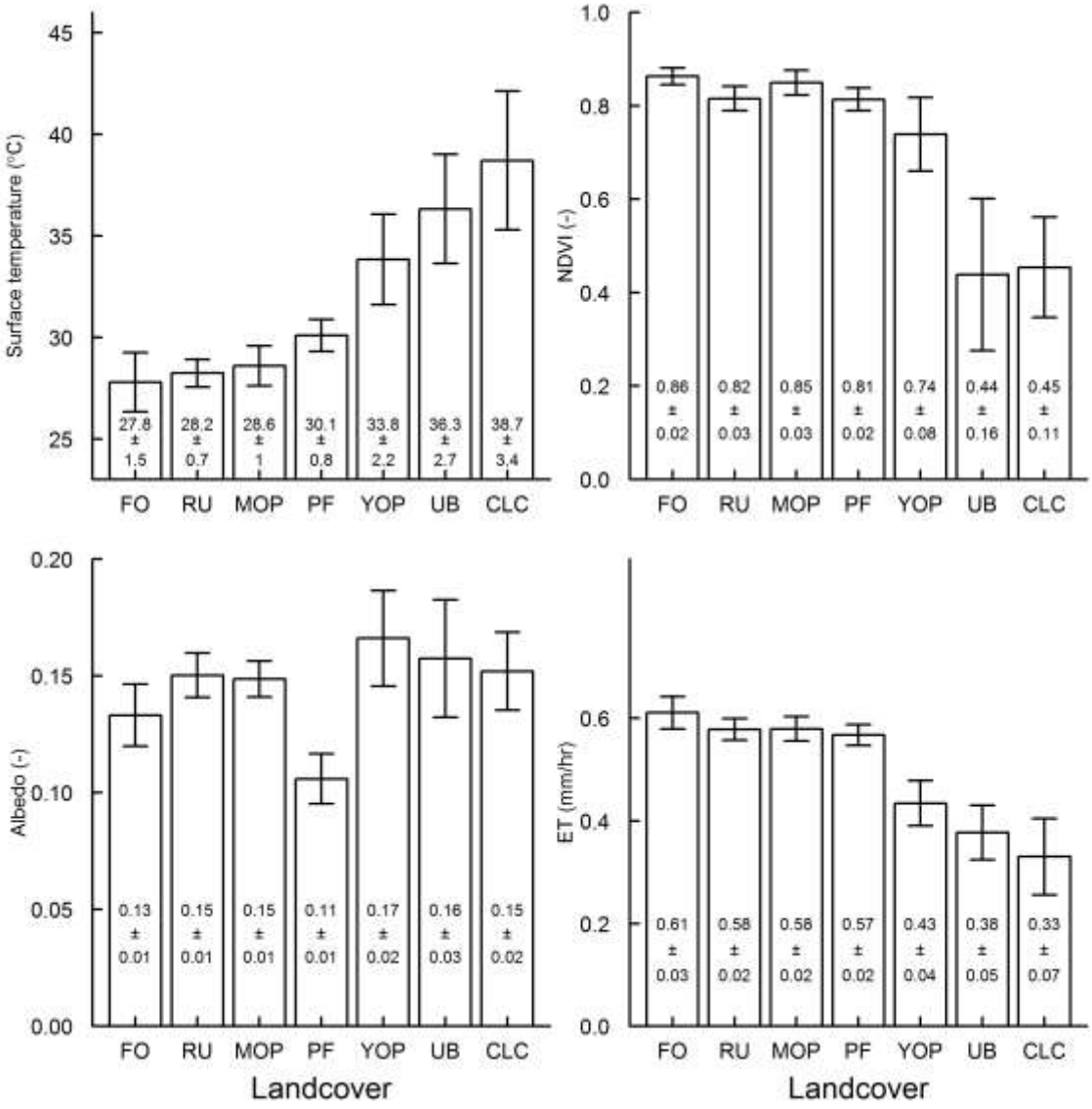

Fig. A3.1 Mean LST, NDVI, Albedo and NDVI extracted from Landsat LST images for 7 land cover types. The values were extracted from small plots that could only be used for Landsat images. (Landsat image was acquired on 19 June 2013 at 10:30 am local time).

A4. Difference in LST, NDVI, albedo and ET between Forest (FO) and 6 other land cover types

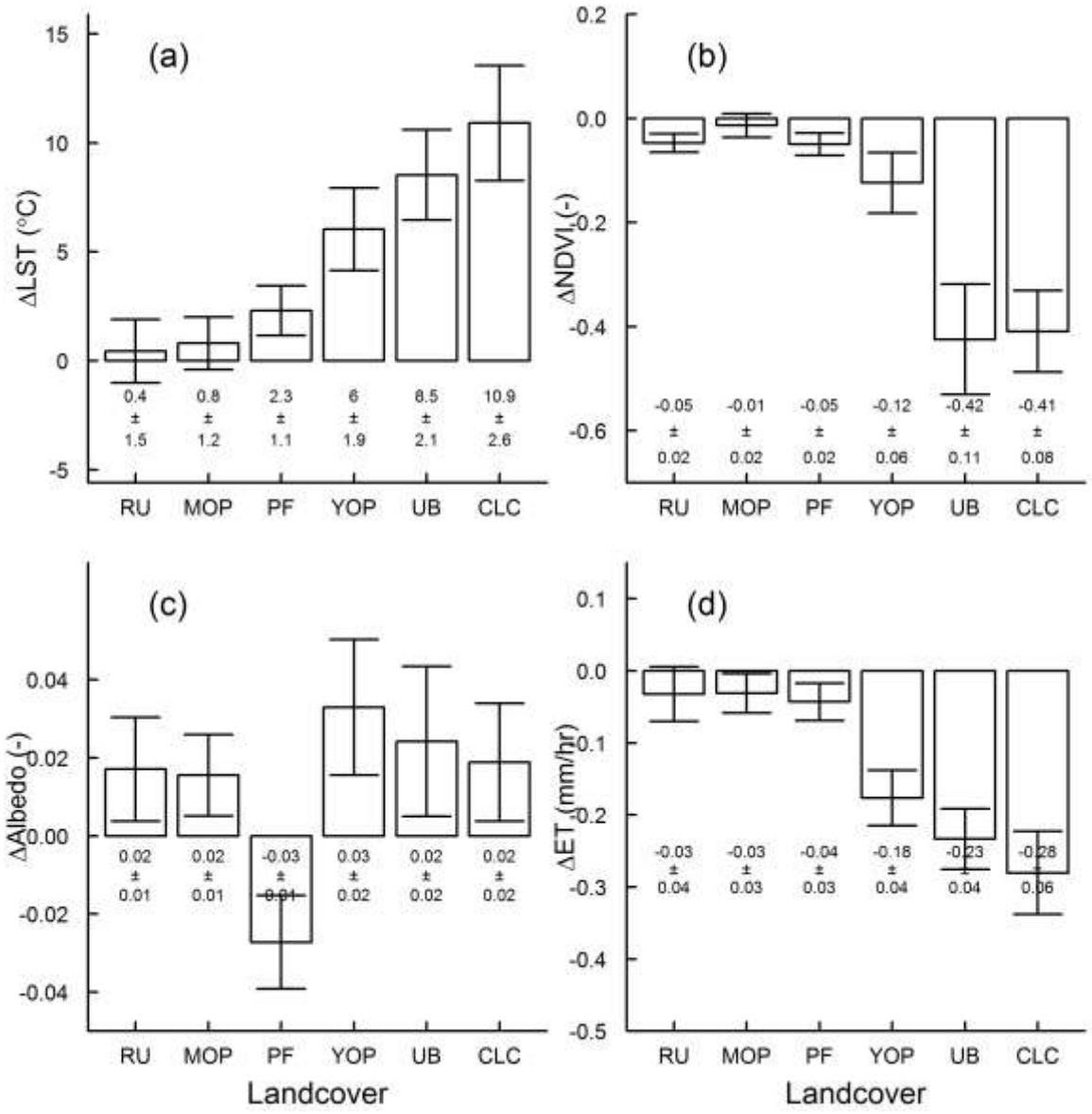

Fig. A4.1 Differences (mean ± SD) in surface temperature (ΔLST), normalized difference vegetation index (ΔNDVI), Albedo (ΔAlbedo) and Evapotranspiration (ΔET) between other land covers (RU, MOP, PF, YOP, UB and CLC) and forest (FO) in the Jambi province, derived from the Landsat LST image acquired on 19 June 2013 at 10:13 am local time.

A5. Statistical analysis

Table A5.1 ANOVA statistics

		Df	Sum Sq.	Mean Sq.	F value	Pr(>F)
L6	Group	6	5033	839	24073	***
	Residuals	41583	1449	0		
Rc	Group	6	13444	2241	25597	***
	Residuals	41583	3640	0		
LST	Group	6	657323	109554	26240	***
	Residuals	41583	173612	4		
Albedo	Group	6	17.0	2.84	11492	***
	Residuals	41583	10.3	0.00		
NDVI	Group	6	1197	200	32402	***
	Residuals	41583	256	0		
ET	Group	6	464	77.3	41141	***
	Residuals	41583	78	0.0		

*** : $p = 2 \times 10^{-16}$

A6. SEBAL steps

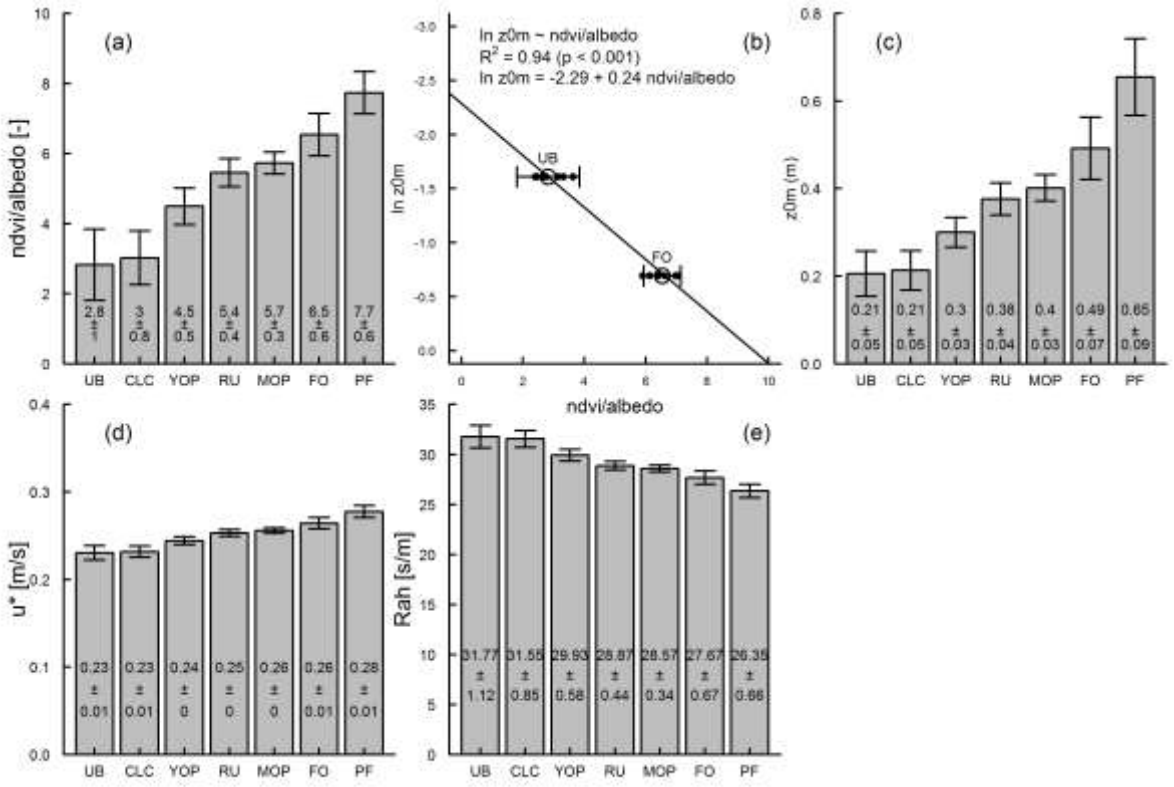

Fig. A5.1 Analysis of the steps involved in deriving the input for deriving ET from Landsat images with SEBAL.

Table A5.2 The relation LST-Albedo-NDVI-ET separated by land cover type.

	Rc			LST		
FO	**α**	**NDVI**	**ET**	**α**	**NDVI**	**ET**
ρ	-0.31	-0.48	-0.96	-0.30	-0.48	-0.96
R^2	0.09	0.06	0.96	0.09	0.06	0.97
β	-4.67	1.42	-6.36	-33.86	10.38	-46.43
Stand. β	-0.31	0.13	-1.01	-0.31	0.126	-1.01
Modelfit (R^2)	0.99			0.99		
RU	**α**	**NDVI**	**ET**	**α**	**NDVI**	**ET**
ρ	0.20	-0.48	-0.89	0.20	-0.48	-0.89
R^2	0.12	0.18	1.29	0.12	0.18	1.29
β	-5.59	1.34	-6.50	-40.89	9.74	-47.47
Stand. β	-0.57	0.37	-1.45	-0.57	0.37	-1.45
Modelfit (R^2)	0.99			0.99		
PF	**α**	**NDVI**	**ET**	**α**	**NDVI**	**ET**
ρ	0.26	-0.30	-0.98	0.26	-0.30	-0.98
R^2	0.07	0.06	1.12	0.07	0.06	1.12
β	-2.87	0.87	-6.22	-20.74	6.26	-44.55
Stand. β	-0.28	0.19	-1.15	-0.28	0.19	-1.146
Modelfit (R^2)	0.99			0.99		
MOP	**α**	**NDVI**	**ET**	**α**	**NDVI**	**ET**
ρ	-0.15	-0.41	-0.95	-0.15	-0.41	-0.95
R^2	0.05	0.11	1.07	0.05	0.11	1.07
β	-5.32	1.42	-6.51	-38.50	10.36	-47.26
Stand. β	-0.30	0.27	-1.12	-0.302	0.27	-1.13
Modelfit (R^2)	0.99			0.99		
YOP	**α**	**NDVI**	**ET**	**α**	**NDVI**	**ET**
ρ	-0.71	-0.58	-0.93	-0.72	-0.58	-0.92
R^2	0.25	0.12	0.87	0.26	0.12	0.86
β	-5.55	0.85	-6.79	-39.11	6.06	-47.52
Stand. β	-0.36	0.21	-0.93	-0.36	0.21	-0.94
Modelfit (R^2)	0.99			0.99		
UB	**α**	**NDVI**	**ET**	**α**	**NDVI**	**ET**
ρ	-0.44	-0.72	-0.89	-0.44	-0.72	-0.89
R^2	0.20	0.02	0.77	0.19	0.02	0.78
β	-6.95	-0.08	-6.40	-47.69	-0.51	-44.22
Stand. β	-0.45	-0.03	-0.87	-0.45	-0.03	-0.87
Modelfit (R^2)	0.99			0.99		
CLC	**α**	**NDVI**	**ET**	**α**	**NDVI**	**ET**
ρ	-0.13	-0.68	-0.98	-0.13	-0.68	-0.98
R^2	0.03	0.05	1.02	0.03	0.04	1.01
β	-6.21	0.35	-7.10	-42.87	1.97	-47.66
Stand. β	-0.20	0.07	-1.05	-0.21	0.06	-1.04
Modelfit (R^2)	0.99			0.99		

All metrics were highly significant ($p = 2\times10^{-16}$).

Abbreviations: FO = Forest, RU = Rubber, PF = Acacia Plantation Forest, MOP = Mature Oil Palm, YOP = Young Oil palm, CLC = Clear cut land, UB = Urban Areas

Integrity declaration

I hereby declare that:
I am the authentic author of this research
I have done the present work independently
I have not used any unauthorized aids
I have not attempted / started a doctoral study before.
In accordance with academic rules and ethical conduct, I have fully cited and referenced all material and results that are not original to this work.

Integritätserklärung

Hiermit erkläre ich dass:
ich der authentische Autor dieser Forschung bin
ich die vorliegende Arbeit selbständig angefertigt habe,
ich keine unerlaubten Hilfsmittel verwendet habe
ich bisher noch keinen Promotionsversuch unternommen habe.
In Übereinstimmung mit akademischen Regeln und ethischem Verhalten habe ich alle Materialien und Ergebnisse, die nicht originell zu dieser Arbeit sind, vollständig zitiert und referenziert.

Déclaration d'intégrité

Je déclare que:
je suis l'auteur authentique de cette recherche
j' ai fait la recherche actuelle indépendamment
je n'ai utilisé aucune aide non autorisée
Je n'ai pas commencé un doctorat avant.
Conformément aux règles académiques et à la conduite éthique, j'ai entièrement cité et référencé tout le matériel et les résultats qui ne sont pas originaux pour ce travail.

Integriteitsverklaring

Hierbij verklaar ik dat:
ik de authentieke auteur van dit rapport ben
ik het huidige onderzoek onafhankelijk gedaan heb
ik geen ongeoorloofde hulpmiddelen gebruikt heb
ik niet eerder aan een doctoraatsstudie begonnen ben.
In overeenstemming met academische regels en ethisch gedrag, heb ik alle materiaal en resultaten die niet origineel zijn in dit werk, volledig geciteerd en gerefereerd

Clifton R. Sabajo

Date 22 June 2018